MODELLING CONCRETE DURABILITY USING SYSTEM DYNAMICS

R. Arunothayan 168017 D

Master of Science of Engineering (Honours)

Department of Civil Engineering

University of Moratuwa

Moratuwa

Sri Lanka

December, 2018

MODELLING DURABILITY OF CONCRETE USING SYSTEM DYNAMICS

R. Arunothayan 168017 D

The Research Thesis was submitted in partial fulfilment of the requirements for the

Degree of Master of Science of Engineering

Supervised by Prof. W.P.S. Dias

Department of Civil Engineering

University of Moratuwa

Moratuwa

Sri Lanka

December, 2018

DECLARATION

I declare that this is my own work and this thesis does not incorporate without acknowledgement any material previously submitted for a Degree or Diploma in any other University or institute of higher learning and to the best of my knowledge and belief it does not contain any material previously published or written by another person except where the acknowledgement is made in the text.

Also, I hereby grant to University of Moratuwa the non-exclusive right to reproduce and distribute my thesis, in whole or in part in print electronic or other medium. I retain the right to use this content in whole or part in future works (such as articles or books)

…… Date: December 10, 2018

R. Arunothayan

"The undersigned hereby certified that they have read and recommended the thesis for the acceptance in partial fulfilment of the requirements for the Degree of Master of Science of Engineering"

…… Date: December 11, 2018

Prof. W.P.S. Dias

ABSTRACT

MODELLING CONCRETE DURABILITY USING SYSTEM DYNAMICS

Corrosion of reinforcement is the major deterioration mechanism of the durability of reinforced concrete. Chloride ingress and carbonation are the main contributors to the corrosion. This work was aimed to model the corrosion processes using system dynamics which has a closed-loop structure that brings results from past actions of the system back into the model to control future actions.

Two separate models are built for chloride ingress and carbonation. In each case, after the model is built, it is validated, and then parametric studies carried out on the influence of water / binder ratio (varied from 0.3 to 0.8) and fly ash percentage of binder (varied from 0 to 50%). Models were in good agreement with the published experimental studies. The obtained results predict the long-term characteristics of corrosion, and the changes in corrosion parameters such as crack width (chloride ingress into concrete) and carbonation depth (carbonation) over a design period of 50 years.

Chloride ingress process is a positive or reinforcing loop in the system dynamics understanding where such ingress leads to the onset of cracking that in turn increases the ingress. The carbonation process on the other hand is a negative or balancing loop, since the diffusion of CO_2 causes a carbonated region with reduced porosity that in turn decreases the diffusion.

The effects of fly ash differ in the two models. In both cases, fly ash replacement (up to an optimum of around 30%) reduces porosity and hence increases strength and reduces diffusion, whether of chlorides or CO_2. However, in the chloride ingress model, the reduction of OH- ions by the fly ash further reduces the ingress; whereas in the carbonation model, the same reduction increases the CO_2 diffusion.

Key Words: *Concrete, Reinforcement Corrosion, Carbonation, Chloride Ingress, Fly Ash*

ACKNOWLEDGEMENT

I would like to pay gratitude to everyone who gave support during the research study as it would have never got succeeded without them.

I would like to express my profound gratitude and warm regards to the supervisor of the research, Prof. W.P.S. Dias Senior Professor, Department of Civil Engineering, University of Moratuwa, for guiding me with continuous supervision and sharing his broad knowledge and time for my research project. I would also like to thank him for being the motivational support at the time of need.

I appreciate the financial assistance given by Millennium Concrete Technologies (Pvt) Ltd, Kelaniya, Sri Lanka.

I am obliged to thank Prof. S.M.A. Nanayakkara, Prof. R.U. Halwatura Dr. K. Baskaran and Dr. J.C.P.H. Gamage for their valuable comments and advices given during discrete discussions and research progress evaluations.

Finally, I am truly grateful to the technical staffs in the department laboratories and my colleagues who have supported me in many ways during my research. I would like to take this opportunity to express my sincere gratitude to them.

TABLE OF CONTENTS

LIST OF FIGURES

LIST OF TABLES

LIST OF ABBREVIATIONS

Abbreviation	Description
FA	Fly Ash
OPC	Ordinary Portland Cement
RC	Reinforced Concrete
SCM	Supplementary Cementitious Materials
SD	System Dynamics
SDM	System Dynamics Modelling

1 INTRODUCTION

1.1 Background

Consisting of concrete and embedded steel reinforcement, Reinforced Concrete (RC) is probably the most commonly used construction material across the globe due to its considerable strength and flexibility in properties. It is widely used for bridges, buildings, and underground structures. Properly designed, built, and maintained, reinforced concrete structures remain in service for many decades, even under severe corrosive conditions. There are many factors which influence the performance and the durability of concrete structures during service life. Different physico-chemical processes take place in reinforced concrete structures and result in deterioration. It is widely accepted that corrosion of reinforcing steel is one of the major deterioration mechanisms of reinforced concrete and can severely compromise safety and serviceability of the structure.

In the absence of aggressive environment, concrete provides an excellent protection to the steel, both mechanically and electrochemically because the pores in concrete are partially or totally filled with a highly alkaline solution – with a pH larger than 12, typically between 12.5 and 13. In that alkaline medium, the steel is in a passive state due to the formation of a layer of dense, impervious oxide that protects the steel against corrosion. However, under aggressive environment conditions, de-passivation of the layer occurs due to two key mechanisms – carbonation and chloride ingress. In carbonation, the incoming substance – namely carbon dioxide - reacts with alkaline constituents and reduces the pH of the electrolyte in the pores; this removes the protective layer on the steel and leads to corrosion. In chloride ingress, the incoming substance – chloride ions - produce a local pH reduction via ion exchange of OH^- ions and breaks the passivation layer. Consequently, in both cases, this breakdown of steel passivity will lead to the loss of rebar cross section and spalling of the concrete cover.

Corrosion reactions are very complex and influenced by many factors such as supplementary cementitious materials, moisture content, cover depth, temperature, cyclic wetting and drying, sustained loading, concrete resistivity, concrete quality, cracking, dissolved oxygen concentration and exposure conditions (Otieno et al 2010). However, it is important to note that it is hard to explicitly incorporate each of these factors in a model. Some of these factors can be indirectly incorporated in a prediction model, for example - concrete resistivity can be indirectly used to account for temperature, concrete quality, and moisture content of the concrete (Otieno et al 2012).

1.2 Reinforcement Corrosion

Corrosion is an unavoidable deterioration characteristic in reinforced concrete structures. Two phases of reinforcement corrosion can be identified.

1. Corrosion Initiation Phase - The period taken for the reactive substances in the environment to reach the threshold concentration at which the corrosion of steel bars is triggered
2. Corrosion Propagation Phase – The period in which the crack develops in concrete due to continuous access of reinforcement to the reactive substances

Chloride ions or carbon dioxide molecules infiltrate into the concrete and destroy the passivity of concrete pore water to initiate the corrosion. Frequently used service life models for reinforcement corrosion estimate the time required for a critical amount of these aggressive substances to reach the level of the reinforcement through the concrete cover. When that critical amount is reached, corrosion of the reinforcement is probable, and from that point onwards, the corrosion propagation begins. During the propagation, different damage stages can be identified such as crack initiation (chloride ingress), spalling of cover concrete and the total damage. Figure 1.1 shows the corrosion initiation and propagation pattern over the period of structure's life span.

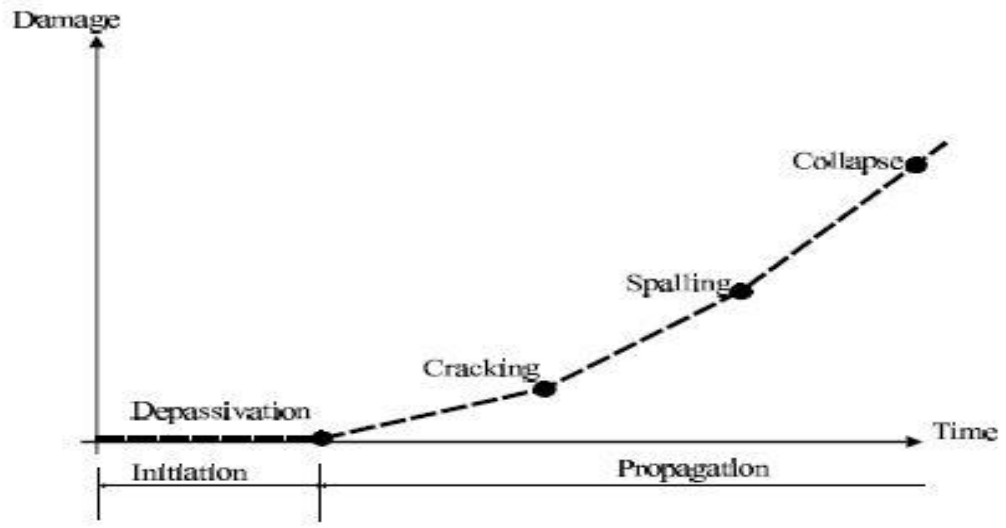

Figure 1.1 Corrosion Initiation and Propagation (Duracrete, 2000)

Corrosion occurs when $Fe2^{+}$ ions are dissolved into the aqueous solution while two electrons are freed in the anode. Corrosion will proceed when the electrochemical circuit is closed in which the freed electrons move into the cathodic region (inside the metal) where they react with other chemical specimens present in the electrolyte. The secondary reactions involve the formation of iron hydroxides and iron oxides. These products have a specific volume greater than that of the steel reinforcement.

Therefore, higher volume of rust will initiate tensile forces in concrete. When the stress exceeds its splitting tensile strength, concrete cracking will be observed on its surface.

Figure 1.2 shows the schematic representation of anodic and cathodic reactions in steel during chloride ingress (Figure 1.2-I) and carbonation (Figure 1.2-II).

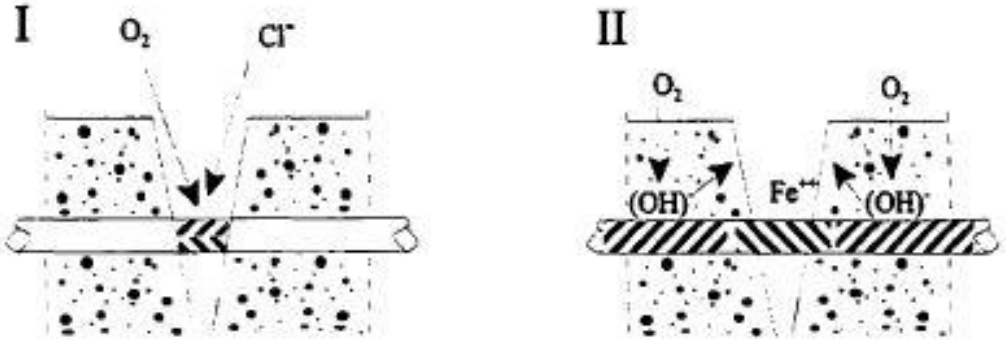

Figure 1.2 Schematic Representation of Corrosion Mechanism (Schiessl and Raupach, 1997)

In Figure 1.2, the anodic steel surface is presented by the hatched lines inclining from left to right and cathodic steel surface, the opposite inclination.

Extensive research has been conducted on modelling the effects of corrosion propagation, including the damage to the concrete cover [Alonso et al., 1998; Liu and Weyers, 1998; Li, 2003; Vu et al., 2005; Li et al., 2008]. However, numerous factors, such as the effects of concrete materials and environmental conditions (temperature and relative humidity) influence the propagation phase, causing uncertainties with such predictions.

1.3 Contribution of Fly Ash in Concrete Corrosion

Supplementary cementitious materials (SCM) such as low calcium fly ash (FA), silica fume or slag are added to the ingredients in the mix design of concrete to increase long-term performance and durability of concrete. Due to economical, technological, and environmental benefits (ACI Committee 232, Reapproved in 2002), the use of fly ash in concrete has significantly increased during the last two decades or so.

For our study, the pozzolanic effects of low calcium fly ash are considered as cementitious additives. Fly ash is a coal combustion by-product, usually found in the residue of coal-burning power plants. After mechanical filtering and separating processes, fly ash is directed to concrete manufacturing industries. Fly ash pozzolans have a slow hydration reaction rate thus gain strength much slower than the cement counterparts. However, as it gains strength, it produces higher strengths in long term than the control OPC which has the same binder content in the mix. Fly ash concrete

also reduces the heat generation in mass structures as the heat generated by hydration of Portland cement is consumed by the pozzolans for initiating the reaction of fly ash (Manmohan and Mehta, 1981). Availability of fly ash will reduce the concrete bleeding, improve pumpability and extend the time of setting by retarding early hydration.

Four principal constituents of fly ash are SiO_2 – due to the presence of clay mineral and quartz impurities of the coal, Al_2O_3 – mainly results from clay and some organic compounds in the coal, Fe_2O_3 – due to the availability of iron containing minerals and CaO – from calcium carbonates and calcium sulphates in the coal.

Fly ash influences the corrosion in concrete due to its pozzolanic reactions. In the mix, fly ash reacts with OH^- ions and produces C-S-H pozzolanic deposits. Therefore, the concrete porosity is reduced. However, when excessive cement is replaced by fly ash, hydration reactions are reduced and hence lesser OH^- ions are produced. This will increase the porosity. In this case, excessive fly ash in the mix cannot participate in pozzolanic reactions due to lack of OH^- ions. Therefore, fly ash replacement in the mix has multiple effects on the concrete porosity and strength development.

Additionally, the pozzolanic reactions of the fly ash separately influence chloride ingress and carbonation. In chloride ingress, higher amount of OH^- ions consumption by fly ash for pozzolanic reactions will lead to the reduction in ion exchange with Cl^- ions. Therefore, anodic corrosion reaction at the steel surface is resisted. In carbonation, fly ash enhances the corrosion. Fly ash consumes OH^- ions for its pozzolanic reactions therefore reduces the amount of the major reactor and hastens the carbonation.

Due to the conflicting effects discussed above, the existing research studies on the effects of cementitious additives on concrete corrosion present inconsistencies. The current research study presents system dynamic models which incorporate the conflicting aspects of fly ash replacement into mathematical models that predict long term deterioration measures.

1.4 System Dynamics Modelling (SDM)

System dynamic modelling illustrates the patterns of behaviour of the interdependent group of variables. The quantitative relationships between the items are represented in a graphical environment via feedback loops. Feedback loop is a closed sequence of causes and effects, that is, a closed path of action and information (Richardson and Pugh, 1981). These loops can be classified into two categories which are balancing feedback loop that seeks stability and reinforcing feedback loop that facilitates an exponential growth.

The system dynamics diagrams represent cause-and-effect chains realistically than verbal explanations of the relationships between variables. The overall performance

of the loop is the integration of the performances of all individual relationships. The process of carbonation and chloride ingress are modelled using system dynamics. Here, chloride ingress process creates a positive or reinforcing feedback loop and, on the other hand, carbonation of concrete creates a negative or balancing feedback loop.

1.5 Outline of the Thesis

The thesis is arranged into six chapters, including this one which introduces the research study.

Chapter 2 introduces the system dynamic modelling and its adaptation to civil engineering practices, especially our use of it for the corrosion in concrete. The chapter also introduces the Vensim system dynamic software which is used for the modelling. Chapter 3 discusses the methodology and the approach to the research study.

Chapter 4 describes the modelling of chloride ingress in concrete. First, the system dynamic model is presented and then it is validated against the experimental results from the available literature. Parametric studies investigating the sensitivity of the influencers such as water / binder ratio and fly ash replacement are analysed and presented.

Chapter 5 describes the modelling of carbonation in concrete. The chapter subdivisions follow the same as chapter 4, as the model is developed, validated, and the parametric studies are analysed and presented.

Chapter 6 summarizes the main conclusions of the thesis and makes a few suggestions for future research.

also reduces the heat generation in mass structures as the heat generated by hydration of Portland cement is consumed by the pozzolans for initiating the reaction of fly ash (Manmohan and Mehta, 1981). Availability of fly ash will reduce the concrete bleeding, improve pumpability and extend the time of setting by retarding early hydration.

Four principal constituents of fly ash are SiO_2 – due to the presence of clay mineral and quartz impurities of the coal, Al_2O_3 – mainly results from clay and some organic compounds in the coal, Fe_2O_3 – due to the availability of iron containing minerals and CaO – from calcium carbonates and calcium sulphates in the coal.

Fly ash influences the corrosion in concrete due to its pozzolanic reactions. In the mix, fly ash reacts with OH^- ions and produces C-S-H pozzolanic deposits. Therefore, the concrete porosity is reduced. However, when excessive cement is replaced by fly ash, hydration reactions are reduced and hence lesser OH^- ions are produced. This will increase the porosity. In this case, excessive fly ash in the mix cannot participate in pozzolanic reactions due to lack of OH^- ions. Therefore, fly ash replacement in the mix has multiple effects on the concrete porosity and strength development.

Additionally, the pozzolanic reactions of the fly ash separately influence chloride ingress and carbonation. In chloride ingress, higher amount of OH^- ions consumption by fly ash for pozzolanic reactions will lead to the reduction in ion exchange with Cl^- ions. Therefore, anodic corrosion reaction at the steel surface is resisted. In carbonation, fly ash enhances the corrosion. Fly ash consumes OH^- ions for its pozzolanic reactions therefore reduces the amount of the major reactor and hastens the carbonation.

Due to the conflicting effects discussed above, the existing research studies on the effects of cementitious additives on concrete corrosion present inconsistencies. The current research study presents system dynamic models which incorporate the conflicting aspects of fly ash replacement into mathematical models that predict long term deterioration measures.

1.4 System Dynamics Modelling (SDM)

System dynamic modelling illustrates the patterns of behaviour of the interdependent group of variables. The quantitative relationships between the items are represented in a graphical environment via feedback loops. Feedback loop is a closed sequence of causes and effects, that is, a closed path of action and information (Richardson and Pugh, 1981). These loops can be classified into two categories which are balancing feedback loop that seeks stability and reinforcing feedback loop that facilitates an exponential growth.

The system dynamics diagrams represent cause-and-effect chains realistically than verbal explanations of the relationships between variables. The overall performance

of the loop is the integration of the performances of all individual relationships. The process of carbonation and chloride ingress are modelled using system dynamics. Here, chloride ingress process creates a positive or reinforcing feedback loop and, on the other hand, carbonation of concrete creates a negative or balancing feedback loop.

1.5 Outline of the Thesis

The thesis is arranged into six chapters, including this one which introduces the research study.

Chapter 2 introduces the system dynamic modelling and its adaptation to civil engineering practices, especially our use of it for the corrosion in concrete. The chapter also introduces the Vensim system dynamic software which is used for the modelling. Chapter 3 discusses the methodology and the approach to the research study.

Chapter 4 describes the modelling of chloride ingress in concrete. First, the system dynamic model is presented and then it is validated against the experimental results from the available literature. Parametric studies investigating the sensitivity of the influencers such as water / binder ratio and fly ash replacement are analysed and presented.

Chapter 5 describes the modelling of carbonation in concrete. The chapter subdivisions follow the same as chapter 4, as the model is developed, validated, and the parametric studies are analysed and presented.

Chapter 6 summarizes the main conclusions of the thesis and makes a few suggestions for future research.

3 OBJECTIVES AND APPROACH

The two main objectives of the research study are

I. to portray the chloride ingress and carbonation phenomenon in concrete as causal loop diagrams; and
II. to investigate the influences of fly ash replacement of cement and water / binder ratio on these two major concrete deterioration mechanisms

The existing knowledge on concrete durability is a collection of independent distinctive studies on the influencers of concrete corrosion. However, existing researches do not capture the interrelations between major influences; instead treating parts of the complex system separately.

The current research investigates the inter-relationships among the factors extensively, validates the processes and provides a detailed illustration of the influencers and its effects on the concrete durability through system dynamic modelling. In Vensim environment, all the influencers are interconnected using mathematical relationships available in the literature.

It should be noted that the chloride ingress process is a positive or reinforcing loop in the system dynamics understanding, since such ingress leads to the onset of cracking that in turn increases the ingress. This is presented in Figure 3.1. It should be noted that cracking occurs parallel to the corroding bar and not in a transverse direction (as caused by flexural stress).

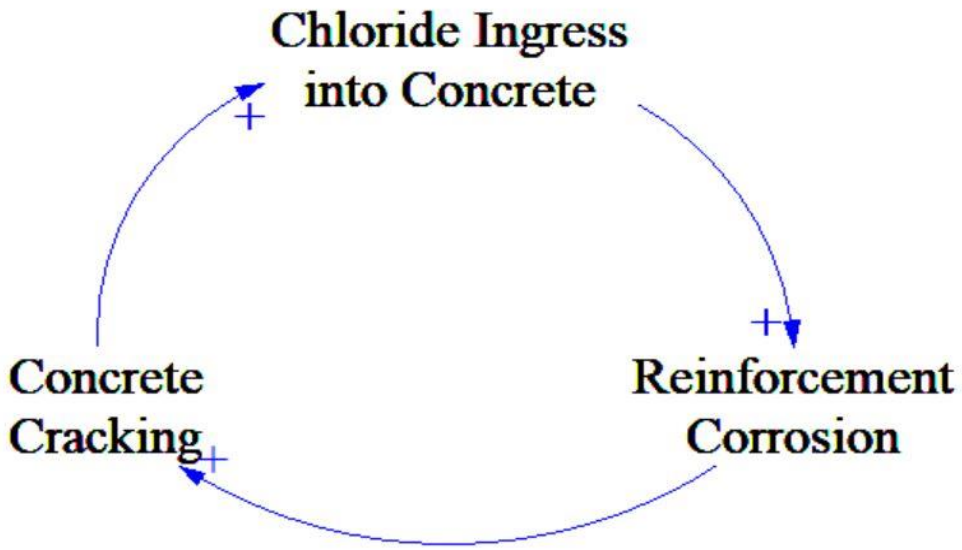

Figure 3.1 Reinforcing Loop of Chloride Ingress (Vensim)

The carbonation process on the other hand is a negative or balancing loop, since the diffusion of CO_2 causes a carbonated region with reduced porosity that in turn decreases the diffusion. This is presented in Figure 3.2.

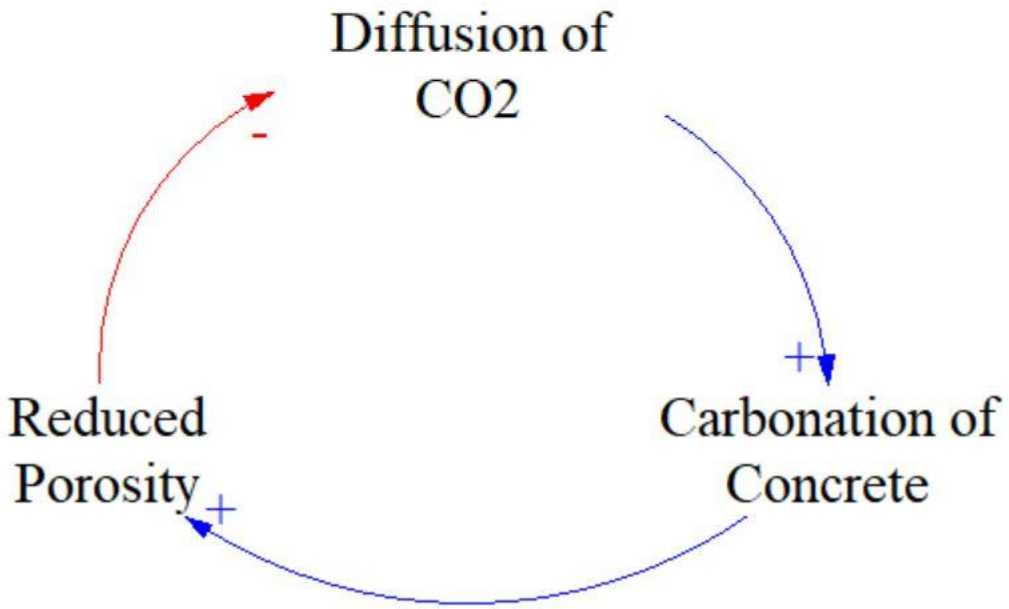

Figure 3.2 Balancing Loop of Carbonation (Vensim)

We can see that (in Figure 3.1 and Figure 3.2), the signs of the arrows, when combined, give the sign of the loop. An odd number of negative signs in the arrows results in a negative (balancing) loop whereas an even number (including zero) of negative signs results in a positive (reinforcing) loops.

Two separate models are built for chloride ingress and carbonation. No attempt is made to combine them. In each case, after the model is built, it is validated, and then parametric studies carried out on the influence of water / binder ratio (varied from 0.3 to 0.8) and fly ash percentage of binder (varied from 0 to 50%).

The effects of fly ash differ in the two models. In both cases, fly ash replacement (up to an optimum of around 30%) reduces porosity and hence increases strength and reduces diffusion, whether of chlorides or CO_2. However, in the chloride ingress model, the reduction of OH- ions by the fly ash further reduces the ingress; whereas in the carbonation model, the same reduction increases the CO_2 diffusion.

Validation is difficult because data on long term behaviour is scarce. In some cases, the same experimental results were used to both build and validate the model, with care exercised to use different aspects of the results for different tasks. The long-term chloride ingress results of Vidal et al (2004) and Zhang et al (2010) were particularly useful in this regard.

It is also important to note that the long-term predictions of the concrete performance are inconsistent due to limitations in long term experimental studies on concrete durability. Majority of the experimental research studies are accelerated experiments under the laboratory conditions. Available literature based on the condition assessments of existing structures provide insight into long term predictions but the data regarding mix constituents are difficult to acquire for those structures. To overcome the gap, the current research provides necessary assistance to predict long term concrete performances and hence support the designers to optimise the mix accordingly. In this model, the changes in the level variables with time is captured over the design life of 50 years. Therefore, the crack width propagation in chloride ingress and the carbonation depth development in carbonation process are studied over the time. Therefore, the model leads to time dependent analyses of the deterioration mechanisms.

Another objective of the study is to introduce system dynamic thinking into structural engineering practices. In an ever-evolving discipline where many new technologies are established on daily basis, it is important to understand the counter intuitive behaviour avoid unexpected dynamics which hinder the progress. Having the complete illustration of the existing problem helps to resolve the problems without unforeseen side effects and delays.

The limitations of the research work are given below

- The research work outputs do not account for the spalling of concrete cover during corrosion propagation phase
- The research study does not consider the onsite workmanship factors which affect the quality of the in-situ concrete.

4 MODELLING CRACKING DUE TO CHLORIDE INGRESS INTO CONCRETE

4.1 Introduction to Chloride Ingress

One of the main causes of concrete degradation is the corrosion due to chloride ingress. Bridge decks, Marine structures, and parking lots are frequently vulnerable to chloride ingress. Chlorides in concrete can arrive from various sources. Occasionally, chloride ions are present in the constituents of concrete. The use of contaminated sea water, inadequately washed aggregates and chloride additives could cast chloride ions into concrete. However, the predominant type of chloride ingress comes from diffusion of chloride ions into the concrete during the service life exposure. The sources of chloride ion supply are either sea water or airborne ions. The supply of chlorides in the concrete is a time-dependent function of the environmental conditions. The mechanisms of chloride supply are complex. The supply processes are not explicitly defined hence not easy to be quantified.

Chloride can be present in concrete in two forms which are free chloride and bound chloride. Free chloride is the concentration of water soluble chloride ions within the pore solution of concrete. Free chloride ions are the primary participants in the corrosion reactions with the steel reinforcement. Meanwhile, chloride ions can be bound physically and chemically in concrete. Chloride binding in concrete is vital since the binding process removes chloride ions from the concrete pore solution into the hydrated solid binder. This binding offers a reduction in chloride ions that delays the ingress of chloride ions. Physical binding is generally assumed to occur at the pore walls. Chemical binding of chlorides with cement forms Friedel's salt ($3CaO.Al_2O_3.CaCl_2.10H_2O$) (Nilsson et al., 1996).

The following equation shows the relationship between the chloride concentrations present in the concrete at any given time.

$$C_{total} = C_{free} + C_{bound} \quad (1)$$

Where C_{total} is the total chloride concentration in concrete in [kg/m3], [moles/volume] or [kg/kg]; C_{free} is the free chloride ion concentration in the given volume of solution [kg/m3 solution]; C_{bound} is the bound chloride concentration in the given volume of concrete solution [kg/m3 solution].

Chloride binding may delay reinforcement depassivation; for only the free (unbound) chloride ions are available to interact with steel reinforcement. However, bound chlorides could be partially liberated if the free chloride concentration reduces. Therefore, the sink in chloride ions provided by binding may switch into a supply source of chloride ions. On the other hand, the risk of reinforcement corrosion cannot

be completely ignored because binding is nearly completely reversible if pore solution pH value drops below approximately 11 [Glass and Buenfeld, 2000].

Chloride supply and distribution into concrete is a complex time-dependent process which is largely controlled by the properties of the concrete cover, water to binder ratio, constituents of concrete and cement minerals, as well as by exposure conditions such as temperature, moisture, chloride concentration at the concrete surface, and so on. The chloride penetration is a dependent on its diffusion mechanisms. The major diffusion characteristics rely upon the moisture condition of concrete or degree of saturation. Due to the complexity, lack of comprehensive knowledge on this theme does not help the dependable quantification of their effects.

Vensim model for chloride ingress incorporates the inter-dependency of the influencers and proposes a detailed background for the prediction of long-term crack width development and the time for the crack initiation.

4.2 Chloride Ingress Model Formulation

4.2.1 Model Overview

Identifying the system of processes that affect the reinforcement corrosion and understanding the inter relationship among those sub systems are two key important features in the modelling of chloride ingress using system dynamics. Every interrelation entered into the model has been repeatedly checked for accuracy and correctness by referencing multiple sources.

As discussed, chloride amount at steel level is a function of exposure conditions and the diffusion mechanism of chloride ions. As the chloride amount in the steel level exceeds the chloride threshold value, the corrosion is initiated. After the initiation, the corrosion propagation is expressed in terms of corrosion rate (corrosion current density). The rate of corrosion presents the ratio of cathodic and anodic processes of corrosion in concrete. Rate of corrosion depends on the available chloride concentration at the reinforcement level. Continuous supply of chloride ions coupling with the pore structure and the resistivity of concrete will determine the amount of current produced per square area of steel corrosion.

Attack Penetration (loss of reinforcement thickness) is the accumulation of total corrosion which is represented by the gradual loss of reinforcement diameter thickness in concrete. It is important to note that the concrete specimen are not homogeneous, therefore the corrosion is localised and non-uniform. Electron probe micro-analyses are usually applied to identify and evaluate the experimental penetration depth and the profiles of attack penetration.

On the other hand, the corrosion products are settled inside concrete and the volume of the corrosion products (rust) are greater than the original reinforcement corroded. This will result in the volume expansion of the concrete hence the tensile stress

development. When the tensile stress due to corrosion exceeds the splitting tensile strength of concrete, the crack in concrete initiates. Crack width measures the crack propagation in concrete with time.

Crack in concrete will invite more chloride molecules into concrete. Large voids will be established, and chloride ions have greater access to reinforcement. In marine environments where the continuous uniform chloride supply is guaranteed, the diffusion of chloride ion will increase, and thus more cracks will occur. This will form a reinforcing feedback loop in system dynamics where the past activities (concrete cracking due to chloride ions) will increase the probability for the future occurrence (more chloride ions will penetrate through the cracks). This feedback loop is chloride ingress model is presented in Figure 4.1.

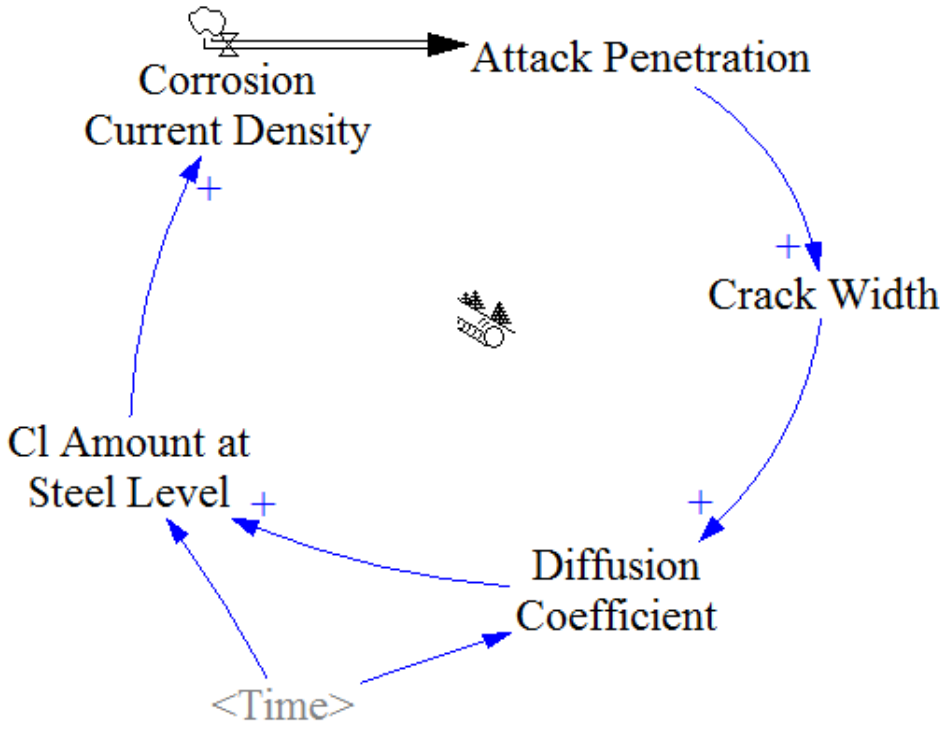

Figure 4.1 Chloride Ingress Model Feedback Loop

In the system dynamic model, the factors affecting the feedback loop and its contributions to corrosion are incorporated using mathematical expressions. The life-span of the model predictions are considered as 50 years.

4.2.2 Attack Penetration

Attack penetration is the accumulation of loss of reinforcement and it is identified by the corrosion rate. The corrosion current densities of steel in concrete vary in the range of 10^{-2} to 10^{2} $\mu A/cm^2$ (Broomfield et al, 1993).

Duracrete (2000) discussed the electrochemistry-based method to model the attack penetration of the corrosion. Corrosion current density (corrosion rate) is measured using 3LP (Clear, 1992) and Gecor (Broomfield et al, 1993) devices. Both devices use the same linear polarization technique. 3LP is a potentio-static test with a rectangular counter electrode of 76 mm x178 mm while Gecor uses the galvanostatic method to measure the change in potential between control and the test specimen. The guidelines of 3LP and Gecor are shown below in Table 4.1.

Table 4.1 Corrosion Current Density in 3LP and Gecor Devices

i_{corr} (μA/cm^2)	Gecor Device corrosion state	i_{corr} (mA/ft^2)	3LP Device Expectation
< 0.1	Passive	<0.2	No damage expected
0.1 -0.5	Low Corrosion	0.2-1.0	Damage possible 10-15 years
0.5 -1.0	Moderate	1.0-10.0	Damage possible 2-10 years
>1.0	High Corrosion	>10.0	Damage possible < 2 years

Very low current densities indicate passivity. When the current density is lower than 0.1 μA/cm^2, corrosion is very rarely triggered (Broomfield, 1993). Higher current densities (greater than 1 μA/cm^2) indicate very active corrosion. This state is not naturally encountered; rather only exhibited in accelerated chloride penetration test under laboratory conditions. It is also important to note that the current density is influenced by time as the anodic and cathodic concentration of ions change with time.

Using Faraday's law of electrochemistry, the corrosion rate in terms of amount of steel dissolving and forming hydroxide/oxide shall be calculated using the Equation 2 given below.

$$m = \frac{i \times t \times a}{n \times F} \qquad (2)$$

Where m is the mass of reinforcement per area dissolved at the anode (g/m2); i is the electric current density (A/m2); t is time (s); a is the atomic mass of iron (55.8 g/mol) n is number of electrons liberated in the anodic reaction (2 for Fe → Fe2+ + 2e−) and F is Faraday's constant (96487 As/mol)

Considering the mass density of reinforcement steel to be 7.87 kg/dm^3, the Faraday's law can be modified and rearranged into a simpler equation as given in Equation 3.

$$V_{corr} = 11.6 \times I_{corr} \qquad (3)$$

Where V_{corr} is the corrosion rate (μm/year) and I_{corr} is the corrosion current density (μA/cm^2)

Integration of corrosion rate over the propagation period will measure the accumulation of reinforcement loss at time t. Duracrete (2000) model proposes Equation 4 as a function for Attack penetration P(t) at a given time t. This function gives the advancement of corrosion with time as a function of the corrosion rate V_{corr}.

$$P(t) = \int_{t_i}^{t} V_{corr}(t)\, dt \qquad (4)$$

Where $V_{corr}(t)$ is the corrosion rate at the given t, t_i is the time of corrosion initiation;

The time-independent expression for the corrosion rate, V_{corr} based on Faraday's electrochemistry model is used to develop a simpler penetration attack. Assuming a uniform corrosion rate during the propagation period, the gradual loss of rebar diameter (attack penetration) can then be expressed by incorporating Equation 3 and Equation 4 as given in Equation 5:

$$P(t) = \int_{t_i}^{t} 11.6 \times I_{corr}(t)\, dt \qquad (5)$$

However, uniform corrosion rate is reliable for cases where the material is homogeneous. Concrete is highly non-linear in characteristics and therefore, localized corrosion effects should be considered. Therefore, Duracrete (2000) model included the pitting factor α into the model and proposed the Equation 6. Details on Pitting Factor will be further discussed in section 4.2.3.

$$P(t) = \int_{t_i}^{t} \alpha \times 11.6 \times I_{corr}(t)\, dt \qquad (6)$$

This Equation 6 is then converted into the form that is applicable to Vensim system dynamic modelling as follows.

Attack Penetration = INTEG (11.6*Corrosion Current Density*PITTING FACTOR); Initial value = 0

However, the corrosion rate is usually not constant but evolves due to the corrosion process itself (progressive production of rust and extension of the corroded area leads to crack and therefore further ingress of substance). Therefore, $I_{corr}(t)$ must be initially determined. In this model, system dynamic of the corrosion process has been used to determine this time variant $I_{corr}(t)$. Vensim model uses time steps to calculate the time variant $I_{corr}(t)$ and use that value at each time steps in the calculation of next time step.

In the Vensim model, the connector in the box variable is a stock and the rate valves control the amount of stock inside the box. Under this circumstance, corrosion

current density will function as the rate valve and attack penetration will accumulate the stocks. The relationship is graphically shown in Figure 4.2.

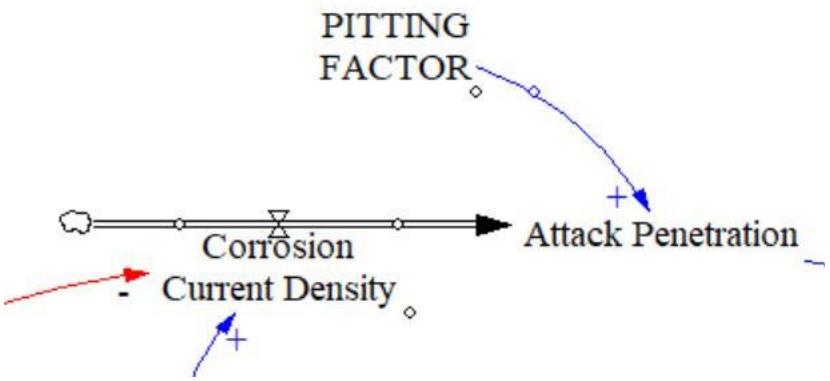

Figure 4.2 - Vensim Model for Attack Penetration

Complex corrosion models based on electrochemical principles and Butler-Volmer kinetics have been developed [Maruya 2003, Kranc and Sagüés 2001, Sagüés et al 1993, Kranc and Sagüés 1993]. These models included localization of pits, effects of future variations in exposure conditions, etc. which are not required in Vensim model because those effects are considered at separate stages of the model.

4.2.3 Pitting Factor

Corrosion in reinforced concrete can be of two types which are general corrosion and pitting corrosion. When the surface attack in the steel is uniform throughout, it is classified as general corrosion. In aggressive chloride environments, general corrosion is very rare. Localized or pitting corrosion is non-uniform and the reinforcement loss at different locations in the steel surface could be of different magnitudes. This corrosion arises particularly at places where the chloride ions diminish the protective layer. Figure 4.3 shows the difference between general and pitting corrosion.

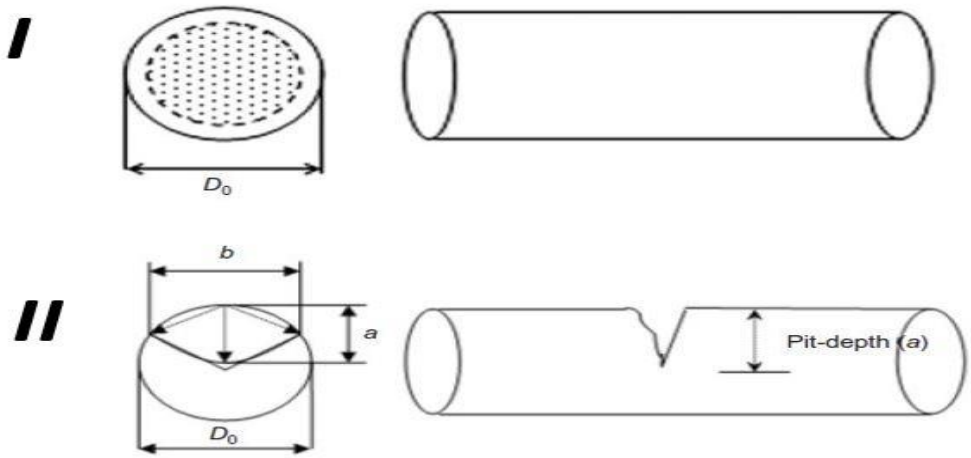

Figure 4.3 General Corrosion (I) and Pitting Corrosion (II) in Steel (Val and Melchers, 1997)

To account for this variation of corrosion depth that depends on the type of corrosion, user can input a constant value to the Vensim model for pitting factor. Pitting factor defines the amount of times the maximum localized loss of rebar exceeds the average general corrosion penetration. Values between four and eight are suggested by various research outputs [Darmawan, 2010; Broomfield, 2003; Rodriguez et al, 1996; Gonzalez et al, 1995] depending on the aggressive nature of the chloride environment. Pitting factor of five (5) is used in Vensim model as derived from Darmawan (2010).

However, pitting factor of 2 is used in the long-term analyses. As more chloride particles enter the concrete, the chloride amount at steel level reaches an equilibrium state where the corrosion process becomes homogeneous. Rodriquez et al (1996) proposed a pitting factor of two (2) for the general corrosion. This was later validated by Zhang et al (2010) experimentally. The difference between general corrosion and pitting corrosion is further discussed in section 4.3.3.

4.2.4 Corrosion Current Density

As discussed in Section 4.2.2, corrosion current density is a time dependent rate of corrosion and decides the severity of it. The increase in the corrosion rate which induces the change in concrete from passive corrosion to active corrosion has aroused the interest of the researchers, but the arithmetic values of corrosion rates are not accurately measured or estimated.

Corrosion rate (I_{corr}) is a complex process and indirectly affected by many influencers. To account for them, empirical models were proposed interrelating corrosion rate with resistivity. Since the interrelationships of other factors on I_{corr} values are considered in this model at separate individual locations, simple equation representing only I_{corr} with resistivity is essential for the modelling purpose.

Based on extensive research performed on mortars prepared with different cements and subjected to a wide range of exposure conditions, Alonso et al (1988) proposed a relationship between resistivity of concrete and the corrosion rate as shown in Equation 7.

$$I_{corr} = \frac{K_{corr}}{\rho_{ef}} \qquad (7)$$

Where K_{corr} is a constant regression coefficient equals to 3×10^4 mA/cm^2.kOhm.cm and ρ_{ef} is the resistivity of the concrete (Ohm m) at its actual degree of saturation;

However, as this relationship is experimentally derived from concrete samples with no embedded reinforcement and under indoor conditions, the relationship was omitted from the model. However, a similar, simpler but a more generalized equation is preferred.

Detailed study of existing literature gives a variety of models to predict the I_{corr} [Yalcyn and Ergun's model (1996), Katwan et al.'s model (1996), Liu and Weyers' model (1998), Duracrete model (1998), Vu and Stewart's model (2000), Scott's model (2004), Takewaka et al.'s model (2003), GuoYisen (2011)].

The model by Yalcyn and Ergun (1996) was developed by studying the chloride and acetate ions on I_{corr}. Accelerated corrosion results were measured for cylindrical specimens with 10% pozzolanic replacement and no embedded reinforcement. The model is presented in Equation 8.

$$I_{corr} = I_o . e^{-Ct} \qquad (8)$$

Where I_{corr} is the corrosion rate at time t, I_o is the initial corrosion rate and C is a corrosion constant which Yalcyn and Ergun (1996) consider to be 1.1 x 10^{-3} day^{-1}

Even though the model gives a simpler relationship to empirically calculate the corrosion rate, the model has its limitations. It predicts the corrosion rate only for uncracked conditions and the rate may not be applicable for cracked concrete structures. The model also assumes that the exposure conditions remain constant and the I_{corr} is a sole dependent on time. Also, since the model used accelerated corrosion results for derivation, this model is also avoided in the Vensim model.

Liu and Weyers (1998) proposed an empirical model based on statistical analyses of experimental results obtained from accelerated experiments. I_{corr} prediction model is a non-linear regression relationship following a rigorous statistical approach to the problem. The model is presented in Equation 9.

$$I_{corr} = 102.47 + 10.09.\ln\,(1.69.Cl) - 39038.96.(T^{-1}) - 0.0015R + 290.91.t^{-0.215} \qquad (9)$$

Where I_{corr} is the corrosion rate measured in 3LP (μA/cm^2), Cl is the total chloride content at the steel level, T is the temperature at the steel surface, R is the resistivity of the cover concrete and t is the corrosion time (Lui and Weyers, 1998).

Similar to previous models, this empirical model is also derived from accelerated corrosion and the combined effects of all factors is included in the statistical analyses. Since those effects are considered in Vensim model separately, this model is not adopted.

Duracrete model (1998) proposed a factorial approach for the chloride effect. It was an attempt to improve the Alonso et al.'s model (1988) and proposed the inclusion of other I_{corr} influencing factors to the original model by the introduction of coefficients/correction factors as shown in Equation 10.

$$I_{corr} = \frac{K_{corr}}{\rho(t)} \times F_{cl} \times F_{gal} \times F_{o2} \times F_{oxide} \qquad (10)$$

where K_{corr} is a constant regression parameter (10^4), F_{cl}, F_{gal}, F_{o2} and F_{oxide} are factors to take into account the influence of chloride content, galvanic effects, continuous formation and ageing of oxides and availability of oxygen on I_{corr} respectively, and $\rho(t)$ is the resistivity of concrete (Ω-m) at time t and is derived from Equation 11;

$$\rho(t) = \rho_0 f_e f_t (t/t_0)^n \qquad (11)$$

where ρ_0 is the resistivity of concrete (Ω-m) at time t_0, n is a factor which takes into account the influence of ageing on ρ_0, f_e is a factor which modifies ρ_0 to take into account the influence of the exposure environment and f_t is a factor which takes into account the influence of the resistivity test method; (Duracrete, 1998)

Although the above factors are suggested, no guidelines are given on how to obtain or predict the values. Therefore, quantification of several factors in the model creates misperception.

A direct relationship between resistivity and I_{corr} was developed using empirical relationships by Morris et al (2004). They proposed that electrical resistivity of concrete is the most effective parameter to estimate the risk of reinforcing steel corrosion and experimented electrochemical analysis for reinforced concrete cylinders in natural and seaside environments. Morris et al (2004)'s relationship is presented in Equation 12.

$$I_{corr} = 55000\rho^{-1.3} \qquad (12)$$

Where I_{corr} is corrosion current density in $\mu A/cm^2$ and ρ is resistivity of concrete in Ωcm.

Guo (2011) modified Alonso et al (1988)'s original model and introduced new constants which are in similar nature for the prediction of the I_{corr}. Guo's proposal of F_{cl} accounts for the increase in the conductivity of the concrete due to the increase in chloride concentration. The relationship was developed based on the results reported by Liu and Weyers (1998) and presented in Equation 13.

$$F_{cl} = \frac{Cl_S + Cl_{th}}{2Cl_{th}} \qquad (13)$$

Where $Cl_{th}$is the chloride threshold level at which the corrosion initiates (kg/m^3) and $Cl_s$is the water soluble (free) chloride concentration at steel level (kg/m^3);

Guo's (2011) contribution was coupled with Morris et al (2004) to generate the combined effect of chloride and resistivity on corrosion current density (I_{corr}). The combined effect is presented in Equation 14.

$$I_{corr} = F_{cl} \times 55000\rho^{-1.3} \qquad (14)$$

Equation format fed into the Vensim model is presented below.

Corrosion Current Density = 55000*((Resistivity in Cement)^-1.3)*Factor for Chloride level at Steel Surface

Figure 4.4 shows the presentation of corrosion current density and its influencers in Vensim environment.

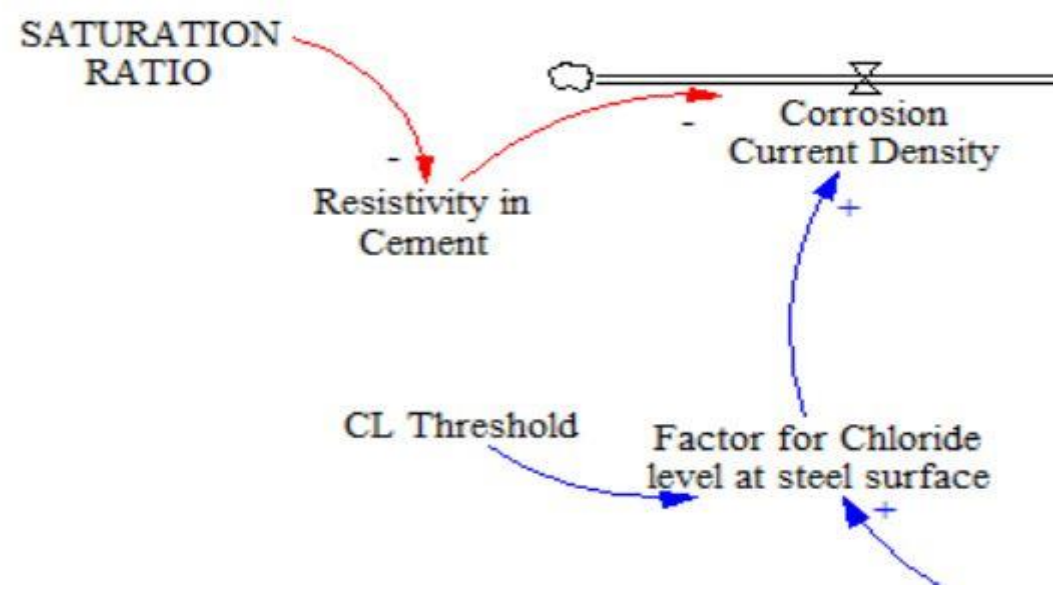

Figure 4.4 - Corrosion Current Density in Vensim Environment

4.2.5 Resistivity of Concrete and Saturation Ratio

The resistivity of concrete varies based on the wet-dry condition of the concrete. Gjorv (1977) reported resistivity values of 7 × 10^3 Ωcm and 6 x 10^6 Ωcm for 100%

and 20% saturated concrete, respectively. An empirical relationship between electrical resistivity and moisture content of concrete was developed by Saleem et al (1996) for chloride contamination and the outputs agree with Gjorv (1977). Therefore, the resistivity of concrete is noticeably dependent on the degree of pore saturation. Different results between resistivity and the pore saturation relationship can be found in literature (Backe et al, 1998, Andrade et al, 2002, Lopez and Gonzalez 1992). A direct relationship between resistivity and the pore saturation in equation format is provided only in the Andrade (2002) experiment. Therefore, the Andrade (2002) equation is used in Vensim model to evaluate the relationship between the resistivity and pore saturation as given in the Equation 15 below.

$$\rho = 932.6e^{-0.0409(SW)} \qquad (15)$$

Where, ρ is the resistivity in kΩ cm and SW is pore saturation with respect to the capillary porosity of the volume

Andrade et al (2002) reported that, below a minimum value of SW, corrosion rate (Icorr) is lower than 0.1 µA/cm^2 which indicates passive corrosion (as discussed in Section 4.2.2). The pore connectivity below the minimum value is negligible and the corrosion process shall not be initiated. On the other hand, 100% saturation of concrete represents the reduction in the transportation of oxygen content in the pore solution – which also reduces corrosion. Naturally, the saturation ratio fluctuates over the time unceasingly and an average value shall be considered for long-term predictions. Considering all above references, pore saturation percentage of 80% is inserted in the model.

Porosity and related pore connectivity also affect the resistivity of concrete. Well-known relationship between the porosity and resistivity is known as the Archie law (Archie, 1942). Archie investigated the relationship between the electrical conductivity and the porosity of rocks saturated with conducting water. The appropriateness of the application of Archie's law to cement slurries is addressed my many reports (Nigmatullin et al., 1992, Tumidajski et al., 1996) and presented in Equation 16.

$$F = \frac{\sigma_f}{\sigma_c} = \frac{a}{\varepsilon^m} \qquad (16)$$

where F - the resistivity formation factor, σ_c - the conductivity of the cement, σ_f - the conductivity of the pore fluid, ε is the porosity of the medium and a and m are constants.

Constant values (a and m) for different cement pastes and concrete are calculated by different authors (Tumidajski et al, 1996, Backe et al, 2001) and were used for calculating the formation factor of concrete material. Tumidajski et al (1996) prepared 12 mix types varying the water / binder ratio and coarse / fine aggregate ratio and hydrated the specimens in sealed rubber membranes containing a small

amount of saturated lime water for periods up to 29 years. Paste conductivity and porosity are measured and plotted into Archie's model to determine the constants. His outcomes fitted the experiments carried out by Christensen et al (1994) and Taffinder and Batchelor (1993). Though they found a varying range for the constants for cement paste, the value of m for cement mortar is proposed to vary in between 2.5 and 3.5. Wong et al (1984) also found similar outcomes under comparable conditions. Therefore, m = 3 is considered for the model.

Since these two relationships propose the influences of pore saturation and porosity effect on resistivity separately, the Vensim model cannot be defined. Therefore, a coupling mathematical formula combining the influences of both parameters is proposed in the model. Based on literature, pore saturation of concrete has the greater effect on resistivity and therefore effect of porosity is added as a multiplication factor. The Andrade (2002) experiment was conducted at initial porosity of 0.3. Hence, resistivity of concrete for the generalized case is presented in Equation 17.

$$\rho = 932.6 \times e^{-0.0409 \times SW} \times \left(\frac{\varepsilon}{0.3}\right)^{-3} \qquad (17)$$

This equation is entered in to the Vensim software as below.

Resistivity in Concrete = 932.6*EXP (-0.0409*SATURATION RATIO)*((Porosity) ^ (-3))/ ((0.3) ^ (-3))

Resistivity of concrete and its contribution to the overall model is graphically shown in Figure 4.5.

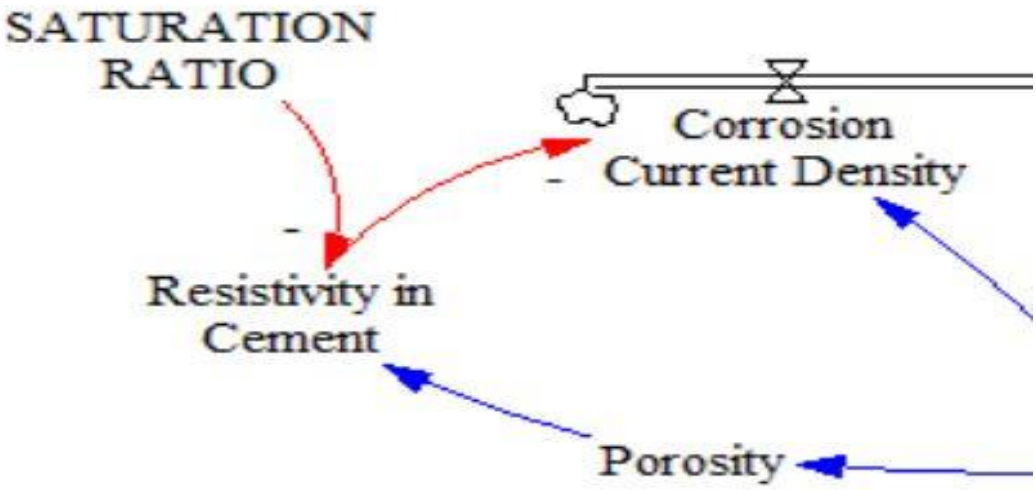

Figure 4.5 - Resistivity of Concrete in Vensim model

4.2.6 Porosity of Concrete

Porosity is the measure of voids in the specimen, given by the fraction of volume of voids by the total bulk volume of the specimen. Porosity is solely a material property. In concrete, it depends on the constituents of the concrete. It is well-known that when the water in the design mix is higher, the concrete porosity is higher because the lesser the cement particles are, the voids in the concrete are larger and it increases the porosity.

The addition of fly ash into the mix will further affect the porosity. Replacing cement with fly ash has multiple effects on porosity. Due to lower density, fly ash occupies a large volume in comparison to the same mass of cement. In the short term, fly ash particles are involved in chemical reactions forming ettringite which will fill more voids in the concrete. In the long-term performance, the C-S-H products of pozzolanic action of fly ash increase the cohesiveness of the concrete particles. Therefore, fly ash replacement reduces the porosity of concrete.

Relationships between water / binder ratio, fly ash replacement and porosity have been empirically proposed (Parrot 1985, Dhir 1989) based on experimental results. Lam et al (2000) developed relationship between gel / paste ratio, fly ash replacement and water / binder ratio using fly ash concrete samples. Lam et al (2000) also incorporated the reactive nature of fly ash by appreciating the efficiency of fly ash which will be discussed in Section 4.2.7) into their model. The relationship is presented in Equation 17.

$$x_{fc} = \frac{2.06 \times v_c \times c + 2.56 \times v_c \times \alpha \times f}{v_c \times c + v_c \times \alpha \times f + w} \quad (17)$$

Where x_{fc} is the gel / paste ratio, c , w are the cement content and water content respectively, α is the efficiency of fly ash and f is the fly ash replacement of cement; v_c is the specific volume of cement (v_c = 1/3.15 = 0.317) and v_f is the specific volume of the fly ash (for general low calcium F class fly ash; v_f = 1/2.31 = 0.433)

Poon et al (2000) produced the correlation between gel / paste ratio and porosity measured in percentage (%) using Mercury Intrusion Method. They observed that the data of gel / paste ratio correlates linearly with the data of porosity. The linear relationship is presented in Equation 18.

$$\varepsilon = (-49.203 \times x_{fc} + 59.515)/100 \quad (18)$$

Where $\boldsymbol{\varepsilon}$ is the porosity and $\boldsymbol{x_{fc}}$ is the gel / paste ratio; This equation is valid for gel / paste ratio greater than 0.4 which fits almost all natural cases

Therefore, the equation for porosity is entered in the Vensim model as given below.

Porosity = (0.59515-0.49203*((0.653*Degree of cement hydration*(1-FLY ASH REPLACEMENT) +1.0825*Efficiency of fly ash)/ (WATER BINDER RATIO+0.317*Degree of cement hydration*(1-FLY ASH REPLACEMENT) +0.433*Efficiency of fly ash)))

4.2.7 Fly Ash Replacement and Fly Ash Efficiency

Fly ash replacement can be categorized as cement replacement and aggregate replacement. Though the physical manufacturing application is the same in both cases, the performance of the concrete significantly varies. When fly ash replaces cement, the early age strength is reduced due to lower activity of fly ash particles but as the time proceeds, the gap is eliminated gradually. When fly ash replaces the aggregate, the strength is reasonably increased from the beginning as the concrete mix should behave as a higher-grade concrete than to the control Ordinary Portland Cement (OPC). To ensure the effects of cement replacement, fly ash replacement is defined as a mutually exclusive user-defined constant from the water / binder ratio user-defined constant (even though the binder in the ratio is the summation of the cement content and fly ash content in concrete mix).

Research efforts over many years towards effective and efficient utilization of fly ash in concrete provide contrasting observations. Though the beneficiaries of fly ash are well established, the quantitative understanding in optimization of fly ash consumption in the mix is inadequate. Vast variations in concrete grade and wide ranges in the amount of constitutions of fly ash mineral halt the generalization of the fly ash contribution of the concrete.

Smith (1967) first proposed 'fly ash cementing efficiency factor' (k) as such that the strength of the strength to water cement ratio relation for normal concretes is also valid for fly ash concretes considering the "effective water cement ratio", as given by $w/(c+kP)$ where w is the water content, c is the cement content and P is the fly ash content. Based on experimental results, he proposed a constant efficiency factor of 0.25 for fly ash replacements up to 25%. Several Standards followingly accepted the mathematical formula but proposed different efficiency factors based on continuous research conclusions. Schiessl and Hardtl (1991) reported that for the concretes with different types of cements and fly ashes (up to 28% replacement and w/c ratio between 0.5 and 0.65) a value of 0.5 is more appropriate for the efficiency factor.

Babu and Rao (1995) concluded that the efficiency factor depends on percentage on fly ash replacement and the age of the structure. They defined 'overall cementing efficiency' which is the arithmetic addition of above two influences (Equation 19). Values for age are defined as distinctive constants up to 90 days. Quantitative representation of fly ash replacement is formulated as in Equation 20 at replacement levels varying between 15 – 75%.

$$Ko = Ke + Kp \tag{19}$$

$$Kp = 2.54\,p^2 - 3.64p + 1.73 \tag{20}$$

Where Ko is the overall efficiency of fly ash, Ke is the efficiency of fly ash due to aging of structure, Kp is the efficiency of fly ash due to fly ash replacement, p is the fly ash replacement.

Due to variations in cement and fly ash properties and curing conditions, the authors proposed permissible provisions and advised to limit the fly ash percentage replacement to a maximum of 50%.

Oner et al (2005) proposed optimization of fly ash using Bolomey and Feret equations. They experimented the changes in strength development for different cement dosage and proposed equivalent cement dosage for fly ash replacement. The study also represented fly ash efficiency as a function of fly ash replacement based on experimental results for 180 days. All their experimental results were fitted into Equation 21 that covers 0% - 50% fly ash replacement.

$$k = 33.522p^2 - 43.987p + 13.971 \tag{21}$$

The equation was independently validated against the experimental results of the previously mentioned authors and it fitted reasonably well. Therefore, Equation 21 is presented to represent the fly ash efficiency in the Vensim model.

4.2.8 Crack Initiating Penetration

Concrete is a heterogeneous material the porosity of which is dependent on the quality of the material. As corrosion products are generated, they attempt to precipitate into the surrounding concrete. While some of the corrosion products may fill the voids or pores of concrete without generating stresses on the surrounding concrete, the rest of the corrosion products may migrate away from the steel - concrete interface. Due to the expansion in volume of corrosion products, bursting tensile forces are generated in the surrounding concrete. Cracks develop once the tensile strain capacity of the concrete is exceeded. Continued corrosion may then lead to further cracking and spalling of the concrete cover.

Studies on the crack width initiation and chloride penetration are carried out [Al-Sulaimani et al (1990), Clark and Saifullah (1993), Andrade et al (1993), Rodriguez et al (1994)] under various conditions. Liu and Weyers [1998] introduced a model to determinate the initiation of cracking in concrete by considering the physical properties. Their model is an adaptation of Bazant's (1997) work for the similar parameters, and it directly governs the time required for corrosion products to fill the porous zone at the steel - concrete interface before applying pressure on surrounding concrete. In their model presented in Equation 22, the time from corrosion initiation to cover cracking, t_{crack}, is given as a function of the critical amount of rust product needed to induce cracking of the concrete cover (W_{crit}) and the corrosion rate, K_p:

$$t_{crack} = \frac{W_{crit}^2}{2K_p} \qquad (22)$$

This is a fundamental relationship in which W_{crit} is accumulated over the time in the concrete. To find the attach penetration that induces crack initiation, several other researches were studied.

In a review of models for predicting the attack penetration for onset of cracking of cover concrete under DuraCrete [1998], a relationship was proposed that relates the amount of corrosion (attack penetration of the reinforcing bar to cause cracking) to the cover/bar diameter ratio and the splitting tensile strength as presented in Equation 23.

$$x_{crack} = 83.8 + 7.4\,\frac{c}{\Phi} - 22.6\,fc,sp \qquad (23)$$

Where: x_{crack} is the attack penetration of steel (μm) to cause cracking, c/Φ = cover/bar diameter ratio and fc,sp is characteristic value of the splitting tensile strength of the concrete [MPa]. Since there was no guideline given in the DuraCrete model for splitting tensile strength values, x_{crack} will become a negative value for some tensile strength values in the model. Negative crack widths are not applied to real world problems and therefore this relationship is needed to be limited.

Alonso et al (1998) predicted the attack penetration required for corrosion cracking initiation to be independent of tensile capacity of concrete to evade the negative values for attack penetration. The empirical relationship is presented in Equation 24.

$$x_{crack} = 7.53 + 9.32 \frac{c}{\Phi} \qquad (24)$$

where, x_{crack} is the attack penetration needed to initiate cracking (μm). Cover depth is represented by c (mm) and Φ (mm) is the initial diameter of ordinary reinforcement bar.

Andrade (1993) has proposed similar empirical equation (Equation 25) for the estimate of the radius reduction causing initial cracking.

$$x_{crack} = 74.5 + 7.3 \frac{c}{\Phi} - 17.4\, ftd \qquad (25)$$

where $ftd\ (MPa)$ is the concrete characteristic tensile strength (obtained from the Brazilian test), which has values between 3 MPa and 4 MPa which shall be in accordance with the standard classes of each proposed concrete composition. Cover depth is represented by c (mm) and Φ (mm) is the initial diameter of ordinary reinforcement bar. Within the boundary values given in the equation, x_{crack} will not become a negative value.

From the Equations 23, 24 and 25, it can be noted that, though higher cover to reinforcement delays the corrosion initiation, the curves have no significant variations in the gradient for various cover to reinforcement ratios.

As the attack penetration is already defined in the model, the crack initiation period should be accommodated to the model using an empirical equation that proposes the attack penetration required to initiate cracking. Therefore, out of above equations, relationship proposed by Andrade (1993) was used in this model (Equation 25).

Instead of introducing a range for splitting tensile strength of concrete which limits the functionality of the model, Vensim facilitates 'IF THEN ELSE' function where any negative output will be considered as zero. Accordingly, the equation used in the Vensim model as given in the expression below. This representation of crack initiating penetration in Venism model is shown in Figure 4.6.

Crack Initiating Penetration = IF THEN ELSE ((74.5+7.3*(COVER/BAR DIAMETER)-17.4*Characteristic Value of the Splitting Tensile Strength of Concrete) <0, 0, (74.5+7.3*(COVER/BAR DIAMETER)-17.4*Characteristic Value of the Splitting Tensile Strength of Concrete))

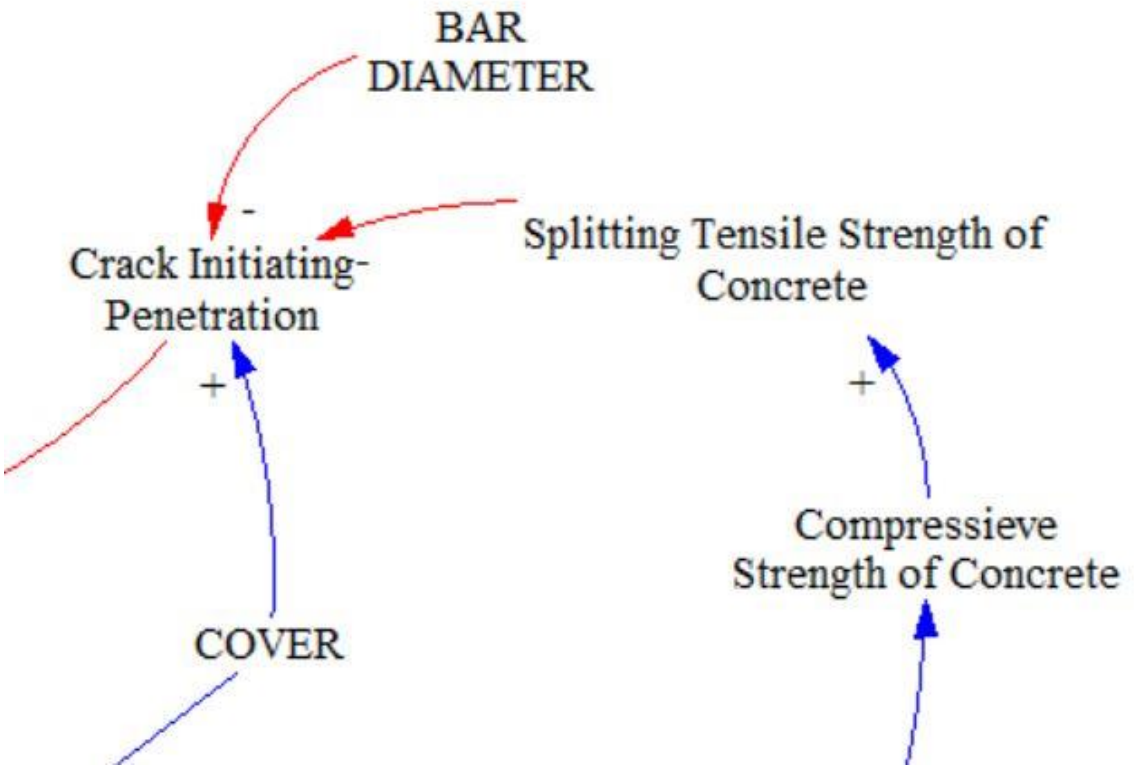

Figure 4.6 Crack Initiating Penetration Vensim Model

4.2.9 Splitting Tensile Strength of Concrete

Splitting tensile strength of concrete is the capacity up to which the tensile stresses are restrained in concrete. It is a well-known fact that concrete is vulnerable to tension forces. Under normal conditions, the value of splitting tensile strength of concrete does not exceed 5 MPa. During the routine design phase, splitting tensile strength of concrete is assumed to be non-existent. The main interest of researches and designers are the compressive strength of concrete.

The empirical relationship between the compressive strength and tensile strength of concrete is proposed by many researches (Sideris and Konsta-Gdoutos, 1996, Zain et al, 2002, Felekog lu et al. 2007). Felekog˘lu et al. (2007) proposed a simpler correlation between the strengths as presented in Equation 26.

$$f_t = 0.43 \times \rho_c^{0.6} \qquad (26)$$

Where, f_t is the tensile strength and ρ_c is the compressive strength of concrete.

The equation entered in the Vensim model is as follows.

Splitting Tensile Strength of Concrete = 0.43*Compressive Strength of Concrete^0.6

Compressive strength of concrete is not an input parameter in the model. It is widely agreed that the compressive strength depends on water / binder ratio and the replacement of cement. Water / binder ratio has an inversely proportionate relationship with compressive strength. Lesser water used in the mix increases the connectivity of concrete and hence higher strength is achieved. However, water content is essential for the hydration reactions of cement hardening. Therefore, a minimum limit of water / binder is defined, above which the compressive strength reduces with the increase in water.

Assuming a cement class and aggregate type, BRE/DOE mix design charts are used to propose compressive strength as a function of water / binder ratio. Felekoglu et al. (2007) validated experimental compressive strengths against the BRE designs and proposed distinct values.

However, in the model, porosity is defined as a function of water / binder ratio and fly ash replacement. It is evident that the pore structure of concrete determines the hydrated content and the strength development in concrete. Therefore, instead of separately proposing a correlation for compressive strength from water / binder ratio, correlation between porosity and the compressive strength is preferred in the model.

Lam et al (2000) proposed an empirical equation for fly ash concrete for low water content mixes that fits their experimental results. Their proposed model is presented in Equation 27.

$$f_c = 315.7 \times e^{-0.0707 \times \varepsilon} \qquad (27)$$

Where $f_c$is the compressive strength of concrete and ε is the Mercury Intrusion porosity measured;

Chindaprasirt and Rukzon (2008) proposed a simpler model for the similar purpose for fly ash concrete. Unlike Lam et al (2000), this experimental research was carried out for water / binder ratio varying between 0.4 and 0.6 which is common in design practices. They developed the relationship by curve fitting the three-month experimental results. Their proposed correlation is presented in Equation 28. However, we have modelled water / binder ratio to be varied from 0.3 to 0.8.

$$f_c = 1147.04 \times \varepsilon^{-1.15} \qquad (28)$$

This equation is entered in the Vensim model as given below.

Compressive Strength of Concrete = 1147.04*(Porosity*100)^-1.15

The Vensim environment of the section is shown in Figure 4.7.

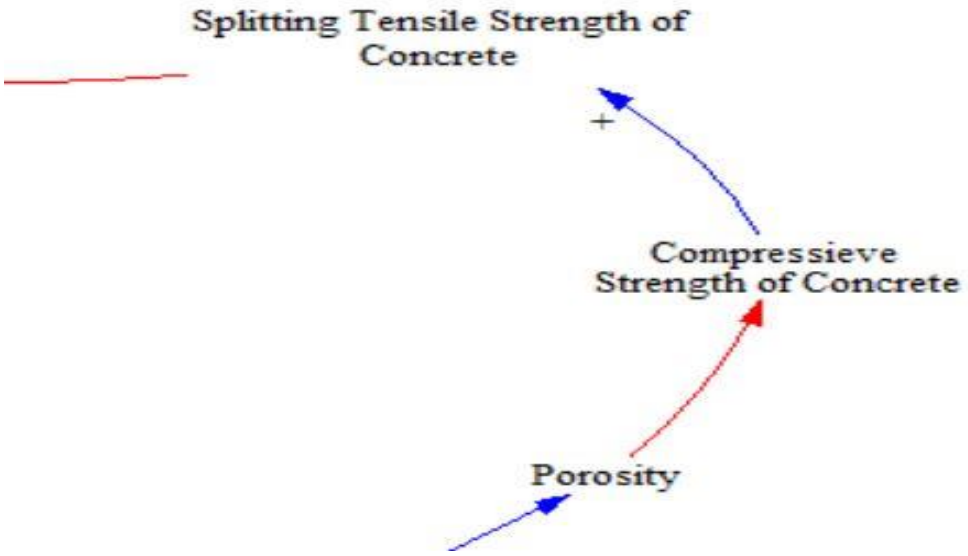

Figure 4.7 Splitting Tensile Strength in Vensim Environement

4.2.10 Crack Width

Crack width is the physical presentation of crack propagation. The propagation is mainly influenced by the diffusion of chloride ions and its availability in the environment to facilitate the ion exchange reactions. The crack initiates when the attack penetration due to corrosion exceeds the attack penetration required to initiate the crack. Therefore, crack width can be directly attributable to the loss of reinforcement in the concrete.

Under favourable circumstances, smaller cracks can exhibit autogenous healing. Due to inter molecular forces, the smaller cracks are automatically rectified in concrete. The critical parameters for crack healing are exposure conditions, access to moisture, and crack size.

An empirical expression between the characteristic crack width and the corrosion propagation was proposed by Rodriguez et al [1996]. The expression is presented in Equation 29.

$$w = 0.05 + \beta(x - x_{crack}); \qquad (29)$$

where: w is characteristic crack width in mm, x is crack penetration (reduction in the bar radius) in μm, x_{crack} is attack penetration leading to cracking initiation in μm, β = coefficient which depends on the arrangement of the bars in concrete surface to its direction to applied load (β = 0.01 for top cast bars and 0.0125 for bottom cast bars); 0.05 is a constant provided for the initial cracks in concrete.

IF THEN ELSE function in Vensim environment is used to avoid any negative values of crack width during the early periods where the attack penetration does not exceed the initiating penetration. The equation used in the model is given below.

Crack Width = IF THEN ELSE ((0.05+(COEFFICIENT FOR ARRANGEMENT*(Attack Penetration - Crack Initiating Penetration))) < 0.05, 0.05, (0.05 + (COEFFICIENT FOR ARRANGEMENT*(Attack Penetration-Crack Initiating Penetration))))

The model graphical representation is as the Figure 4.8 below.

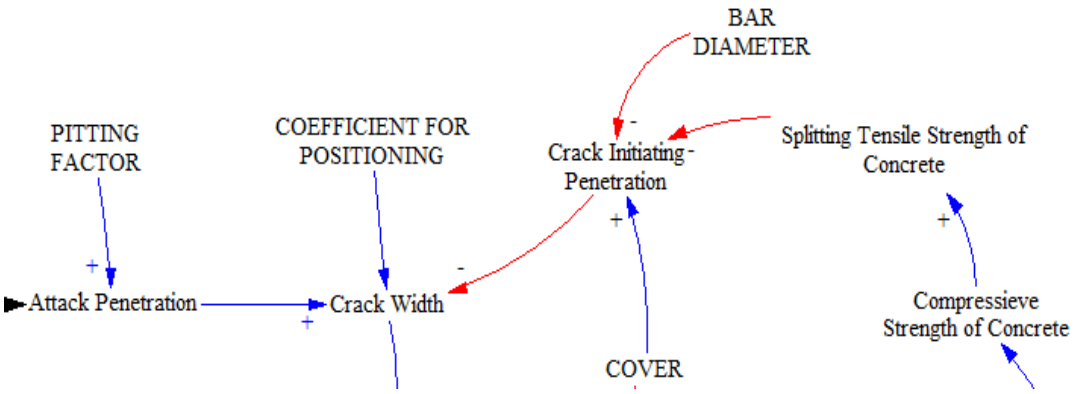

Figure 4.8 Crack Width in Vensim Environment

4.2.11 Diffusion Coefficient and Crack Propagation

The diffusivity of chloride ions into the concrete is influenced by the propagation of the cracks in the concrete surfaces. Effects of crack propagation on the chloride diffusion converts the entire process into a reinforcing loop; therefore Vensim model is developed to depict and account for the effect of this reinforcing loop on corrosion.

The entire chloride diffusion flux can be divided into two; flux in uncracked concrete and flux in cracked concrete. Chloride diffusion in cracked concrete is much larger than the diffusion in uncracked concrete.

Initial cracks due to plastic shrinkage are assumed to have not contributed to the initial diffusivity of chlorides due to their significantly smaller sizes. Research outcomes (Takewaka et al 2003, Djebri 2008) reported that crack widths up to 0.03 mm (w_1) have no influence on the diffusion coefficient because of the self-healing characteristic of concrete. Therefore, the crack's effect on chloride diffusion is ignored when the crack width is lesser than its lower limit (w_1). This is presented in Figure 4.9 (a). Only the effects of cracks caused by the expansion of corrosion reaction products are represented in the model.

The crack propagates between w_1 and w_2 (upper limit) when the subsequent products of hydration cannot block the crack completely. Primarily, the crack propagates

perpendicular to the concrete surface, with unidirectional diffusion. The diffusion rate is comparatively slower and unsteady. This is presented in Figure 4.9 (b).

Crack width also has an upper limit above which the products of subsequent hydration cannot block the crack, and the diffusion through the crack walls can be represented by the diffusion of sound concrete (discussed in Section 4.2.12). At this stage, chloride ions will rapidly diffuse into crack and reach stability. Then, the chloride ions inside the crack further penetrates concrete matrix through the surfaces opened by the propagation of the cracks. This causes a three-dimensional diffusion inside the existing crack which further reinforces the crack propagation. In this case, it is assumed that the chloride ion concentration inside the crack is equal to the atmospheric chloride ion concentration and the medium is in equilibrium. This diffusion mechanism is presented in Figure 4.9 (c).

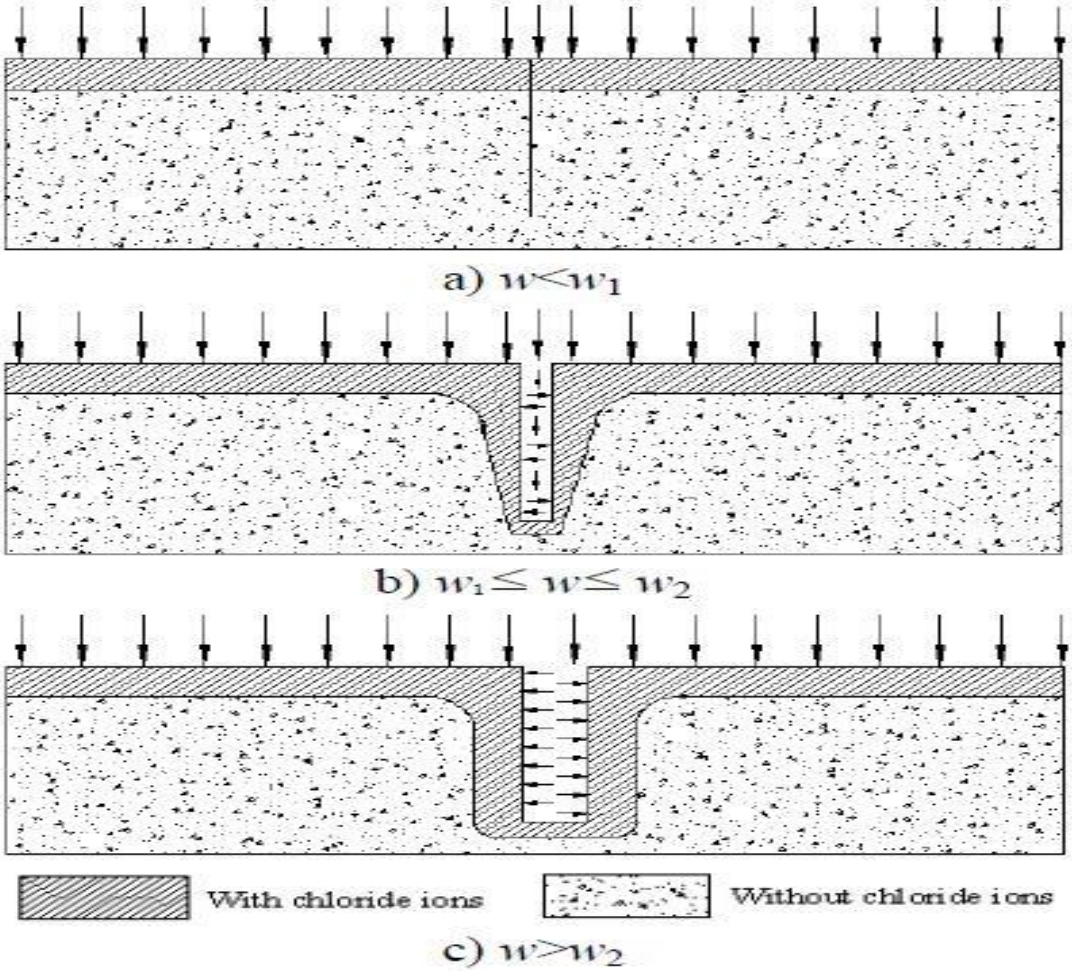

Figure 4.9 Chloride diffusion through crack widths (Jin et al, 2010)

The values of upper limit and lower limit of crack widths were proposed by many researchers based on their experiments on chloride ion diffusion through different mediums. These values are listed in Table 4.2.

Table 4.2 Upper and Lower limit of Crack Width Influencing Chloride Diffusion

Authors	Lower Limit (micro m)	Upper Limit (micro m)	Medium
Takewaka et al (2003)	50	100	Concrete
Ismail et al (2004)	30	99	Brick
Francois et al (2005)	30	Undefined	Concrete
Kato and Uomoto (2005)	Undefined	75	Concrete
Djerbi et al (2008)	30	80	Concrete
Ismail et al (2008)	30	125	Mortar

In the Djebri model (2008), diffusion coefficient increases linearly with the increase in crack width between 30 to 80 micro m and arrives at a constant when the crack width is greater than 80 micro m. Figure 4.10 shows the relationship between the crack width and the diffusion coefficient of chloride ions through the crack proposed by Djerbi (2008).

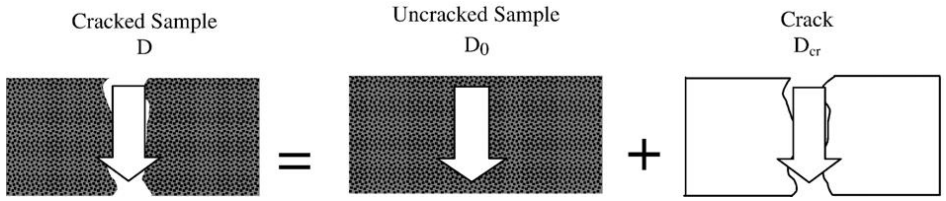

Figure 4.10- Partition hypothesis of chloride diffusion through cracked discs- A. Djebri et al. 2008

$$D_{cr}\left(\frac{m^2}{s}\right) = 2 \times 10^{-11} w - 4 \times 10^{-10} \qquad 30\mu m \leq w \leq 80\mu m \qquad (30)$$

$$D_{cr}\left(\frac{m^2}{s}\right) \approx 14 \times 10^{-10} \qquad w \geq 80\mu m \qquad (31)$$

According to the Djebri (2008), the diffusion coefficient is a constant above the crack with of 0.08 mm as presented in Equation 31. However, the argument was challenged by many researchers (Park et al.2012, Park et al.2009, Jang et al.2011, Lu et al 2014) who proposed diffusion coefficients for the effective diffusivity of cracked concrete above the crack width of 0.08 mm.

Park et al. (2012) equation is given below

$$D_{cl}(w) = (4189.27w^3 - 1642.57w^2 + 3478w + 1).D \qquad (32)$$

Park et al. (2009) equation is given below

$$D_{cl}(w) = (31.61w^2 + 4.73w + 1).D \qquad w > 0.1mm \qquad (33)$$

Where D is diffusion before crack, $D_{cl}(w)$ diffusion value of cracked concrete at crack width and w is the crack width.

Lu et al (2014) proposed a new relationship by incorporating the counter arguments (S.-S. Park et al.2012, S.-S. Park et al.2008) into the Djebri model (2008). The relationship is presented in Equation 34.

$$f(w) = 31.08w^2 + 71.54w + 1 \qquad w < 0.35mm \qquad (34)$$

where; $f(w) = \frac{D_{eq}}{D}$ with D is apparent diffusion coefficient (sound concrete) and D_{eq} is the effective diffusive coefficient at a crack width of w;

Compared with the regression formulas given in the published reports, this equation results are greater than the values calculated from Equation 32 (Park et al., 2012) and less than the values calculated from Equation 33 (Park et al., 2009) and appropriate with the test results in (Djerbi et al., 2008). The equation also agrees with the proposals of Park et al (2012) and Park et al (2008) that the upper limit of the crack widths is significantly greater than 80 micro m. Lu et al (2014) proposed the upper limit of 0.35 mm.

Therefore, Equation 34 is used in Vensim model. The model also assumes that crack width propagation is uniform in its entire crack length. The equation fed into the model is presented below.

IF THEN ELSE (Crack Width<0.35, (31.08*(Crack Width^2) + 71.54*(Crack Width) + 1) *Diffusion Coefficient of Sound Concrete, (31.08*(0.35^2) +71.54*(0.35) +1) * Diffusion Coefficient of Sound Concrete)

4.2.12 Diffusion Coefficient of Sound Concrete

The apparent diffusion of chloride ions into concrete is depended on the mix composition of the concrete, cementitious additives added to the mix, compaction technique, exposure conditions and time. According to Equation 34 (discussed in Section 4.2.11), diffusion coefficient of cracked concrete depends on apparent diffusion coefficient (sound concrete) of concrete.

Liu and Weyers (1998) presented apparent diffusion coefficient values calculated from chloride profiles for bridges in different locations of United States of America. These values were found to range from 1.0 x 10^{-12} m^2/s to 6.7 x 10^{-12} m^2/s, influenced by the geography of the bridges. However, these values represent "lifetime average" diffusion coefficients (i.e., the time dependent effects have been averaged out over the period of lifetime from the first salt exposure to the time of sampling) and relate to structures exposed to lower average temperatures.

Papadakis et al (1996) presented a model to calculate the apparent diffusion coefficient. The relationship is presented in Equation 35.

$$D = D_{H2O} \times 0.15 \times \frac{1 + \rho_c \frac{c}{w}}{1 + \rho_c \frac{c}{w} + \frac{\rho_c}{\rho_a}\frac{a}{c}} \times \left(\frac{\rho_c \frac{c}{w} - 0.85}{1 + \rho_c \frac{c}{w}} \right)^3 (cm^2/s) \qquad (35)$$

where a/c is the aggregate-to-cement ratio, ρ_c and ρ_a are the mass densities of cement and aggregates respectively and D_{H2O} is the chloride diffusion coefficient in an infinite solution (=1.6× 10^{-5}cm^2/s for NaCl).

However, the relationship proposed by Papadakis et al (1996) is not adopted into Vensim model due to its complicated nature with many input parameters.

Stewart (1998) suggested a model for diffusivity using 16 different experimental data for OPC concrete. That relationship is presented in Equation 36.

$$D = 10^{(-10+4.66(w/c))} \qquad (36)$$

Where D is the apparent diffusion coefficient and w/c is the water cement ratio of OPC concrete;

It is noted that apparent chloride diffusion coefficient tends to decrease with time. Bamforth and Price (1997) proposed that the reduction in apparent diffusion coefficient is most rapid during the first 5 years of exposure and after that approaches a constant value. However, the function of time is not considered in the proposed equations by Papadakis et al (1996) and Steward (1998).

Life 365 service life prediction model proposed apparent chloride diffusion coefficient as a function of time, water / binder ratio of the mix and the cementitious additives. Equation 37 is used in Life 365 model to account for the influence of time-dependent variations in the apparent diffusion coefficient.

$$D(t) = D_{ref} \times (\frac{t_{ref}}{t})^m \qquad (37)$$

Where $D(t)$ is the diffusion coefficient at time t; D_{ref} is the diffusion coefficient at time t_{ref}, m is the diffusion decay index which is a constant;

In Life 365 model, reference period of 28 days is assumed to incorporate the experimental data into the model. The relationship between diffusion coefficient at 28 days (D_{28}) and water / binder ratio (w/b) was developed for the model using unpublished data from tests at the University of Toronto and published data for the same. The relationship is presented in the Equation 38.

$$D_{28} = 10^{(-12.06+2.4(w/c))} \qquad (38)$$

Effects of fly ash and slag are captured in the model by incorporating the decaying constant m. Neither fly ash nor slag are assumed to affect the early age diffusion

coefficient. However, the rate of reaction in chloride diffusivity will be impacted in the long-term. Life 365 defines m as a function of fly ash replacement and slag content as below in Equation 39.

$$m = 0.2 + 0.4 \times \left(\%\frac{Fly\ Ash}{50} + \%\frac{Slag}{70}\right) \qquad (39)$$

The relationship is only valid up to replacement levels of 50 percent fly ash or 70 percent slag and m itself cannot exceed 0.6. In the Vensim model, only the effects of fly ash admixture is considered. Therefore, slag percentage is assumed as 0.

Therefore, the combination of Equations 37, 38 and 39 are fed into the model. The equation for diffusivity of sound concrete is presented below.

Diffusivity of Sound Concrete = 10^(-12.06+2.4*WATER BINDER RATIO)*(28/(Time*365+1))^(0.2+0.4*FLY ASH REPLACEMENT/0.5)

Figure 4.11 shows the causal loop diagram established in the Vensim environment to incorporate the effects of diffusion coefficient of sound concrete and the effects of diffusion coefficient due to crack width variations.

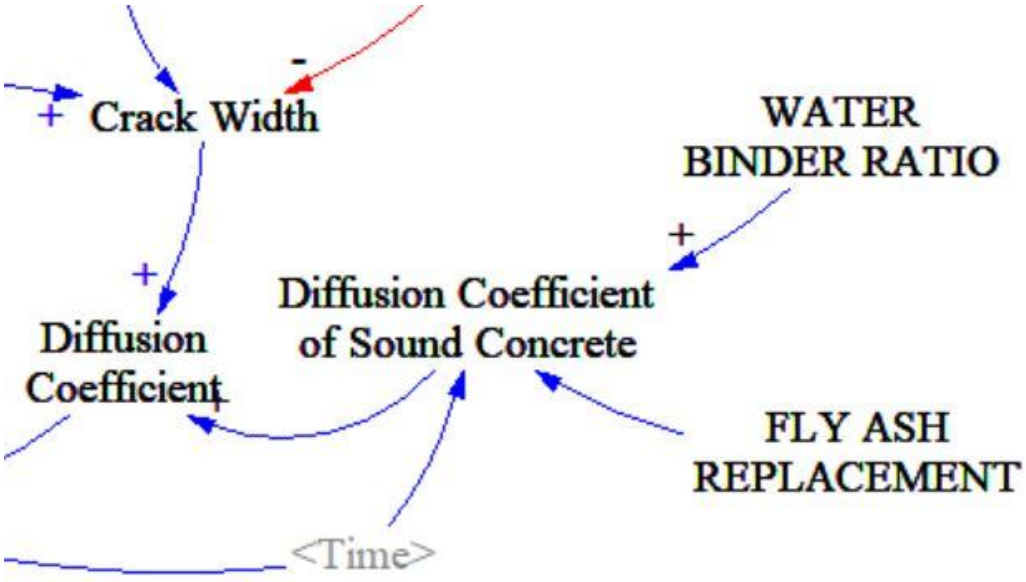

Figure 4.11 Diffusion Coefficient Presentation in Vensim Model

4.2.13 Chloride Amount at Steel Surface

The supply and transport of chlorides in concrete is mainly a function of the environmental conditions and the concrete material properties. The main influencer of chloride supply is the chloride concentration and the duration of which the

chloride substances are in contact with the concrete surface. In the concrete structures located closer to marine environment, available chloride concentration is usually higher; for salt water is frequently supplied to the concrete surface and the surface intermittently dries out.

Chloride amount at the steel level is mainly influenced by the diffusivity of chloride, chloride concentration on the surface, time, and the cover depth (Thomas, 1996). Time and cover depth are used defined variables in the Vensim model. Diffusion coefficient of cracked concrete id discussed in Section 4.2.11. Therefore, to calculate the chloride level at steel surface, chloride concentration on the concrete surface need to input to the model as another variable.

Chloride level on the concrete surface is not a constant. Chloride ions are accumulated in the surface during the service period of the structure and the chloride level builds up with time. The importance of continuous supply of chloride ions for reinforcement corrosion in concrete has led to the concept of the chloride threshold level or critical chloride concentration, which may be defined as the minimum chloride level at the depth of the reinforcement which could trigger the corrosion.

In the Vensim model, it is assumed that surface chloride level increases linearly up to a maximum chloride concentration at the given time and then becomes a constant (Life 365). User defined maximum chloride concentration and the time taken to reach the maximum concentration values are fed into the model. The maximum concentration of chloride is dependent of the exposure conditions and the geographical location. Life 365 proposes the build-up rate and the maximum concentration for four regions as presented in Table 4.3.

Table 4.3 Build-up Rates and Maximum Surface Concentration of Chloride Ions (Life 365)

Region	Build-up Rate (%/year)	Maximum (%)
Marine Splash Zone	Instantaneous	0.8
Marine Spray Zone	0.1	1.0
Within 800 m of the ocean	0.04	0.6
Within 1.5 km of the ocean	0.02	0.6

For the model, Marine Spray Zone is considered to be appropriate. The chloride surface build-up for the marine spray zone is presented in Figure 4.12.

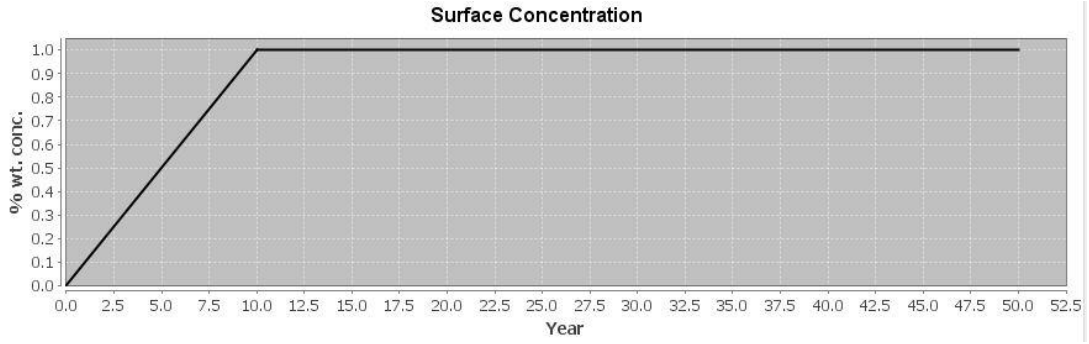

Figure 4.12 Surface Chloride Build-up for Marine Spray Zone (Life 365)

The main transportation mechanisms of chloride ions are capillary suction, diffusion, and migration. Capillary suction occurs due to the surface tension of the capillary pores under submerged conditions where concrete surface quickly dries off. This mechanism is predominant in the tidal and splash zone as well as in concrete road applications where de-icing salts are used (Bertolini et al. 2013).

Diffusion is the main transportation mechanisms of airborne deposits when concrete is not submerged. Diffusion occurs due to concentration gradients. For non-steady-state conditions, such as in the case of concrete, where the concentration gradient changes with time, the flux can be described according to Fick's second law of diffusion. The driving force for diffusion of airbone deposits, such as oxygen or chloride ions, is the presence of concentration gradients. The Fick's law is presented in Equation 40.

$$\frac{\partial C}{\partial t} = D\frac{\partial^2 C}{\partial x^2} \qquad (40)$$

Where, c is the chloride concentration at the surface, t is the time, D is the diffusion coefficient and x is the depth.

The ingress of chloride in concrete is not a pure diffusion process as discussed above. However, as the model is developed for structures which are not submerged in the chloride ion supply medium, the predominant effect of diffusion is adopted to the model.

For chloride ingress modelling, the error-function solution is applied to resolve the differential equation (Equation 40). In its simplest form, this function is given in Equation 41.

$$C(x,t) = C_s\left(1 - erf\left(\frac{x}{2\sqrt{D_{eff} \times t}}\right)\right) \qquad (41)$$

Where $C(x,t)$ is the chloride content at depth x and time t, erf is the Gauss error function, D_{eff} is the effective chloride diffusion coefficient, m^2/s C_s is the surface or near surface chloride content, x is the depth from the surface, m t is the time. When x

approaches the cover to reinforcement in concrete, the chloride content at steel level is determined by solving the above.

When solving Equation 41, Guass error function ($\mathrm{erf}(x)$) is applied to the Vensim software as a tabular input. The function is a special function of sigmoid shape and used for integrating the normal distribution. The function is presented in its integration form as in Equation 42.

$$\mathrm{erf}\,(z) \equiv \frac{2}{\sqrt{\pi}} \int_0^z e^{-t^2}\, dt. \qquad (42)$$

Gauss error function (erf(z)) can also be defined as a Maclaurin series as shown in Equation 43.

$$\begin{aligned} \mathrm{erf}\,(z) &= \frac{2}{\sqrt{\pi}} \sum_{n=0}^{\infty} \frac{(-1)^n z^{2n+1}}{n!\,(2n+1)} \\ &= \frac{2}{\sqrt{\pi}} \left(z - \tfrac{1}{3} z^3 + \tfrac{1}{10} z^5 - \tfrac{1}{42} z^7 + \tfrac{1}{216} z^9 + \ldots\right) \end{aligned} \qquad (43)$$

Entire chloride diffusion equation cannot be entered to the Vensim software due to software limitations. To lessen the complexity of the differential equations in the model, tabular format of the error function (lookup function in Vensim software) is used. Here, the error function is modelled as another series that feeds to the main variable in the causal loop of the model.

User-defined Lookup function can specify an arbitrary nonlinear relationship in Vensim. Put simply, a Lookup is a list of numbers representing an x axis and a y axis. The inputs to the Lookup are positioned relative to the x axis, and the output is read from the y axis (Vensim manual). Due to the complexity of the error function, it is incorporated as a Lookup function. Values related to the error function is entered to the software using Table 4.4 and the Vensim software coverts that into the exact error function as given in the Figure 4.13.

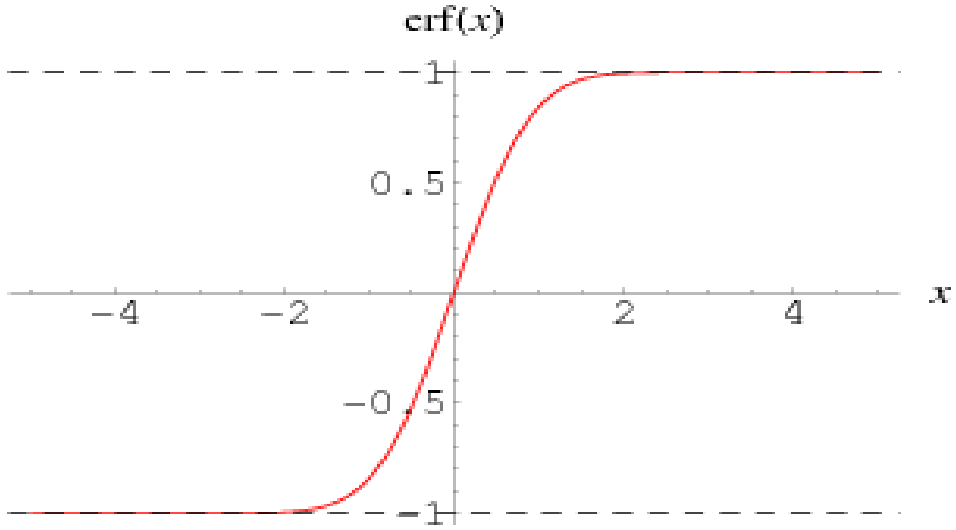

Figure 4.13 Gauss Error Function

The inputs in axis-x is given as z and the outputs of error function in axis-y is presented as erf(z) in Table 4.4.

Table 4.4 Gauss Error Function

z	*erf (z)*	*z*	*erf (z)*	*z*	*erf (z)*
0	0	0.55	0.5633	1.3	0.9340
0.025	0.0282	0.60	0.6039	1.4	0.9523
0.05	0.0564	0.65	0.6420	1.5	0.9661
0.10	0.1125	0.70	0.6778	1.6	0.9763
0.15	0.1680	0.75	0.7112	1.7	0.9838
0.20	0.2227	0.80	0.7421	1.8	0.9891
0.25	0.2763	0.85	0.7707	1.9	0.9928
0.30	0.3286	0.90	0.7970	2.0	0.9953
0.35	0.3794	0.95	0.8209	2.2	0.9981
0.40	0.4284	1.0	0.8427	2.4	0.9993
0.45	0.4755	1.1	0.8802	2.6	0.9998
0.50	0.5205	1.2	0.9103	2.8	0.9999

Equation for the chloride amount at steel level, incorporating all the necessary equations discussed in the chapter, is fed into Vensim software as given below.

Chloride Amount at Steel Level = Surface Chloride Buildup*(1-(Table Effect EF((COVER)/(1000*(2*SQRT(Diffusion Coefficient*(Time+0.001)*365*24*60*60))))))

Furthermore, time is a dividend in the equation and analysis starts at t =0 which causes a mathematical error state. Therefore, an initial value of t+0.001 years is used.

Figure 4.14 shows the Vensim environment presentation of the chloride amount at steel level and the factors influencing the causal loop.

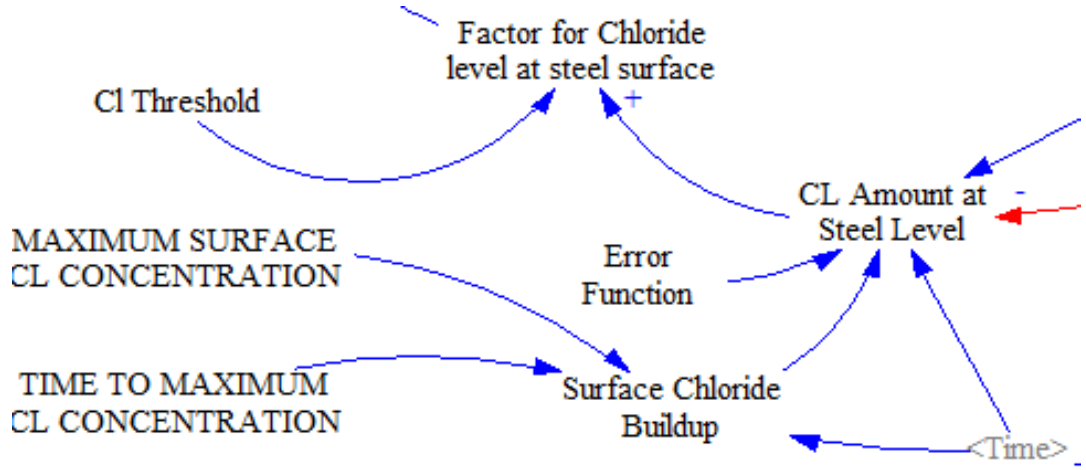

Figure 4.14 Chloride Amount at Steel Level Presentation in Vensim Model

Taking all these chapters into consideration, the complete system dynamics model of Chloride Ingress in Concrete is developed as a reinforcing loop in Vensim software. The model analyses the influences in the diffusion of concrete due to the propagation of crack width by means of past behaviours. The complete chloride ingress model is presented in Figure 4.15.

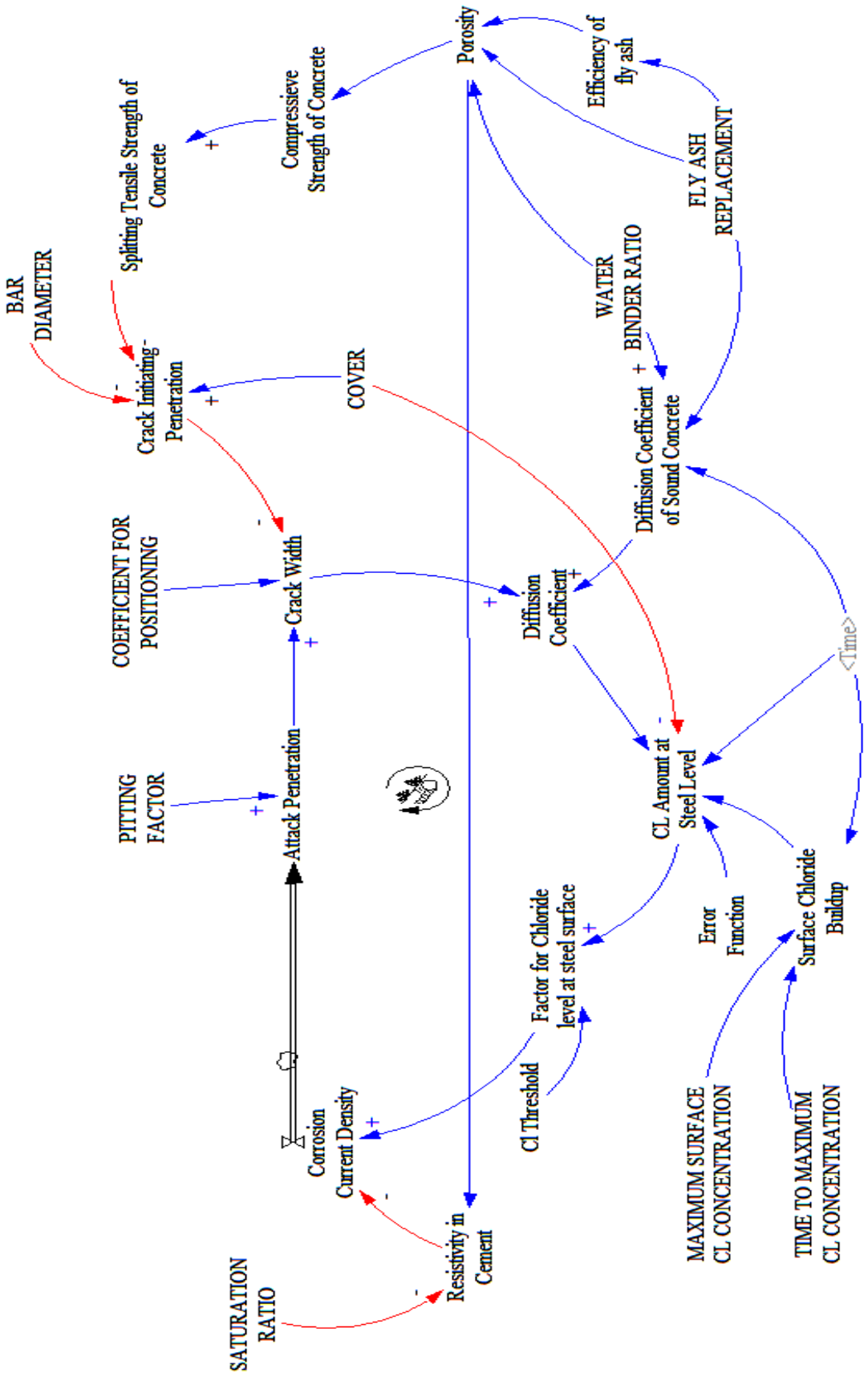

Figure 4.15 Chloride Ingress in Concrete Reinforcing Loop in Vensim Model

4.3 Validation of Chloride Ingress Cracking Model

The state-of-the-art model for chloride ingress in concrete provides an overview of the factors affecting the phenomenon and the magnitude of its effects in the corrosion process and the subsequent formation of cracks. The model predicts the initiation time for the cracks and the propagation of cracks throughout its lifespan.

Determination of the cracking characteristics is difficult. As exposure condition changes over the years and the concrete diffusion mechanism is not constant over the years, the model outputs for long-term analysis should be validated against the existing experimental analysis. However, most of the available literature discusses the effects of chloride ingress in concrete for short term analysis. In addition, the approaches adopted by different researches and models considerably vary in results and conclusions.

To overcome this discrepancy, model results can be validated against the chloride ingress analysis of existing concrete structures. Though the effects of exposure conditions can be modelled, the concrete mix design properties and the cement minerals used are often unavailable. Therefore, establishing a comprehensive stage to validate the model output characteristics spanning over 50 years under natural conditions is extremely difficult.

Considering the difficulties, following model outcomes (Section 4.3.1) and research outcomes (Section 4.3.2 and 4.3.3) were considered for validation of Vensim chloride ingress model.

1. Life 365 Model Outputs for Initiation Time
2. Vidal et al (2004) for Crack Width
3. Zhang et al (2010) for Crack Propagation

4.3.1 Life 365 Model for Initiation Time

Life 365 is a freely available computer program for predicting service life of reinforced concrete exposed to chlorides. The program (v1.0) and the manual were primarily written by E.C. Bentz and M.D.A. Thomas and later, M.A. Ehlen adopted the influences of additives into the program (v2.2).

Life 365 predicts the corrosion initiation period assuming diffusion to be the dominant mechanism of chloride supply. Corrosion initiation period in Life 365 model is defined as the time it takes for sufficient chlorides to penetrate concrete cover and accumulate in sufficient quantity at the depth of the embedded steel to initiate corrosion in the steel. Specifically, it represents the time taken for the critical threshold concentration of chlorides to reach the depth of the cover (Life 365 User Manual).

In Vensim model, corrosion initiation time is measured as the time taken for chloride amount at steel level to exceed the critical threshold concentration of chlorides. According to the model, this value is not a user defined variable but a dependent on the surface chloride build up and the diffusion mechanism. The surface chloride builds up represents the environmental conditions (as discussed in Section 4.2.13).

Corrosion initiation time for different fly ash replacement amounts and different water binder ratios is analysed for validation purposes. The results are provided in following Table 4.5.

Table 4.5 Validation of Chloride Ingress Model vs Life 365

Fly Ash Replacement	w/b ratio	Initiation Time (Years)		
		Vensim	Life 365	Difference
0	0.3	18.5	19.2	-3.78%
0	0.4	16.25	15.8	2.77%
0	0.5	14.25	13.5	5.26%
0	0.6	13	11.8	9.23%
0	0.7	11	-	
0	0.8	10.5	-	
0.1	0.5	15	15.1	-0.67%
0.2	0.5	16.75	17.2	-2.69%
0.3	0.5	20	20.2	-1.00%
0.4	0.5	24	24.3	-1.25%
0.5	0.5	28.5	30.4	-6.67%

The crack initiation values are higher in Vensim than in Life 365 when the water in the mix is increased. With the increment in fly ash replacement, Life 365 shows a slightly higher time-period for the corrosion to initiate. However, the difference between Vensim and Life 365 values are very small and less than 5% in majority of the cases as seen in Table 4.5. For water binder ratio of 0.6, the inconsistency between the two models is around 9% but it should be noted that Life 365 does not entertain water / binder ratios greater than 0.6 in their program.

It is a fact that some of the data used by Life 365 is also considered in the generation of the Vensim model. The basic theoretical approach of chloride diffusion and fly ash contribution is similar in both models. However, it can be argued that Vensim model is superior as it comprises of more in-depth research data and incorporates additional influencers such as saturation of pore water, resistivity to ion exchange and localized corrosion into the feedback loop. Life365 model would be programmed for the average constant values of such parameters. Therefore, the results of the Vensim model can be validated with a simpler program (Life 365) output which has a similar approach in some respects.

4.3.2 Vidal et al (2004) for Crack Width

Since 1984, Laboratoire Mate´riaux et Durabilite´ des Constructions (LMDC) in Toulouse has been conducting a major research project on development of reinforcement corrosion in aggressive environments. Initially, 36 reinforced concrete beams were cast and stored under loading in a chloride environment. Beams were extracted at different stages and experimental tests are carried out at different stages and time periods. Vidal et al (2004) presented the results of a study obtained from two beams naturally corroded in a saline environment and subjected to wetting – drying cycles over the periods of 14 years and 17 years. Compared to accelerated tests that produce poor substitute for real corrosion, this study gives much closer representation of the natural conditions with respect to corrosion distribution, crack propagation and corrosion types.

Two types of reinforced concrete beams were tested; Beam A and Beam B. According to French standards at the time of manufacturing (1983), maximum cover of 40 mm (Beam A) and minimum cover of 10 mm (Beam B) was adopted. Beam A was provided with bottom reinforcement of ribbed 16 mm diameter bars and top reinforcement of ribbed 8 mm diameter bars. In Beam B, bottom reinforcement was ribbed 12 mm diameter bars and the top reinforcement was ribbed 6 mm diameter bar. The comprehensive details of the reinforcement arrangement of beams A and B are presented in Figure 4.16.

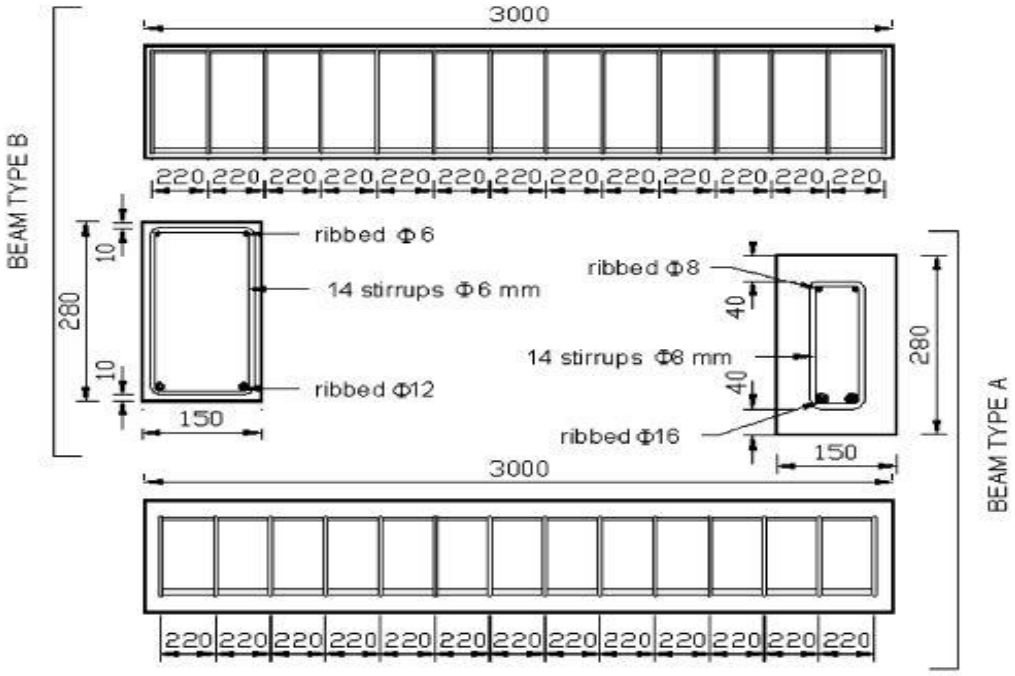

Figure 4.16 Layout of reinforcement for Beams A and B (Vidal et al, 2004)

For Beam A and Beam B, Vidal et al (2004) developed the correlation of crack width evolution with attack penetration (attack penetration) at different locations of the beams. Due to pitting corrosion, various crack widths are recorded in various locations along the beam, leading to a cluster of results represented in the graphical form. Vidal et al (2004) proposed a common linear trend curve for each condition by curve fitting the experimental results.

Validation of the model was plotted against the linear trend curve for given values of concrete cover, diameter, cover / bar diameter ratio, exposure conditions (saline) and the time. These graphs for Beam A and Beam B are presented in Figure 4.17 and Figure 4.18 respectively.

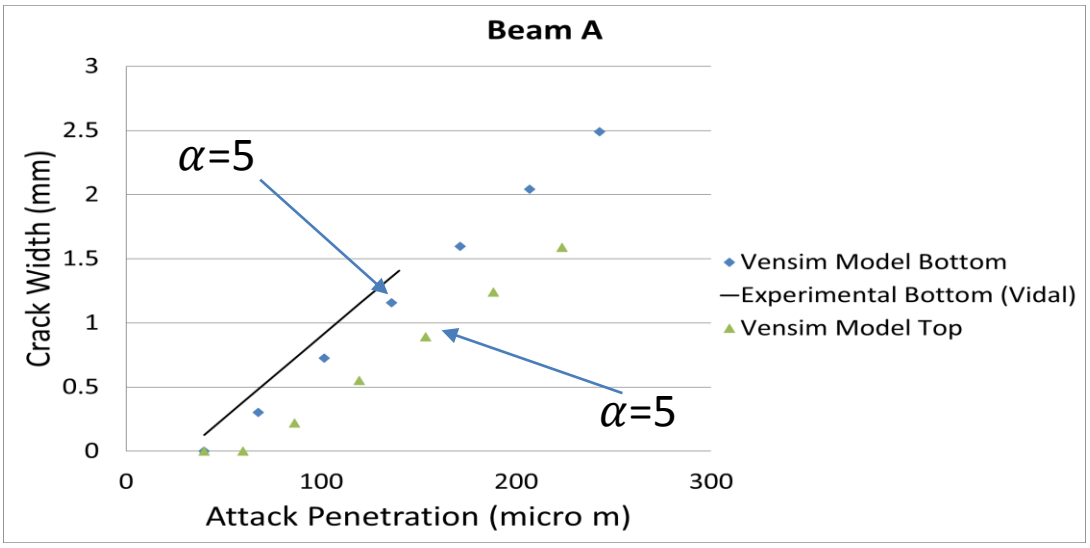

Figure 4.17 Crack width vs Attack penetration validation of Beam A (Vidal et al, 2004)

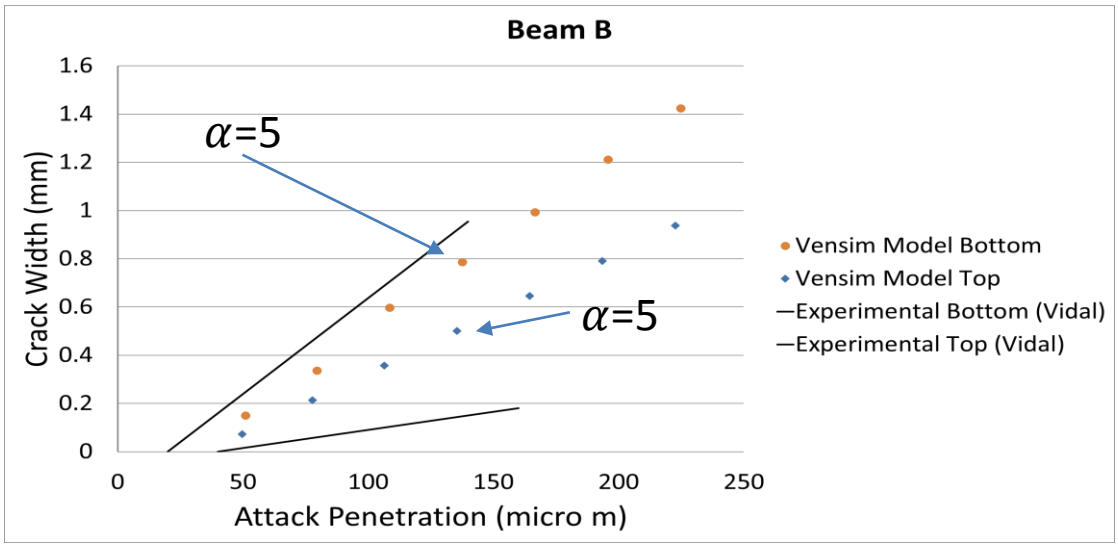

Figure 4.18 Crack width vs Attack penetration validation of Beam B (Vidal et al, 2004)

The differing experimental crack widths along the length of the beams is explained as arising out of different attack penetration values resulting from differing pitting factors.

The graphs show that the Vensim model outputs align with the linear trend curves between crack width and attack penetration of the experimental results. The experimental results of top reinforcement of Beam A is not given by Vidal et al (2004).

It is observed that the highest experimental crack width corresponded to a pitting factor equal to 5. This is true for all cases discussed. Experimental results of Darmawan (2010) also recommended the pitting factor of 5, which justifies our use of it in the model.

4.3.3 Zhang et al (2010) for Crack Propagation

Subsequent research outcomes of the same research series in Section 4.3.2 were published by Zhang et al (2010). This paper deals with the evolution of the corrosion pattern based on two beams corroded by 14 years (Beam C) and 23 years (Beam D) under chloride environment. Reinforcement arrangement in both beams were identical to the reinforcement arrangement in Beam B (as in Section 4.3.2).

Based on the experimental outcomes of steel cross section loss at different locations along the Beam D (23 years), Zhang et al (2010) proposed a new model for crack propagation.

- Localized corrosion (pitting corrosion) is predominant at the cracking initiation stage and the early stage of crack propagation.

- As the cracks propagate further, general corrosion develops rapidly and gradually becomes predominant.

Zhang et al (2010) also argued that Vidal et al (2004)'s results couldn't represent the second part of his model and therefore should be amended. Zhang et al (2010) anticipated that Vidal et al (2004) model could not have gone beyond the first stage of crack propagation under localized corrosion at the time of experimental testing. It is equally important to note that Beam C tested by Zhang et al (2010) would also only be at the localized corrosion stage. Zhang et al (2010)'s proposed new model is graphically presented in Figure 4.19.

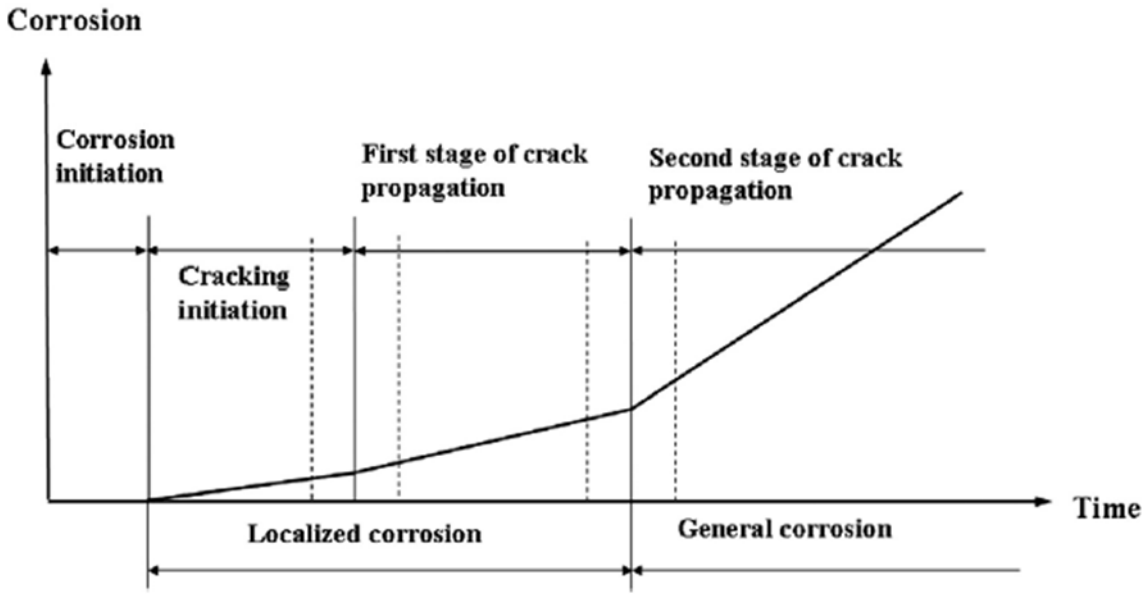

Figure 4.19 Stages of Crack Initiation and Crack Propagation (Zhang et al, 2010)

In the Vensim model, Beam C and Beam D were modelled. Due to identical reinforcement arrangement and cover to concrete, the model is similar to Beam B in Vidal et al (2004) experiment validation. In order to model Zhang et al (2010)'s observations of crack width against time, a pitting factor of 5 is selected according to the validation against Vidal et al (2004). For the general homogeneous corrosion, pitting factor of 2 was proposed by Rodriguez et al (1996). Zhang et al (2010) also suggested pitting factor of 2 for general corrosion.

The graph plotted for Beam C and D is presented in Figure 4.20 where pitting factors of 2 and 5 have both been used.

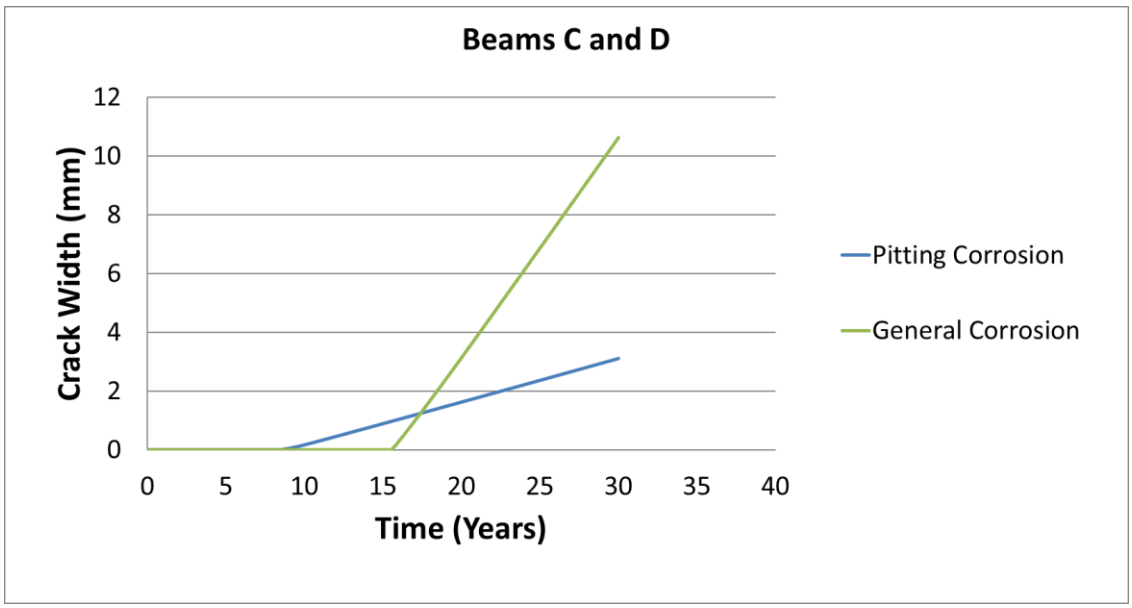

Figure 4.20 Crack Width Propagation from Vensim against Time for Beam C and D (Zhang et al, 2010)

From the crack width evolution graph against time shown in Figure 4.20, it can be noted that general corrosion predominates the pitting corrosion in concrete in the long term. The time taken for general corrosion to predominates the pitting corrosion depends on the causal loop of Vensim model. From the model outputs, general corrosion predominates the pitting corrosion in Beams C and D at 17.5 years. Therefore, the model can be validated against Zhang et al (2010)'s claims of crack width evolution.

The similar approach was tried to Beam A (Vidal et al, 2004) and the graph is plotted in Figure 4.21. In this case, the general corrosion predominates at 24 years. It can be argued that the experimental tests of Vidal et al (2004) were carried out before general corrosion predominates the crack width phenomenon in both beams (Beam A and Beam B) which could be why Vidal et al (2004) couldn't observe the second stage of Zhang's model.

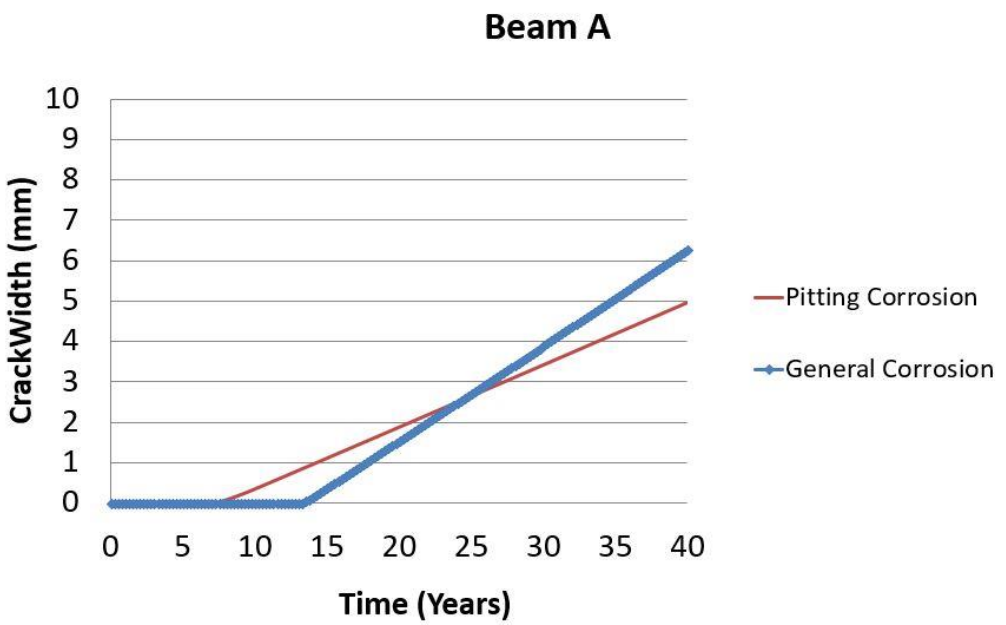

Figure 4.21 Crack Width Propagation from Vensim against Time for Beam A (Vidal et al, 2004)

The above two graphs derived from Vensim models predict the change in crack width propagation (from pitting corrosion to general corrosion) over time similar to what Zhang et al (2010) proposed. It can be argued that the amount of chloride at the steel level reaches equilibrium and hence the corrosion is homogeneous across the length of the reinforcement over time. Therefore, the effects of general corrosion dominate the crack characteristics after a certain period of time which Zhang et al (2010) identifies to be longer than 15 years.

Therefore, it can be concluded that the model predictions are good enough to study the chloride ingress into the reinforced concrete structures with time. The predictions would equip the designer with additional control over efficient material usage.

4.4 Parametric Analysis

Parametric analysis of the chloride ingress model was carried out to identify the effects of the major influencers in the concrete mix design – the water / binder ratio and the fly ash replacement of cement. This analysis would help to optimize the use of materials at the design stage and counteract the chloride ingress corrosion in concrete.

4.4.1 Influence of Water / Binder Ratio

Water / binder ratio directly contributes to the porosity and the chloride diffusion coefficient in the model. Sensitivity analysis were carried out to investigate the behavioural patterns of crack width propagation with the changes in water / binder ratio.

Table 4.6 presents the crack initiation time and the crack width at the end of 50 years design life period (assumed) for various water / binder ratio under the marine spray zone conditions (Section 4.2.13). Cover to reinforcement of 40 mm and the bar diameter of 10 mm is assumed for the analysis. Fly ash replacement is 0%.

Table 4.6 Effects of Water / Binder Ratio on Crack Propagation

Water / binder ratio	Crack Width (mm)	% Increment	Crack Initiation Time (years)	% Reduction
0.3	4.02	-	12.5	
0.4	4.57	14%	12	4%
0.5	5.03	25%	11.25	10%
0.6	5.47	36%	10.5	16%
0.7	5.81	45%	10	20%
0.8	6.09	51%	9.5	24%

Crack initiation time is assumed when the crack width exceeds 0.3 mm. Lesser crack widths will close-down due to the self-healing phenomenon of concrete (Takewaka et al 2003). From Table 4.6, it is observed that the crack width increases with the water / binder ratio. Due to increase in water / binder ratio, up to 50% crack width increment was achieved. Higher water content in the mix increases the pore volume hence more chloride ions penetrate the concrete. Therefore, higher current densities are formed due to increase in ion exchange and as a result, crack width increases.

On the other hand, porosity of concrete increases with higher water content. This will result in the reduction of crack resisting ability of the concrete (Archie's Law). Therefore, crack width initiates quicker in higher water / binder ratio mixes. Figure 4.22 presents the Vensim model output of crack width propagation with time for water binder ratio varies from 0.3 to 0.8, as increments of 0.1. The tabular format of the results is presented in Appendix A.1

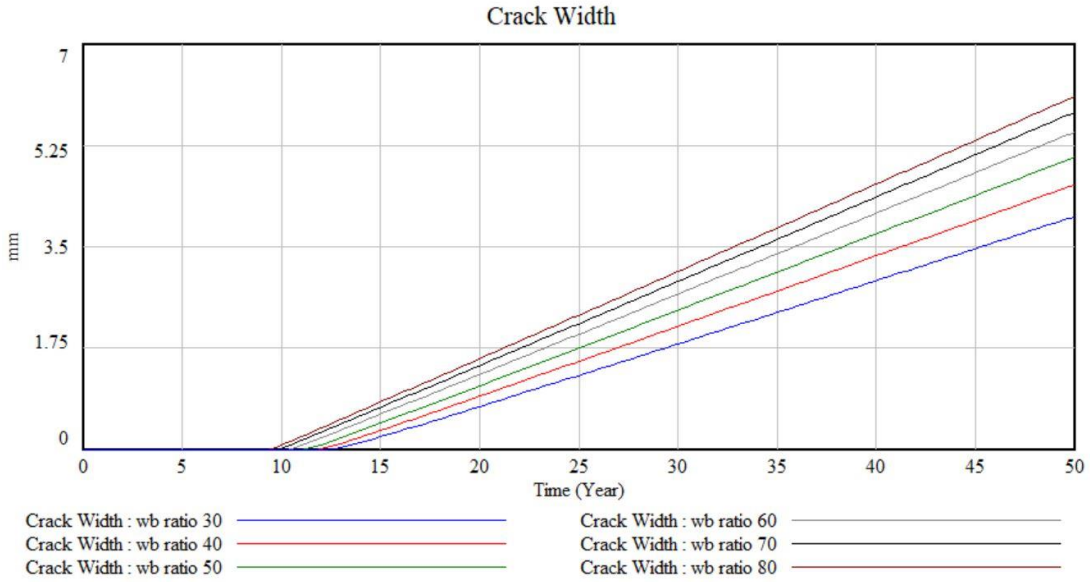

Figure 4.22 Vensim Model Output for Effects of W/B ratio in Crack Width Propagation

4.4.2 Influence of Fly Ash Replacement

Fly ash replacement of cement in the mix separately contributes to the porosity and the chloride diffusion coefficient. Sensitivity analysis on the effects of replacing cement with fly ash was carried out. Crack width (at 50 years design period time) and the initiation time were plotted for the variations in fly ash replacement of cement while the rest of the factors (water / binder ratio, cover to reinforcement and bar diameter) are kept constant (0.5, 40 mm and 10 mm respectively). Table 4.7 presents the results of the analysis.

Table 4.7 Effects of Fly Ash % Replacement in Crack Width Propagation

Fly Ash %	Initiation Time (Years)	% Increment	Crack Width (mm)	% Reduction
0	11.5	-	5.03	-
0.1	12.25	7%	4.76	6%
0.2	13.25	15%	4.37	13%
0.3	15	30%	4.02	20%
0.4	17.55	53%	3.70	26.%
0.5	22	91%	3.44	32%

Identical to the analyses in the previous section (Section 4.4.1), Crack initiation time is assumed when the crack width exceeds 0.3 mm. From Table 4.7, it is observed that crack width reduces with the increase in fly ash replacement of cement. This can be explained by the reduction of OH^- ions due to pozzolanic reaction of fly ash in the mix. Decrease in OH^- ions reduces the ion exchange with chloride ions therefore, the corrosion is counteracted. Up to 32% reduction is achieved in crack width propagation with the replacement of fly ash up to 50%.

The crack initiation time is increased by the addition of fly ash. As the fly ash in concrete mix increases, they hydration product of $Ca(OH)_2$ will react with the fly ash to produce more hydration products and reduce porosity. Consequently, the resistivity of concrete is increased and therefore, the crack initiation time is extended. From Table 4.8, more than 90% increment in the crack initiation time is observed in 50% fly ash replacement of cement compared to OPC concrete. Figure 4.23 presents the Vensim model output of crack width propagation with time for fly ash replacements varies from 0 to 50%, as increments of 10%.

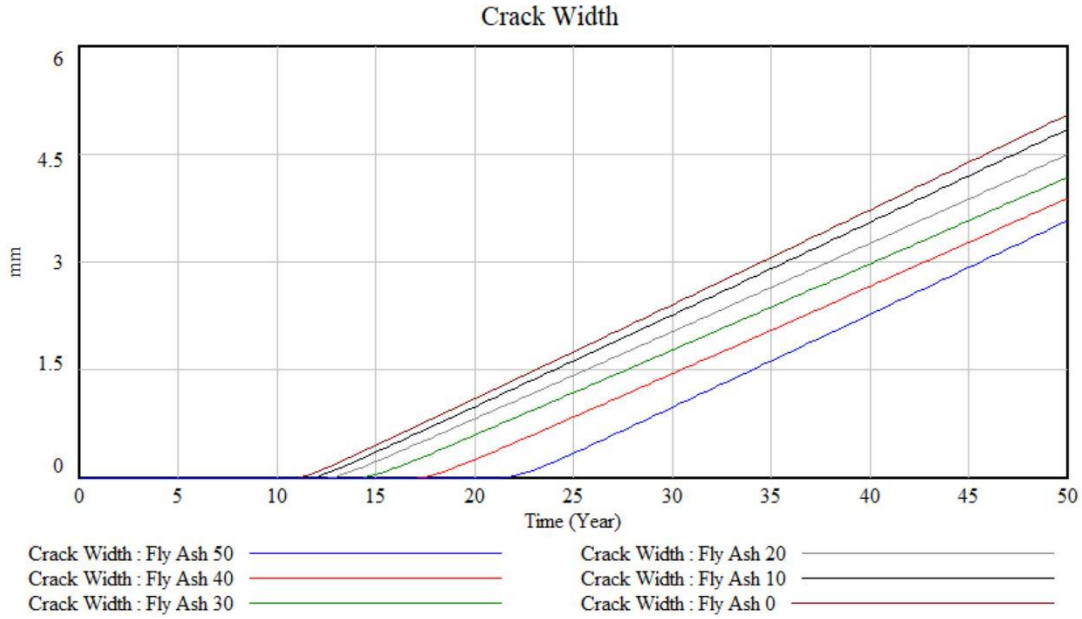

Figure 4.23 Vensim Model Output for Effects of Fly Ash Replacement in Crack Width Propagation

From the above results, crack width at the end of 50 years at 80% saturation percentage is plotted in Figure 4.24 against both water / binder ratio and fly ash replacement. The rate of increase in crack width against water / binder ratio is almost constant for any fly ash replacement up to 50%. As the water / binder ratio increases, the crack width variation caused by % fly ash replacement diminishes; and becomes almost negligible when water / binder ratio is 0.8.

Therefore, it can be concluded that higher percentages of fly ash replacement of cement improve the life period of the structure against chloride ingress. It can also be noted that the influence of fly ash on crack width is restricted by the increasing amount of water in the mix. Due to imitations in model definition, fly ash replacement higher than 50% and water / binder ratio higher than 0.8 cannot be predicted using the Vensim model.

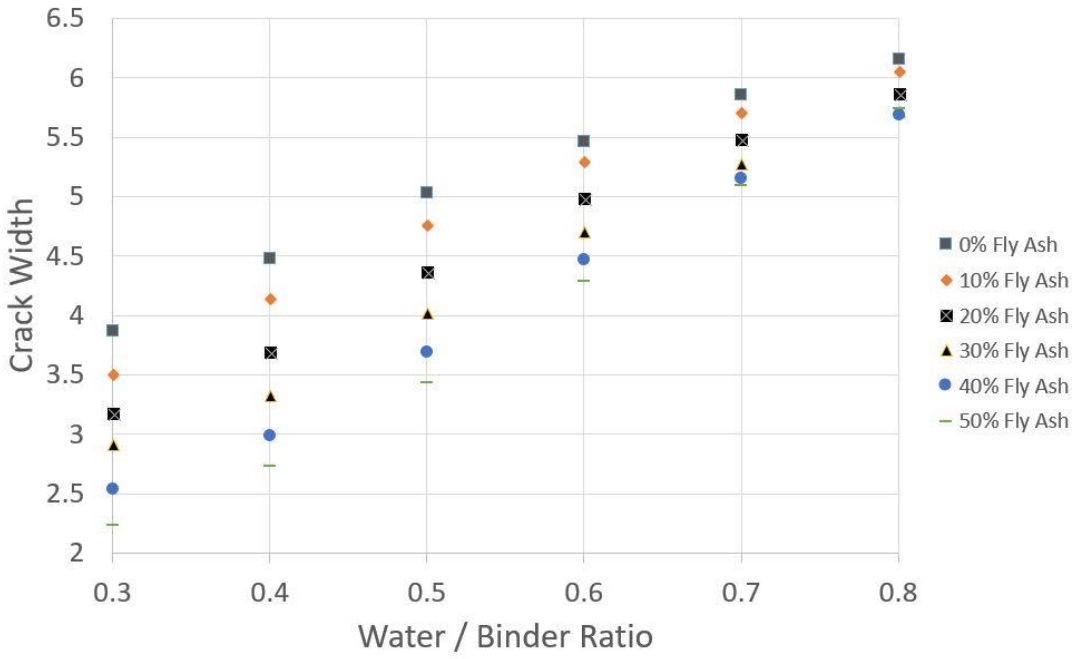

Figure 4.24 Crack Width vs Fly Ash Replacement

Table 4.8 presents the average influence of fly ash replacement and water / binder ratio on the crack width propagation at 80% saturation percentage. Appendix B.1 provides additional tables for saturation ratio at 65% and 100%. This table can help to study the relative influences of changes in water / binder ratio and replacement percentage of fly ash for ranges of 0.3 – 0.8 and 0- 50% respectively. Over the above practically utilized range, the influence of water / binder ratio is about double that of fly ash replacement. This is consistent with the established knowledge that the water / binder ratio is the most significant determinant of the concrete properties.

Table 4.8 Average Influence of W/B Ratio and Fly Ash Replacement

		Water / Binder Ratio						Influence	Average Influence
		0.3	0.4	0.5	0.6	0.7	0.8		
Fly Ash	0	3.87	4.48	5.03	5.47	5.86	6.15	2.28	2.83
	0.1	3.51	4.18	4.76	5.30	5.70	6.06	2.54	
	0.2	3.18	3.70	4.37	4.98	5.48	5.86	2.68	
	0.3	2.91	3.33	4.02	4.70	5.28	5.72	2.80	
	0.4	2.54	3.00	3.70	4.47	5.16	5.69	3.14	
	0.5	2.24	2.74	3.44	4.29	5.10	5.74	3.50	
Influence		1.64	1.73	1.59	1.17	0.76	0.47		
Average Influence		1.22							

4.5 Conclusion

System dynamic thinking implements reinforcing and balancing loops where the effects of past behaviour increase and decrease the rate of action respectively. In the chloride ingress model, existing crack widths in the concrete encourage the diffusivity of chloride ions into the crack pores. The incoming chloride ions further reacts and increases corrosion which ultimately results in the increase in crack width. Therefore, the rate of chloride ingress increases with time. This phenomenon is considered as a reinforcing loop in system dynamics.

5 MODELLING THE CARBONATION OF CONCRETE

5.1 Introduction to Concrete Carbonation

The carbonation of concrete is a slow process of the breakdown of passive oxide and hydroxide layer that protects the steel from deterioration. This phenomenon has been studied a lot in recent years as the associated risk of corrosion of steel reinforcement is not desirable.

Embedded steel reinforcement in concrete is usually protected from corrosion by a thin oxide layer that is formed and maintained on the surface due to the highly alkaline environment of the surrounding concrete pH value above 12.5. The passive layer on the steel surface will no longer remain stable when the alkalinity of the concrete surrounding the steel drops to approximately 11.5. (Sulapha et al 2003).

The pH stays at the value of the saturated $Ca(OH)_2$ solution, i.e. around 12.5, until all $Ca(OH)_2$ has reacted. Therefore, the content of $Ca(OH)_2$ of concrete is a decisive parameter of the carbonation resistance of concrete since it determines the time of the decrease of the pH to values below 12.5 (Böhni - 2005)

Carbon dioxide from the atmosphere reacts with cement components to form carbonates – this is referred to as carbonation. During the carbonation process, $Ca(OH)_2$ in pore water is converted to $CaCO_3$ and henceforth alkalinity in pore water is significantly reduced. This will cause the pH of pore water to drop below the limits below which the passive layer is not present anymore to protect the steel. This will initiate the carbonation process in concrete. Though calcium hydroxide shows greater reactivity, non-hydrated cement phases such as tricalcium silicate and dicalcium silicate also take part in the reactions. The chemical reaction of calcium hydroxide (major reactor), tricalcium silicate and dicalcium silicate are as given below respectively.

$$Ca(OH)_2 + H_2O + CO_2 \rightarrow CaCO_3 + 2H_2O$$

$$3CaO.SiO_2 + 13CO_2 + m\ H_2O \rightarrow SiO_2.mH_2O + 13\ CaCO3$$

$$2CaO.SiO_2 + 12CO_2 + m\ H_2O \rightarrow SiO_2.mH_2O + 12CaCO_3$$

In addition, the calcium silicate hydrates, mostly found in supplementary cementitious materials such as fly ash, will also react with carbon dioxide. There are various discrepancies between researchers over the investigation of mineral additives in concrete. The addition of supplementary additives has its direct influence in the reaction of carbon dioxide as the pozzolanic reaction consumes calcium hydroxide from the paste and therefore reduces the amount of major reactor and fastens carbonation. However, pore refinement through formation of additional C-S-H may lead to a denser microstructure of the cement matrix, thus reducing the rate of

diffusion. Therefore, supplementary cementitious materials have conflicting effects on long term carbonation process.

5.2 Carbonation Model Definitions

5.2.1 Model Outline

Like chloride ingress model discussed in Chapter 4, the carbonation model is developed in Vensim using mathematical relationships proposed by significant research studies in the field of concrete carbonation. Every interrelation has been repeatedly checked for accuracy and correctness by referencing multiple sources.

The depth of carbonation is roughly proportional to the square-root of time, doubling between 1 and 4 years, then doubling again between 4 and 16 years (Neville, 1981). The rate of carbonation depends upon factors such as water / binder ratio, amount of cement replaced by mineral additives and the environmental exposure conditions like the relative humidity of the ambient air. If diffusion of carbon dioxide through the concrete is very slow, a pre-equilibrium is reached where the diffusion of CO_2 and resulted carbonation are negligible. Diffusion of air through concrete depends on the porosity and the pore connectivity structure. Additionally, if the relative humidity is low in the ambient air, the lack of water in the atmosphere will severely reduce the carbonic acid formation and hence the carbonation process is reduced.

Relative humidity influences the carbonation process by the amount of water in atmosphere and in concrete. As discussed before, water is an essential participant in the reaction between CO_2 and $Ca(OH)_2$ to produce $CaCO_3$. As CO_2 is less soluble in water than air, the carbonation reactions are restricted during the periods when relative humidity is higher. However, very low relative humidity conditions will also limit the amount of water available for the carbonation reactions, thus reducing the carbonation. Therefore, as relative humidity varies from 0% to 100%, the rate of carbonation passes through a maximum, generally in between 50% and 80%.

The $CaCO_3$ is the product of carbonation process and it will settle inside the accessible pore space thus reducing the porosity further, which in turn reduces the carbonation process. It is widely understood that concrete becomes denser when carbonating. This phenomenon can be identified as a balancing loop in system dynamics modelling. Balancing loop conveys the reduction in performance in the system caused by the past performance of the system itself. Consequently, the effect converges to an equilibrium at one point where the products of carbonation reaction adversely influence the continuation of the process in the long term. This effect of porosity reduction due to carbonation is not considered by many authors due its minimal influence on the overall carbonation depth in short term. However, this effect predominates and reduces the incremental rate of carbonation in aged structures which again is confirmed in a study by Dias (2000). This effect of porosity reduction is used to model the carbonation process using Vensim.

Figure 5.1 presents the overview of the carbonation model in Vensim environment.

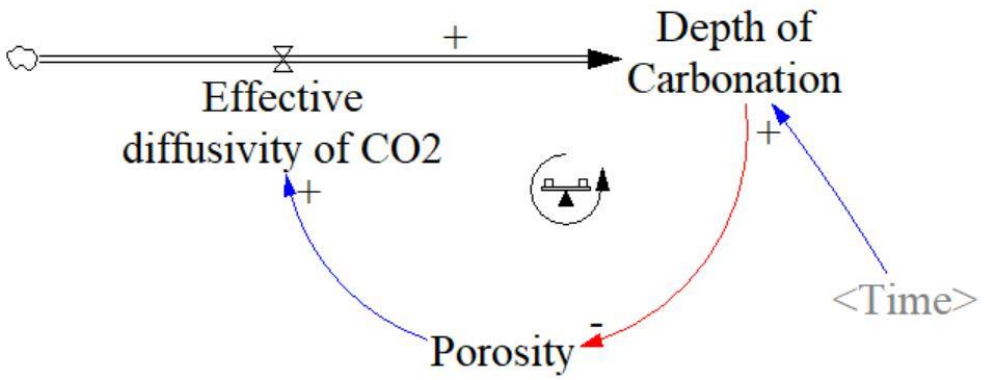

Figure 5.1 Carbonation Model Overview

5.2.2 Carbonation Kinetics and Depth of Carbonation

The carbonation kinetics can be defined as a first approximation, to be a diffusion process of a gas (CO_2) through a porous material. By applying Fick's first law, the Equation 35 is developed to calculate the depth of carbonation with time. This equation exhibits the square root of time relationship introduced by Neville (1981).

$$x = \sqrt{\frac{2Dc}{a}}\sqrt{t} \qquad (35)$$

Where x is the carbonated depth at time t, D the effective diffusivity of CO_2, c its concentration in the atmosphere and a is the concentration of reactive compounds which includes cementitious materials and mineral additives

Numerous researchers have attempted methodologies to propose a common equation for the prediction of depth of carbonation by incorporating all these factors. Therefore, literature provides us with several numerical models consist of assumptions for each of its own. Marques and Costa (2010) took some of the experimental results by Lausanne (1997) into account and proposed a series of factors for influencers as given in the Equation 36 below. In this equation Marques and Costa (2010) had tried a factorial approach to account for all those factors.

$$x = \sqrt{2\frac{D}{a}\Delta C t\sqrt{K_0 K_1 K_2}\left(\frac{t_0}{t}\right)^n} \qquad (36)$$

here x is the carbonation depth (m); D, the coefficient of diffusion of the CO_2 through the carbonated concrete in equilibrium with an environment of 65% RH and 20 ^{0}C (m^2/year); a, concentration of reactive compounds and depends on type and amount of cement (kg/ m^3); ΔC, the difference between the external CO_2

concentration and the one at the concrete carbonation front (kg/m^3); K_0, the constant that accounts for the testing method; K_1, the constant that accounts for the presence of relative humidity; K_2, the constant that accounts for the curing influence; t, the time, (year); t_0, the reference period and *n* is the parameter that accounts for the wet/dry cycle influence in time (Marques and Costa, 2010)

For the effective performance of system dynamics modelling, the number of independent constants should be maintained to minimum and mathematical relationships are encouraged. Marques and Costa (2010) defined separate variables for performance-based characteristics such as K_0, the constant that accounts for the testing method of carbonation. In addition, the equation is not in its simpler form, and shows the contribution of many factors at a given time. Therefore, a simpler equation is preferred.

RC Lifetime software, which is based on a deterministic model Papadakis (2000), and Papadakis and Tsimas (2002) used Equation 37 & 38 to calculate the carbonation depth including supplementary cementing materials. The effects of pozzolanic reactions on the carbonation is researched from the first principles and validated against the experimental studies by the authors in Equation 37. The equation was further developed by incorporating a new function f (RH) for the influence of relative humidity, and, by considering the directly attributable environmental conditions to be the variables (Teplý et al, 2010).

$$x_c = \sqrt{\frac{1.09 D_{e,Co2} C_{co2} 10^{-6} t}{0.218\ (c + kP)}} \qquad (37)$$

$$x_c = \sqrt{\frac{1.09 D_{e,Co2} C_{co2} 10^{-6} t}{0.218\ (c + kP)}}\ .f(RH) \qquad (38)$$

Here C_{co2} is the CO_2 content in the atmosphere (mg m^{-3}), k is the efficiency factor of the pozzolanic additives for carbonation resistance, $D_{e,Co2}$ is the effective diffusivity of CO_2 in carbonated concrete (m^{2}s^{-1}) (Papadakis, 2000), and $f(RH)$ is the function that represents the effects of relative humidity (Teplý et al, 2010).

To model the equation in Vensim, stock and flow diagram for the carbonation depth is developed by considering carbonation depth to be a stock which accumulates values over the time and this stock value is controlled by the flow of effective diffusivity of concrete. In Vensim representation, the accumulation of stock should be presented in the mathematical format as a time integration of CO_2 diffusivity. Therefore, Equation 38 is transformed into Equation 39. Furthermore, time is preferred to be calculated in units of years in Venism model as to predict the long-term results of carbonation depth. Papadakis (2000) defined time in the units of

seconds so the conversion factor is introduced. Considering above, Equation 39 is inserted to generate the carbonation depth component in the model.

$$x_c = \int \left(\frac{\sqrt{\frac{1.09 D_{e,Co2} \times C_{co2} \times 10^{-6}}{0.218\,(c + kP)}}}{2\sqrt{t \times 365 \times 24 \times 60 \times 60}} \right) \times f(RH) \times 31 \times 10^9 \, d(t) \qquad (39)$$

5.2.3 Diffusivity Kinetics of CO_2 and Relative Humidity

The one-dimensional diffusion of a gas through a porous material can be expressed phenomenologically by Fick's first law in Equation 40.

$$J = -D.\frac{dc}{dx} \qquad (40)$$

Here J is the flux of the gas, $\frac{dc}{dx}$ is the gradient of concentration and D is the diffusion coefficient

This equation defines the diffusion coefficient of a gas diffusing into another. If the diffusion is encountered by a porous medium such as concrete, the gas must diffuse through the pore structure of the material. Therefore, the distance through pores will be much longer than that in the definition by Fick's law. Therefore, effective diffusivity is determined based on the material characteristics of the pore medium. It also depends on the volume, the structure, and the degree of saturation of pores. Effective diffusive coefficient is defined for this case.

The effective diffusivity is given by the empirical equation (Equation 41) by Papadakis (1991) based on his previous experimental results;

$$D_{e,Co2} = 6.1 \times 10^{-6} \left(\frac{\frac{[w - 0.267(c + kP)]}{1000}}{\frac{c + kP}{\rho_c} + \frac{w}{1000}} \right)^3 f(RH)^{2.2} \qquad (41)$$

Here c, w and P are the cement, water and SCM content in the initial concrete mix (kg m^{-3}) respectively, ρ_c is the mass density of cement (kg m^{-3}), and f(RH) is the piece-wise linear relationship describing the influence of relative humidity (to be discussed later).

Simplifying the equation for effective diffusivity of concrete, Papadakis et al. (1992) introduced following equation (Equation 42) to account for the relative humidity (RH) and porosity (ϵ) of the medium on diffusivity.

$$D_{e,Co2} = 1.64 \times 10^{-6} \varepsilon^{1.8} (1 - RH)^{2.2} \qquad (42)$$

Here, RH is used to accommodate the effect of relative humidity on carbonation depth. However, the equation is valid only for RH values higher than 50%. Further, since a function of RH is directly attributed to depth of carbonation in the model, introducing the exposure condition would result in double counting of the effect of RH on the model. As discussed, carbonation would pass through a maximum as relative humidity increases from 0% to 100%.

Venuat (1997) researched on the carbonation depth variation as per relative humidity and proposed that maximum penetration appears when relative humidity is between 50% and 65% as plotted in Figure 5.2. Therefore, a multiplication factor is introduced to the carbonation depth equation according to the relative humidity variation in Figure 5.2 and the RH factor part of Papadakis et al (1992) was removed from the equation by replacing it with the maximum value at 50% relative humidity level.

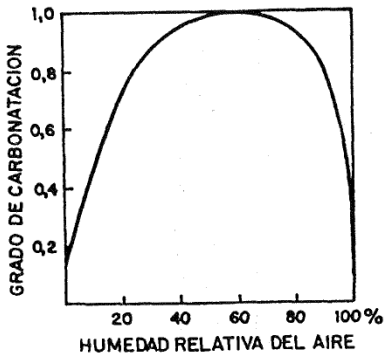

Figure 5.2 - Relative humidity and Carbonation rate (Venuat, 1997)

Thus, f(RH) is given by Equation 43 below and it was derived by using a mathematical formula to represent above data from the figure.

$$f(RH) = -9.1766RH^4 + 18.941RH^3 - 15.539RH^2 + 6.1876RH - 0.0094 \quad (43)$$

Following the modifications, the effective diffusivity coefficient is fed into the model as in Equation 44 where 0.2176 is the diffusivity at 50% RH from Equation 42.

$$D_{e,Co2} = 1.64 \times 10^{-6}\varepsilon^{1.8} \times 0.2176 \quad (44)$$

5.2.4 Porosity of Concrete

Porosity of concrete in the carbonation model is identical to the function used in chloride ingress model. Details have already been given in Section 4.2.6.

In addition, the depth of carbonation has a separate effect on the porosity. This variation is discussed in several papers [(Parrott 1992), (Basheer, Kropp et al. 2001),

(Saetta and Vitaliani 2004)], but those presented data are not consistent. In order to account the effect of porosity reduction due to carbonation, experimental results given by Dias (2000) is used as a multiplying factor on initial porosity (Equation 45). Based on the study, he identified a maximum of 2% change in porosity difference due to the change in carbonation depth. According to the experimental data, the factor for porosity reduction is given as in the Equation 46.

$$\varepsilon = \varepsilon_i \times F_\varepsilon \qquad (45)$$

$$F_\varepsilon = \frac{9.84 - (0.08 \times x_c)}{9.84} \qquad (46)$$

Where, ε is porosity of concrete, ε_i is the initial porosity, F_ε is factor for porosity (Dias, 2000) and x_c is carbonation depth.

5.2.5 Fly Ash Replacement and Efficiency of Fly Ash

Fly ash replacement and fly ash efficiency of the carbonation model is identical to the function used in chloride ingress model. Details of this have already been given in Section 4.2.7

Fly ash, however, has a separate direct effect on the depth of carbonation. Fly ash replacement increases concrete porosity because the reduction in porosity due to pozzolanic activity is lesser than that due to hydration of the same quantity of OPC.

Papadakis et al (1992) proposed a fly ash efficiency coefficient of 0.5 for carbonation of concrete. This is quite different from Section 4.2.7 and incorporated into the carbonation depth equation as an independent term.

Incorporating all these effects, the final mathematical formula for the carbonation depth is inserted into Vensim model as below (Equation 47):

$$x_c = \int \left(\frac{\sqrt{\frac{1.09 D_{e,Co2} \times C_{co2} \times 10^{-6}}{0.218\,(c + 0.5 \times P)}}}{\sqrt{t \times 365 \times 24 \times 60 \times 60}} \right) \times f(RH) \times 0.5 \times 31 \times 10^9 \, d(t) \qquad (47)$$

Depth of Carbonation = ((((1.09*Concentration of CO_2 in atmosphere*Effective diffusivity of CO_2*10^(-6))/(0.218*(CEMENT CONTENT+0.5*FLY ASH REPLACEMENT)))^0.5) *(((Time+0.1)*365*24*60*60)^(-0.5)))*(-9.1766*RELATIVE HUMIDITY ^4+18.941* RELATIVE HUMIDITY ^3-15.539* RELATIVE HUMIDITY ^2+6.1876* RELATIVE HUMIDITY -0.0094)*0.5*31.536*10^9

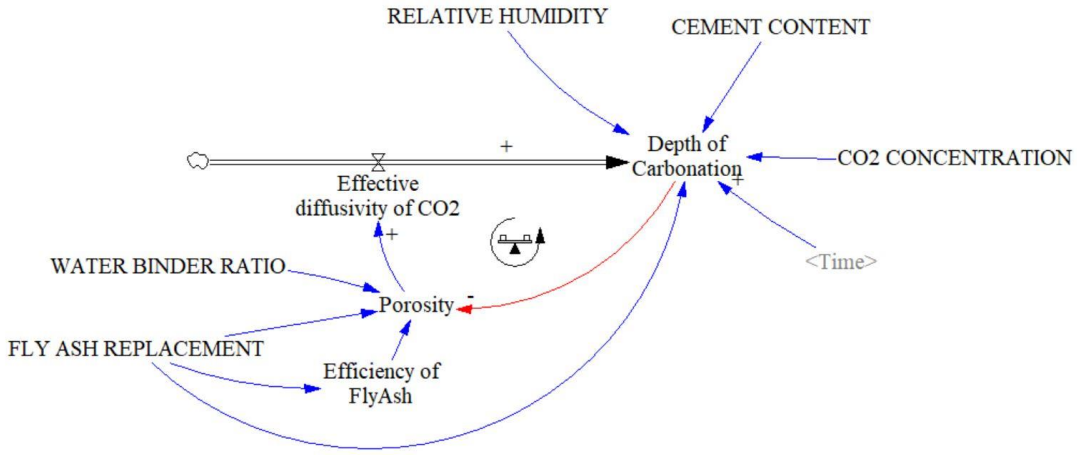

Figure 5.3 - Carbonation balancing loop

5.3 Validation of the Carbonation Model

The proposed model for carbonation in concrete has been developed to provide a general basis for durability analysis of concrete structures. Such a durability analysis can be applied both for obtaining a more controlled durability and long-term performance of new concrete structures, and as an improved basis for condition assessment of existing concrete structures.

However, appropriate determination of concrete carbonation depth is not a trivial problem, considering various concrete materials, complex factors, and exposure conditions. To predict accurate and reliable outputs, the model must be validated against the existing experimental and real-life data. Most of the available literature cover indoor experimental conditions for short term periods. Accelerated carbonation corrosion is exceedingly favoured by researchers where the concentration of carbon dioxide is multiplied by significant times to the real-life conditions to force prompt carbonation reactions. Neither short term laboratory conditions nor accelerated carbonation corrosion do necessarily establish the real-life carbonation phenomenon. Neither do they provide the necessary platform for the validation as the model plots the development of carbonation over the span of 50 years.

It shall also be noted that it is hard to associate the carbonation depth with an exact figure in the experimental analysis. Typically, the ‘‘carbonation front’’, is a transition zone where the degree of carbonation decreases from complete carbonation to zero; The testing procedure (usually Phenolphthalein testing) may not necessarily be accurate regarding the carbonation front. Therefore, discrepancies in the model validation could arise.

Previous research based on condition assessment of existing structures would ideally suit the validation purpose. However, the environmental conditions and the concrete

material characteristics of the existing structures are extremely hard to find. Also in such structures, data regarding mix constituents would typically be difficult to find.

Considering above, three research outputs were used for validation of the carbonation model.

1. Costa and Appleton (2001)
2. Saetta and Vitaliani (2005)
3. Khunthongkeaw et al (2006)

5.3.1 Costa and Appleton (2001)

Costa and Appleton describe an experimental study conducted on the western coast of Portugal in order to evaluate the significance of the carbonation of concrete in marine environment. A few concrete slabs were exposed to natural marine environment conditions (on the estuary of the river Sado) and the carbonation depth was measured by the phenolphthalein test over a period of first six years. Two mixes (C1, C2) were studies for cast-in-situ concrete. The long-term penetration of the aggressive agent was evaluated on the basis of the experimental results obtained. The experiments are part of the inspection and a detailed appraisal study carried out in 1996 to evaluate the deterioration of structures in a large dock yard built in 1970s, located on the west coast of Portugal.

Costa and Appleton developed time functions for carbonation from the results of carbonation depth recorded over six years and extrapolated the curve up to 100 years. They argued that the carbonation depth does not represent Neville's (1981) square root of time relationship in the long-term behaviour. Further, they proposed alternative time exponent values based on concrete mix and exposure conditions. This exponent was found to be 0.44 for mix C1 and 0.40 for mix C2 (see Table 5.1). The reduction in the n value below the 0.5 derived from Fick's law could be attributed to the incremental reduction in the CO2 diffusivity, due to the carbonation itself, a feature captured in our model.

This study is completely independent from the equations used to build the Vensim model. Therefore, the results obtained were modelled in two ways. The models are denoted as Model A – porosity reduction due to carbonation is accounted for; and Model B – porosity reduction due to carbonation is not accounted for.

Table 5.1 and Figure 5.4 give the experimental results of at the end of 6 years and the 100 years predictions. These are compared with those obtained from the Vensim model. Model C1-A represents the C1 mix used in where porosity reduction due to carbonation is accounted for; while Model C1-B does not. Models C2-A and C2-B are also similarly defined for the C2 mix. In computing percentage differences for the 100-year (predicted) values, the Model B outputs are compared with Costa and

Appleton results that assume Fick's law (time exponent is 0.5) and the Model A outputs with those that allow the time exponent to fall below 0.5.

Table 5.1 Validation of Carbonation Model against Costa and Appleton (2001)

Type	Duration	Costa & Appleton (2001)		With porosity reduction (Model A)		Without porosity reduction (Model B)	
C1	6 years	Experimental	9mm	8.13 mm	9.7%	8.34 mm	7.3%
	100 years	$x = k_1 * t^{0.5}$	36mm	29.0 mm	12.1%	32.6 mm	9.8%
		$x = k_2 * t^{0.44}$	33mm				
C2	6 years	Experimental	5mm	4.93 mm	1.4%	5.01 mm	0.2%
	100 years	$x = k_1 * t^{0.5}$	20mm	18.2 mm	13.8%	19.6 mm	2.0%
		$x = k_2 * t^{0.40}$	16mm				

Table 5.1 shows that the model results vary up to 14% from the theoretical results at the end of 100 years. They give a closer representation of the experimental output at the end of first six years. Figure 5.4 shows the shape of the relationship between depth of carbonation and time from Vensim.

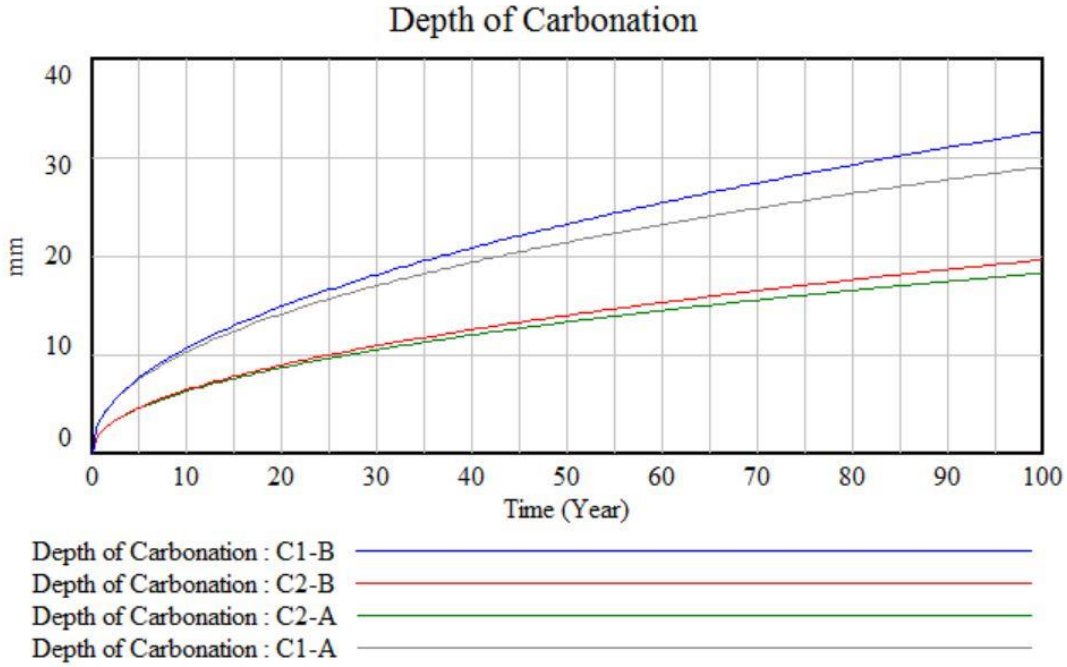

Figure 5.4 Vensim Model (A and B) Output Graph of Depth of Carbonation vs Time (Costa and Appleton, 2001)

The effect of change in porosity reduction with time is carried out in the study and the results are presented in Figure 5.4 and Table 5.1. The carbonation depth is higher

when the porosity reduction is neglected. The model outputs display reasonable agreement with the experimental results (and their extrapolations). Model B outputs appear to show slightly better fit with results. However, we argue that Model A is theoretically superior, because it has a mechanism for the exponent of time to be under 0.5 as proposed by Costa and Appleton (2001).

5.3.2 Saetta and Vitaliani (2005)

Saetta and Vitaliani (2005) developed a mathematical numerical model to predict the corrosion initiation time of reinforced concrete due to carbonation process and they applied their work to some real cases. Two industrial sheds with different ages located in different areas have been analysed performing experimental analyses. The sheds are both situated in the province of Verona, Italy, in the suburbs of the city. Therefore, the exposure conditions such as relative humidity and temperature have no significant differences in the trends but the concentration of carbon dioxide, since one shed (denoted as Shed A) is used for stabling animals and the other (denoted as Shed B) is used for storing tools. Therefore, the data obtained from the tests on the two sheds can be considered as representatives for the model validation.

For Shed A, an experimentally measured carbonation depth of about 11 mm after 16 years of service agrees with the value of depth obtained by the model, which is between 11 and 12 mm; – for Shed B, the experimental finding was about 7 mm after 23 years, while the simulated result is between 7 and 8 mm (Table 5.2).

This study is completely independent from the equations used to build the Vensim model. Therefore, considering the variables gathered by the researchers on the existing sheds, Vensim Model A and Model B (as discussed in 3.3.1) is developed for both the sheds separately for the validation purpose. The model predictions corresponding to the time of carbonation depth testing of real case structures are presented in Table 5.2.

Table 5.2 Validation of Carbonation Model against Saetta and Vitaliani (2005)

Sample	**CO_2 Conc.**	**RH**	**W/B Ratio**	**Experimental Result**	**Model A Results**	**Model B Results**
Shed A	0.08%	72.5%	0.38	11 mm/16yr	11.96 mm/16yr	12.76 mm/16yr
Shed B	0.02%	72.5%	0.38	7 mm/23yr	6.44 mm/23yr	6.72 mm/23yr

From the comparison in Table 5.2, it can be said that the model predictions are closer to real life cases. Model A gives a better prediction than Model B for Shed A (with

both models overpredicting), but this is reversed in the case of Shed B (with both models underpredicting).

5.3.3 Khunthongkeaw et al (2006)

Khunthongkaew, Tangtermsirikul and Leelawat (2006) studied carbonation using fly ash concrete under natural environments. Cubes were casted by varying the water binder ratio and fly ash content, and kept under different exposure conditions such as city, rural and seaside areas.

The test results on the carbonation depth was measured up to 24 months and represented by corresponding carbonation coefficient values which is inversely proportional to the carbonation resistance of concrete and was estimated by the regression analysis using Neville's (1981) empirical relationship (Equation 35).

This study is also completely independent from the equations used to build the Vensim model. Therefore, models in Vensim (Model A where the reduction in porosity due to carbonation is accounted for) were developed for the above conditions. The Vensim predictions of carbonation depth and the experimental test results at the end of 12months and 24 months are displayed in Figure 5.5 and 5.6 respectively.

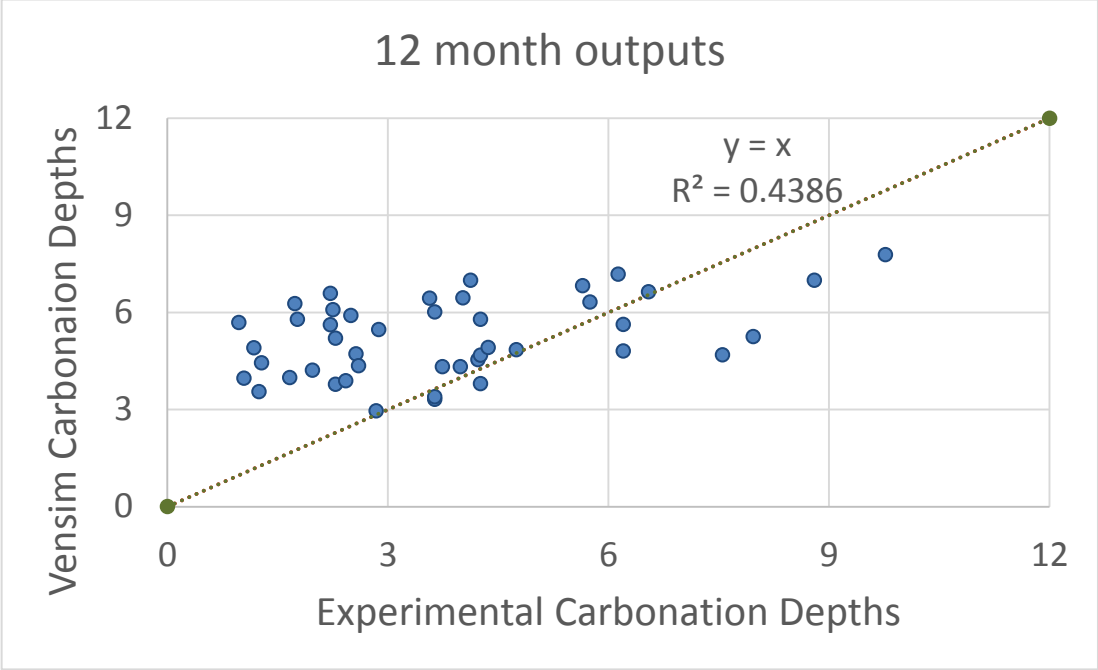

Figure 5.5 Experimental (Khunthongkaew, 2006) Carbonation Depths vs Vensim Carbonation Depths for 12 months period

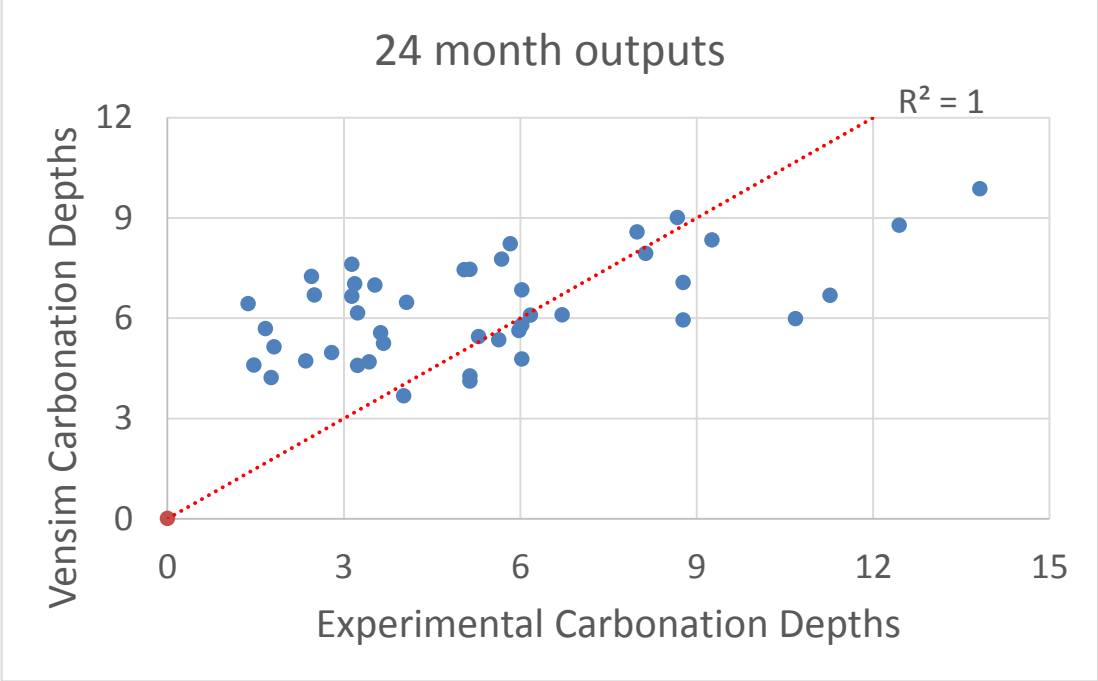

Figure 5.6 Experimental (Khunthongkaew, 2006) Carbonation Depths vs Vensim Carbonation Depths for 24 months period

Both figures show discrepancies between experimental values and model values for some specimens and align with the rest. It can be noted that the model overpredicts when the carbonation depth values are low, and underpredicts when the carbonation depth values are high, When the carbonation depth at the end of 24 months are between 5 mm and 10 mm, Vensim model gives closer approximation to the experimental results.

By taking above three validation exercises into consideration, the following remarks can be made.

- Model outputs display reasonable agreement with the experimental results (and their extrapolations).
- The carbonation depth is higher when the porosity reduction due to carbonation process is neglected.

Therefore, it can be concluded that the model predictions are good enough to study the carbonation depth pattern of the reinforced concrete structures with time during the design stage itself. The predictions would equip the designer with additional control over efficient material usage.

5.4 Parametric Analysis

5.4.1 Influence of Water / Binder Ratio

Sensitivity analyses were carried out for each control variable present in the model and the behaviour patterns of both model conditions were identified. Table 5.3 presents the model A and model B outputs (as discussed in Section 5.3.1) of changes in carbonation depth with water binder ratio when cement content is 300 kg/m^3, RH is 80% and the fly ash replacement is 0%. The table also presents the percentage difference between the model outputs at the end of 50 years design life.

Table 5.3 Effects of Water / Binder Ratio on Models A and B

w/b ratio	Model A (mm)	% Increase	Model B (mm)	% Increase	% Difference between A & B
0.3	16.7	-	17.8	-	6.6%
0.4	20	20%	21.6	21%	8.0%
0.5	22.7	36%	24.8	39%	9.3%
0.6	24.9	49%	27.4	54%	10.9%
0.7	26.7	60%	29.6	67%	10.9%
0.8	28.2	69%	31.5	77%	11.7%

From Table 5.3, the carbonation depth values of both models increase with higher amount of water in the mix. When the water / binder ratio varies from 0.3 to 0.8, rises in carbonation depth up to 69% and 77% are recorded in model A and model B respectively.

The differences between the values from the two models increase as the water content in the mix increases. When the water binder ratio is higher, the large pores allow more CO_2 molecules to react with OH^- ions. More $CaCO_3$ is produced and accumulated hence the porosity reduction is significant.

The reduction in the rate of carbonation can be attributed to the reduction in the time exponent of the carbonation depth equation (Equation 38) as proposed by Costa and Appleton (2001). Model B which does not account for the carbonation reduction gives the carbonation depth values corresponding to the time exponent of 0.5 as in Fick's law. The effect of water / binder ratio on the reduction of the time exponent values predicted by model A are presented in Table 5.4.

Table 5.4 Effect of Water / Binder Ratio on the Carbonation Time Component

Water / binder ratio	Model A Depths (mm)	Time Exponent	% Reduction
0.3	16.7	0.4837	3.26%
0.4	20	0.4803	3.94%
0.5	22.7	0.4774	4.52%
0.6	24.9	0.4755	4.90%
0.7	26.7	0.4736	5.28%
0.8	28.2	0.4717	5.66%

It is also instructive to compare these results with the field observations reported by Dias (2013). When the square root of time law is used for structures ranging from 7 to 125 years of age (all OPC only concrete), the 100-year carbonation depth from the fitted line suggests a carbonation depth of 49 mm, which is admittedly a little more than predicted by even the 0.8 w/c ratio; this may be because of workmanship deficiencies in the real-life structures surveyed by Dias (2013). However, for structures from 7 to 30 years of age (i.e. more recent concretes), the predicted 100-year carbonation depth is 34.5 mm, very close to the values in Table 5.3 between w/c ratios of 0.7 and 0.8; It is important to keep in mind once again that the model outputs would be expected to under-predict field carbonation depths, because the latter would suffer from workmanship defects.

5.4.2 Influence of Fly Ash Replacement

The effect of adding of fly ash into the binder was studied. Model A and model B (as discussed in Section 5.3.1) are used to plot the changes in carbonation depth for different percentages of fly ash replacement of cement. The rest of the factors (water binder ratio, cement content, RH) are kept constant (0.5, 475 kgm^{-3}, 0.6 respectively) and carbonation variation with the fly ash replacement is obtained. The percentage differences between the model outputs are also calculated. The model A and model B outputs at the end of 50 years are provided in Table 5.5. Model A outputs of carbonation depth development over the years is shown in the graphical format in Figure 5.7.

Table 5.5 Effects of Fly Ash in Carbonation Model

Fly ash (%)	Model A (mm)	% Difference	Model B (mm)	% Difference	% Difference between A & B
0	19.03	-	20.36	-	6.99%
10	11.49	40% dec.	11.85	42% dec.	3.13%
20	11.06	42% dec.	11.49	44% dec.	2.35%
25	11.66	39% dec.	12.11	40% dec.	3.86%
30	12.71	33% dec.	13.28	35% dec.	4.48%
35	14.34	25% dec.	15.12	25% dec.	5.44%
40	16.78	12% dec.	17.79	13% dec.	6.02%
50	25.93	36% inc.	28.49	40% inc.	9.87%

(dec – decrease; inc – increase)

From Table 5.5 and Figure 5.7, we can see that carbonation depth is decreased as the fly ash replacement increases to an optimum point during which the fly ash replacement counteracts the carbonation process. At the optimum point, the carbonation depth can be reduced up to 42% in model A and 44% in model B.

Similar to the analysis for the effect of water / binder ratio on the time component in Section 5.3.1, the effect of fly ash replacement is also analysed. Model A which accounts for the porosity reduction due to carbonation is used for the study. The effect of fly ash replacement (as the replacement percentage varies from 0% to 50%) on the time component of carbonation depth is presented in Table 5.6.

Table 5.6 Effect of Fly Ash Replacement on the Carbonation Time Component

Fly Ash Replacement	Model A Depths (mm)	Time Exponent	% Reduction
0	19.03	0.4856	2.88%
10%	11.49	0.4921	1.58%
20%	11.06	0.4903	1.94%
30%	12.71	0.4887	2.26%
40%	16.78	0.4850	3%
50%	25.93	0.4759	4.82%

As the fly ash content in the concrete mixture increases primarily, the hydration product $Ca(OH)_2$ will react with the fly ash to produce more hydration products and reduce porosity. Consequently, fly ash will reduce the depth of carbonation. The carbonation mechanism increases after an optimum point, which would be connected to the existence of excess fly ash in the medium which cannot participate in the reaction. Also, there are increasingly lower cement contents for producing hydrated products. This increases porosity and carbonation. In addition, the increasing amounts of fly ash remove the OH- ions that would otherwise offer resistance to carbonation. This phenomenon is observed in Table 5.6 where the porosity reduction is lower when the fly ash replacement percentage is around 20% - 25%.

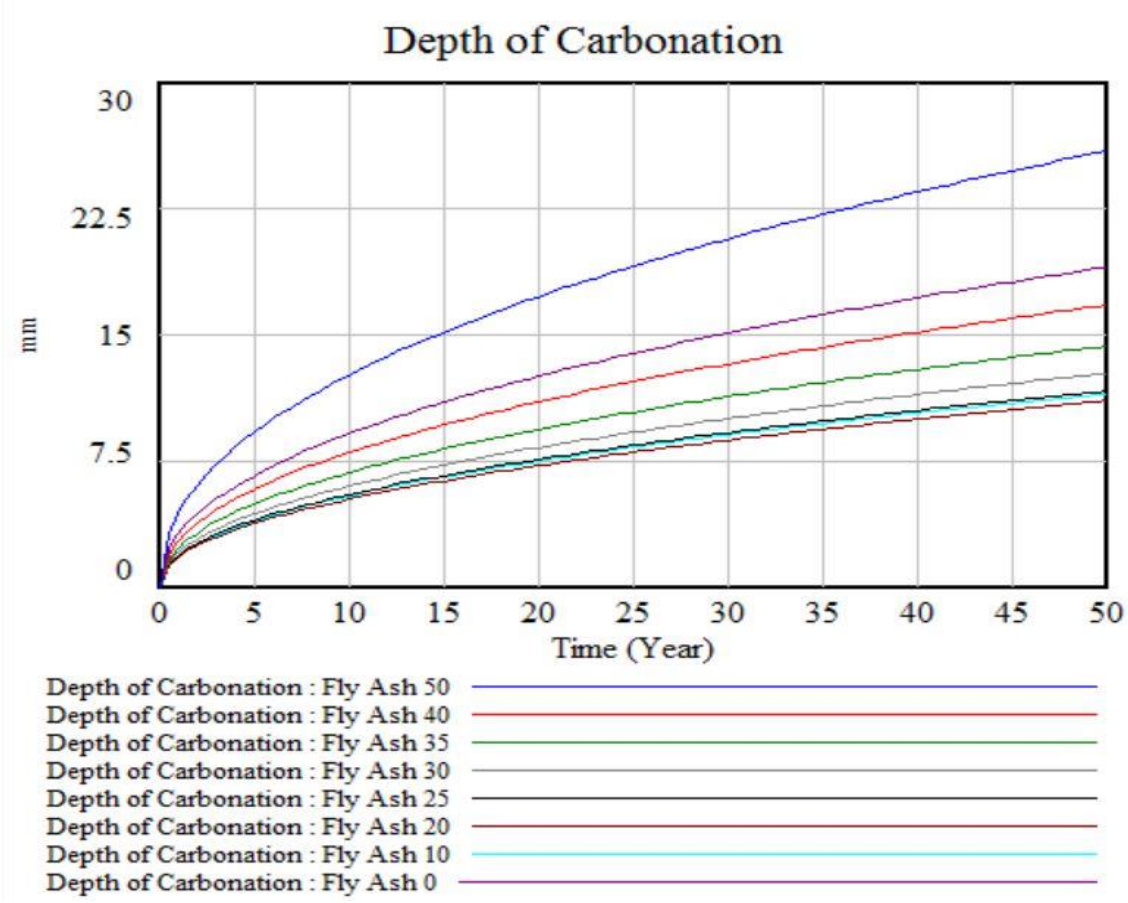

Figure 5.7 Model A Output of Effects of Fly Ash

From the above results, fly ash replacement against carbonation depth graph is plotted in Figure 5.8. This graph shows the carbonation depth at the end of 50 years. From Figure 5.8, it can be observed that an optimum fly ash percentage can be arrived at, with respect to carbonation resistance. The model predicts low carbonation depths when fly ash replacement is around 20%-25%.

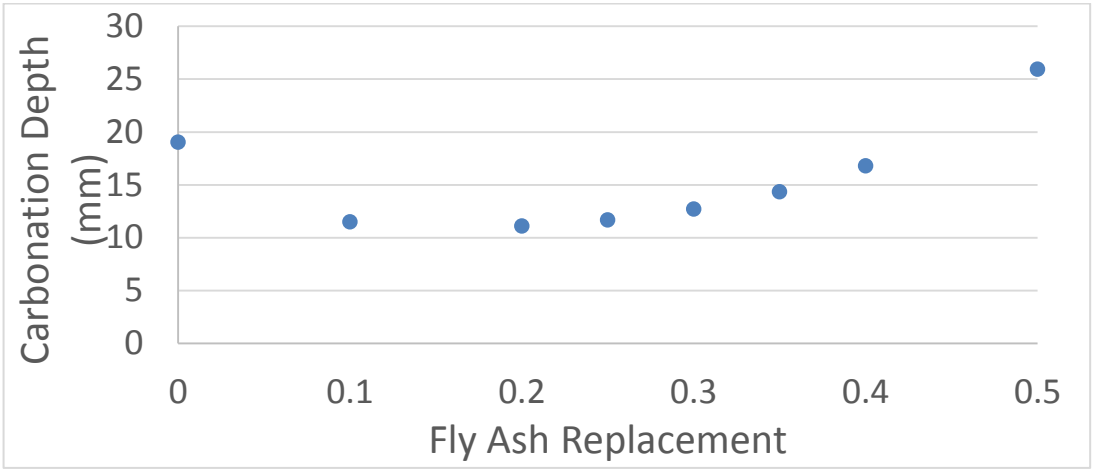

Figure 5.8 Depth of Carbonation vs Fly Ash Percentage

However, the shape of the graph in Figure 5.8 changes with water binder ratio in the mix. For water binder ratio higher than 0.5, the effect of water / binder ratio on carbonation predominates the effect of fly ash. When the pores are larger (high water binder ratio) and the cement content is low, hydration product $Ca(OH)_2$ will be reduced. Therefore, the fly ash reactions and resistance to carbonation are eliminated.

Table 5.7 shows the influences of water / binder ratio and fly ash replacement at relative humidity 65%. Appendix B.2 provides additional tables for same representation at relative humidity at 80% and 100%.

Table 5.7 Combined Influence of W/B ratio and Fly Ash Replacement in Carbonation

		Water / Binder Ratio						Influence	Average Influence
		0.3	0.4	0.5	0.6	0.7	0.8		
Fly Ash	0	9.55	13.89	17.69	20.31	23.67	26.12	16.57	19.83
	0.1	8.71	13.69	17.94	20.87	24.46	27.08	18.36	
	0.2	7.10	12.76	17.52	20.83	24.71	27.53	20.43	
	0.3	7.21	13.30	18.37	21.86	25.91	28.83	21.63	
	0.4	9.89	16.19	21.32	24.72	28.80	31.68	21.78	
	0.5	16.9	23.03	27.80	30.67	34.54	37.11	20.19	
Influence		9.81	10.27	10.28	10.36	10.87	10.99		
Average Influence		10.43							

This table can help to study the relative influences of changes in water / binder ratio and percentage fly ash for ranges of 0.3 – 0.8 and 0- 50% respectively. It can be seen that over the above practically utilized ranges, the influence of water / binder ratio is about double that of fly ash replacement. This is consistent with the established knowledge that the water / binder ratio is the most significant determinant of concrete properties.

5.5 Conclusions

System dynamic thinking implements reinforcing and balancing loops where the effects of past behaviour increase or decrease the rate of action respectively. In the carbonation model, continuous reactions will produce more $Ca(CO)_3$ that will fill the pore spaces, causing the reduction in CO_2 diffusivity and thus the carbonation rate reduces with time. Therefore, this phenomenon is considered a balancing loop in system dynamics.

6 CONCLUSIONS AND RECOMMENDATIONS

In the study, the main deterioration mechanisms of reinforcement corrosion – carbonation and chloride ingress into concrete – are modelled using Vensim causal loops. The obtained results predict the long-term characteristics of corrosion, and the changes in corrosion parameters such as crack width (chloride ingress into concrete) and carbonation depth (carbonation) over a design period of 50 years. Within the above scope, the following conclusions and recommendations can be made.

1. System dynamics modelling can be implemented effectively to model chloride ingress and carbonation in concrete. The rate of chloride ingress increases with time due to the development of cracks and hence the large voids which invite more chloride ion diffusion. Chloride ingress into concrete is considered a reinforcing loop in system dynamics where the effects of past behaviour increase the rate of action. The carbonation rate reduces with time due to the accumulation of $Ca(CO)_3$ in the pores and the consequent reduction of CO_2 diffusivity. Therefore, carbonation is considered a balancing loop where the effects of past behaviour decrease the rate of action.

2. Water / binder ratio and fly ash replacement of cement are the main design-controlled variables of chloride ingress and carbonation. In both models, the average influence of water / binder ratio (varied from 0.3 to 0.8) is about twice the average influence of fly ash replacement (varied from 0% to 50%).

3. Crack width and crack initiation timeare the key parameters in quantifying the chloride ingress into concrete. Crack width increases with water / binder ratio and reduces with fly ash replacement of cement. Around 50% increase in crack width is predicted by the model when the water / binder ratio is increased from 0.3 to 0.8 (while fly ash replacement is 0%). This increase corresponds to 24% reduction in the crack initiation time. On the other hand, around 32% reduction in crack width is predicted when the fly ash replacement is increased from 0% to 50% (while water / binder ratio is 0.5). This corresponds to 91% increase in the crack initiation time.

4. Corrosion can be categorized into general corrosion and pitting corrosion. Pitting corrosion is predominant at the crack initiation phase and the early propagation phase.As the crack propagates further, general corrosion develops rapidly and becomes predominant. The model predicts a time above 15 years for the general corrosion to overtake the pitting corrosion. This prediction is validated by Zhang et al (2010).

5. The rate of carbonation can be associated with a reduction in the exponent of the time function to below the 0.5 suggested by Fick’s Law. The difference

between the carbonation depth values from the two models (one has the constant exponent of 0.5 and the other has an exponent allowed to vary with porosity reduction) increase as the water / binder ratio increases. Around 12% difference in carbonation depth is found between the two model predictions when the water / binder ratio is 0.8. This corresponds to the time exponent component of 0.4717; which is 5.6% less than 0.5 as suggested by Fick's law. Similarly, around 10% difference is found between two model predictions when the fly ash replacement is 50%. This corresponds to the time exponent component of 0.4759; which is 4.8% less than 0.5.

6. The carbonation depth is decreased with the fly ash replacement of cement up to an optimum point; a period during which fly ash reacts with $Ca(OH)_2$to produce more hydration products and reduce porosity. The carbonation mechanism increases after the optimum point, which would be attributed to the existence of excess fly ash that does not participate in the hydration reactions.

7. By optimizing the use of low calcium fly ash replacement to around 20% - 25% of the cement, the carbonation depth at 50-year design period can be reduced by around 42% (when water / binder ratio is 0.5).

8. Future work should use field data if possible and find ways to account for workmanship factors.

9. In addition, since spalling is not covered in these models, some research, at least on incorporating expected time to spalling, can be initiated.

10. Where the Vensim models are concerned, a user friendly interface can be developed inclusive of guidance to users on choice of appropriate parameters.

REFERENCES

Alonso, C., Andrade, C., Rodriguez, J. and Diez, J.M., 1998. Factors controlling cracking of concrete affected by reinforcement corrosion. *Materials and structures*, 31(7), pp.435-441

Andrade, C., Alonso, C. and Molina, F.J., 1993. Cover cracking as a function of bar corrosion: Part I-Experimental test. *Materials and structures*, 26(8), pp.453-464.

Andrade, C., Alonso, C. and Sarrıa, J., 2002. Corrosion rate evolution in concrete structures exposed to the atmosphere. *Cement and concrete composites*, 24(1), pp.55-64.

Archie, G.E., 1942. The electrical resistivity log as an aid in determining some reservoir characteristics. *Transactions of the AIME*, 146(01), pp.54-62.

Backe, K.R., Lile, O.B. and Lyomov, S.K., 1998, January. Characterising Curing Cement Slurries by Electrical Conductivity. In SPE *Western Regional Meeting*. Society of Petroleum Engineers.

Bamforth, P.B., Price, W.F. and Emerson, M., 1997. *International Review of Chloride Ingress Into Structural Concrete: A Trl Report (Trl 359).* Thomas Telford.

Basheer, L., Kropp, J. and Cleland, D.J., 2001. Assessment of the durability of concrete from its permeation properties: a review. *Construction and building materials*, *15*(2-3), pp.93-103.

Bazant, Z.P., 1979. Physical model for steel corrosion in concrete sea structures-theory. *ASCE J Struct Div*, *105*(6), pp.1137-1153.

Bertolini, L., Elsener, B., Pedeferri, P., Redaelli, E. and Polder, R.B., 2013. *Corrosion of steel in concrete: prevention, diagnosis, repair*. John Wiley & Sons.

Böhni, H. ed., 2005. *Corrosion in reinforced concrete structures*. Elsevier.

Brieger, L.M., 1986. Numerical simulation of carbonation of concrete. In *Werkstoffwissenschaften und Bausanierung, Berishtsband zum 2. Internationalen Kolloquium* (pp. 635-640). Technische Akademie Esslingen.

Broomfield, J.P., 2003. *Corrosion of steel in concrete: understanding, investigation and repair*. CRC Press.

BroomfieldJ. P., RodriguezJ., OrtegaL. M., GarciaA. M., 1993.Concrete Bridges in Aggressive Environments, Philip D. Cady International Symposium, Minneapolis, November 9–10, 1993, Weyers, R.E.(Ed.)), Detroit, American Concrete Institute, ACI SP-151, P. 163–181.

Christensen, B.J., Coverdale, T., Olson, R.A., Ford, S.J., Garboczi, E.J., Jennings, H.M. and Mason, T.O., 1994. Impedance spectroscopy of hydrating cement-based materials: measurement, Interpretation, and application. *Journal of the American Ceramic Society*, *77*(11), pp.2789-2804.

Clear, K.C., 1992. Effectiveness of Epoxy-coated Reinforcing Steel-Interim Report.

Comité Européen de Normalisation, 2004. Design of concrete structures—Part 1-1: General rules and rules for buildings. *Eurocode 2*, *EN 1992-1-1: 2004: E*.

Dhir, R.K., Hewlett, P.C. and Chan, Y.N., 1989. Near surface characteristics of concrete: intrinsic permeability. *Magazine of concrete research*, *41*(147), pp.87-97,

Dias, W.P.S., 2000. Reduction of concrete sorptivity with age through carbonation. *Cement and Concrete Research*, *30*(8), pp.1255-1261.

Dias, W.P.S., 2013. Factors influencing the service life of buildings. *Engineer: Journal of the Institution of Engineers, Sri Lanka*, *46*(4).

Djerbi, A., Bonnet, S., Khelidj, A. and Baroghel-Bouny, V., 2008. Influence of traversing crack on chloride diffusion into concrete. *Cement and Concrete Research*, *38*(6), pp.877-883.

Felekoğlu, B., Türkel, S. and Baradan, B., 2007. Effect of water/cement ratio on the fresh and hardened properties of self-compacting concrete. *Building and Environment*, *42*(4), pp.1795-1802..

Gjørv, O.E., Vennesland, Ø.E. and El-Busaidy, A.H.S., 1977, January. Electrical resistivity of concrete in the oceans. In *Offshore technology conference*. Offshore Technology Conference.

Glass, G.K. and Buenfeld, N.R., 2000. The influence of chloride binding on the chloride induced corrosion risk in reinforced concrete. *Corrosion Science*, *42*(2), pp.329-344.

Guo, Y., Trejo, D. and Yim, S., 2014. New Model for Estimating the Time-Variant Seismic Performance of Corroding RC Bridge Columns. *Journal of Structural Engineering*, *141*(6), p.04014158.

Jang, S.Y., Kim, B.S. and Oh, B.H., 2011. Effect of crack width on chloride diffusion coefficients of concrete by steady-state migration tests. *Cement and Concrete Research*, *41*(1), pp.9-19.

Katwan, M.J., Hodgkiess, T. and Arthur, P.D., 1996. Electrochemical noise technique for the prediction of corrosion rate of steel in concrete. *Materials and Structures*, *29*(5), pp.286-294.

Kranc, S.C. and Sagüés, A.A., 1993. Calculation of extended counter electrode polarization effects on the electrochemical impedance response of steel in concrete. In *Electrochemical Impedance: Analysis and Interpretation*. ASTM International.

Kranc, S.C. and Sagüés, A.A., 2001. Detailed modeling of corrosion macrocells on steel reinforcing in concrete. *Corrosion Science*, *43*(7), pp.1355-1372.

Kwon, S.J., Na, U.J., Park, S.S. and Jung, S.H., 2009. Service life prediction of concrete wharves with early-aged crack: Probabilistic approach for chloride diffusion. *Structural Safety*, *31*(1), pp.75-83.

Li, C.Q., 2003. Life-cycle modeling of corrosion-affected concrete structures: propagation. *Journal of Structural Engineering*, *129*(6), pp.753-761.

Li, C.Q., Yang, Y. and Melchers, R.E., 2008. Prediction of reinforcement corrosion in concrete and its effects on concrete cracking and strength reduction. *ACI materials journal*, *105*(1), p.3.

Lindvall, A., 1998, August. Duracrete–probabilistic performance based durability design of concrete structures. In *2nd Int. PhD. Symposium in civil engineering*.

Lindvall, A., 1998, August. Duracrete–probabilistic performance based durability design of concrete structures. In *2nd Int. PhD. Symposium in civil engineering*.

Liu, T. and Weyers, R.W., 1998. Modeling the dynamic corrosion process in chloride contaminated concrete structures. *Cement and Concrete Research*, *28*(3), pp.365-379.

Lopez, W. and Gonzalez, J.A., 1993. Influence of the degree of pore saturation on the resistivity of concrete and the corrosion rate of steel reinforcement. *Cement and concrete research*, *23*(2), pp.368-376.

Lu, C., Gao, Y. and Liu, R.G., 2014. Effect of Transverse Crack on Chloride Penetration into Concrete Subjected to Drying–Wetting Cycles.

Manmohan, D. and Mehta, P.K., 1981. Influence of pozzolanic, slag, and chemical admixtures on pore size distribution and permeability of hardened cement pastes. *Cement, Concrete and Aggregates*, *3*(1), pp.63-67.

Marques, P.F. and Costa, A., 2010. Service life of RC structures: Carbonation induced corrosion. Prescriptive vs. performance-based methodologies. *Construction and Building Materials*, *24*(3), pp.258-265.

Maruya, T., Hsu, K., Takeda, H. and Tangtermsirikul, S., 2003. Numerical modeling of steel corrosion in concrete structures due to chloride ion, oxygen and water movement. *Journal of Advanced Concrete Technology*, *1*(2), pp.147-160.

Mehta, P.K., 1991. *Concrete in the marine environment (modern concrete technology series)*. CRC Press.

Morris, W., Vico, A. and Vázquez, M., 2004. Chloride induced corrosion of reinforcing steel evaluated by concrete resistivity measurements. *Electrochimica Acta*, *49*(25), pp.4447-4453.

Neville, A.M., 1995. *Properties of concrete* (Vol. 4). London: Longman.

Ngala, V.T. and Page, C.L., 1997. Effects of carbonation on pore structure and diffusional properties of hydrated cement pastes. *Cement and Concrete Research*, *27*(7), pp.995-1007.

Nigmatullin, R.R., Dissado, L.A. and Soutougin, N.N., 1992. A fractal pore model for Archie's law in sedimentary rocks. *Journal of Physics D: Applied Physics*, *25*(1), p.32.

Nilsson, L.O., Poulsen, E., Sandberg, P., Sørensen, H.E. and Klinghoffer, O., 1996. HETEK, Chloride penetration into concrete, state-of-the-art, transport processes, corrosion initiation, test methods and prediction models. *Denmark, ISSN/ISBN*, pp.0909-4288.

Otieno, M., Beushausen, H. and Alexander, M., 2011. Prediction of corrosion rate in RC structures-A critical review. In *Modelling of Corroding Concrete Structures* (pp. 15-37). Springer, Dordrecht.

Otieno, M., Beushausen, H. and Alexander, M., 2012. Prediction of corrosion rate in reinforced concrete structures–a critical review and preliminary results. *Materials and corrosion*, *63*(9), pp.777-790.

Papadakis, V.G. and Tsimas, S., 2002. Supplementary cementing materials in concrete: Part I: efficiency and design. *Cement and concrete research*, *32*(10), pp.1525-1532.

Papadakis, V.G., 2000. Effect of supplementary cementing materials on concrete resistance against carbonation and chloride ingress. *Cement and concrete research*, *30*(2), pp.291-299.

Park, S.S., Kwon, S.J. and Jung, S.H., 2012. Analysis technique for chloride penetration in cracked concrete using equivalent diffusion and permeation. *Construction and Building Materials*, *29*, pp.183-192.

Parrott, L.J., 1985. Effect of changes in UK cements upon strength and recommended curing times. *Concrete (London)*, *19*(9).

Parrott, L.J., 1992. Variations of water absorption rate and porosity with depth from an exposed concrete surface: Effects of exposure conditions and cement type. *Cement and Concrete Research*, *22*(6), pp.1077-1088.

Radzicki, M.J. and Taylor, R.A., 2008. Origin of system dynamics: Jay W. Forrester and the history of system dynamics. *US Department of Energy's introduction to system dynamics*..

Richardson, G. and Pugh, A.L., III 1981. Introduction to system dynamics modeling with dynamo.

Rodriguez, J., 1996. Corrosion of reinforcement and service life of concrete structures. In *Proceedings of 7th International Conference on DBMC, 1996* (Vol. 1, pp. 117-126).

Saetta, A.V. and Vitaliani, R.V., 2004. Experimental investigation and numerical modeling of carbonation process in reinforced concrete structures: Part I: Theoretical formulation. *Cement and concrete research*, *34*(4), pp.571-579.

Sagüés, A., Kranc, S.C. and Washington, B.G., 2000. Computer modeling of corrosion and corrosion protection of steel in concrete. *Concrete*, p.1275.

Saleem, M., Shameem, M., Hussain, S.E. and Maslehuddin, M., 1996. Effect of moisture, chloride and sulphate contamination on the electrical resistivity of Portland cement concrete. *Construction and Building Materials*, *10*(3), pp.209-214.

Schiessl, P. and Hardtl, R., 1991. Efficiency of fly ash in concrete evaluation of ibac test results. In *Technical Report of Institut für Bauforschung*. RWTH Aachen.

Sideris, K.K. and Konsta-Gdoutos, M., 1996. Influence of the water to cement ratio W/C on the compressive strength of concrete—An application of the cement hydration equation to concrete. *Applied Composite Materials*, *3*(5), pp.335-343.

Smith L.A., 1967. Proc. Institution of Civil Engineers, London, April,Vol.36, pp.769-790

Snyder, K.A., 2001. *Validation and modification of the 4SIGHT computer program*. US Department of Commerce, Technology Administration, National Institute of Standards and Technology.

Steffens, A., Dinkler, D. and Ahrens, H., 2002. Modeling carbonation for corrosion risk prediction of concrete structures. *Cement and Concrete Research*, *32*(6), pp.935-941.

Stewart, M.G. and Rosowsky, D.V., 1998. Structural safety and serviceability of concrete bridges subject to corrosion. *Journal of Infrastructure systems*, *4*(4), pp.146-155.

Sulapha, P., Wong, S.F., Wee, T.H. and Swaddiwudhipong, S., 2003. Carbonation of concrete containing mineral admixtures. *Journal of materials in civil engineering*, *15*(2), pp.134-143.

Taffinder, G.G. and Batchelor, B., 1993. Measurement of effective diffusivities in solidified wastes. *Journal of Environmental Engineering*, *119*(1), pp.17-33.

Takewaka, K., Yamaguchi, T. and Maeda, S., 2003. Simulation model for deterioration of concrete structures due to chloride attack. *Journal of Advanced concrete technology*, *1*(2), pp.139-146.

Teplý, B., Chroma, M. and Rovnanik, P., 2010. Durability assessment of concrete structures: reinforcement depassivation due to carbonation. *Structures & Infrastructure Engineering*, *6*(3), pp.317-327.

Thomas, M.D.A. and Bentz, E.C., 2002. Computer program for predicting the service life and life-cycle costs of reinforced concrete exposed to chlorides. *Life365 Manual, SFA*, pp.12-56.

Tumidajski, P.J., Schumacher, A.S., Perron, S., Gu, P. and Beaudoin, J.J., 1996. On the relationship between porosity and electrical resistivity in cementitious systems. *Cement and concrete research*, *26*(4), pp.539-544.

Val, D.V. and Melchers, R.E., 1997. Reliability of deteriorating RC slab bridges. *Journal of structural engineering*, *123*(12), pp.1638-1644.

Vensim software (Accessed on multiple dates between 2016 and 2018): https://www.vensim.com/documentation/index.html?users_guide.htm.

Ventana Systems, 2007. Vensim® User Manual.

Vu, K., Stewart, M.G. and Mullard, J., 2005. Corrosion-induced cracking: experimental data and predictive models. *ACI structural journal*, *102*(5), p.719.

Vu, K.A.T. and Stewart, M.G., 2000. Structural reliability of concrete bridges including improved chloride-induced corrosion models. *Structural safety*, *22*(4), pp.313-333.

Yalcyn, H. and Ergun, M., 1996. The prediction of corrosion rates of reinforcing steels in concrete. *Cement and concrete research*, *26*(10), pp.1593-1599.

Zhang, R., Castel, A. and François, R., 2010. Concrete cover cracking with reinforcement corrosion of RC beam during chloride-induced corrosion process. *Cement and Concrete Research*, *40*(3), pp.415-425.

APPENDIX

Appendix A.1

Vensim model outputs in tabular format for the influence of water / binder ratio on the crack width due to chloride ingress into concrete when no cement is replaced by fly ash. (Figure 4.22)

	Water / binder ratio					
Time (Year)	0.3	0.4	0.5	0.6	0.7	0.8
0	0.00	0.00	0.00	0.00	0.00	0.00
0.25	0.00	0.00	0.00	0.00	0.00	0.00
0.5	0.00	0.00	0.00	0.00	0.00	0.00
0.75	0.00	0.00	0.00	0.00	0.00	0.00
1	0.00	0.00	0.00	0.00	0.00	0.00
1.25	0.00	0.00	0.00	0.00	0.00	0.00
1.5	0.00	0.00	0.00	0.00	0.00	0.00
1.75	0.00	0.00	0.00	0.00	0.00	0.00
2	0.00	0.00	0.00	0.00	0.00	0.00
2.25	0.00	0.00	0.00	0.00	0.00	0.00
2.5	0.00	0.00	0.00	0.00	0.00	0.00
2.75	0.00	0.00	0.00	0.00	0.00	0.00
3	0.00	0.00	0.00	0.00	0.00	0.00
3.25	0.00	0.00	0.00	0.00	0.00	0.00
3.5	0.00	0.00	0.00	0.00	0.00	0.00
3.75	0.00	0.00	0.00	0.00	0.00	0.00
4	0.00	0.00	0.00	0.00	0.00	0.00
4.25	0.00	0.00	0.00	0.00	0.00	0.00
4.5	0.00	0.00	0.00	0.00	0.00	0.00
4.75	0.00	0.00	0.00	0.00	0.00	0.00
5	0.00	0.00	0.00	0.00	0.00	0.00
5.25	0.00	0.00	0.00	0.00	0.00	0.00
5.5	0.00	0.00	0.00	0.00	0.00	0.00
5.75	0.00	0.00	0.00	0.00	0.00	0.00
6	0.00	0.00	0.00	0.00	0.00	0.00
6.25	0.00	0.00	0.00	0.00	0.00	0.00
6.5	0.00	0.00	0.00	0.00	0.00	0.00
6.75	0.00	0.00	0.00	0.00	0.00	0.00
7	0.00	0.00	0.00	0.00	0.00	0.00
7.25	0.00	0.00	0.00	0.00	0.00	0.00
7.5	0.00	0.00	0.00	0.00	0.00	0.00
7.75	0.00	0.00	0.00	0.00	0.00	0.00
8	0.00	0.00	0.00	0.00	0.00	0.00
8.25	0.00	0.00	0.00	0.00	0.00	0.00
8.5	0.00	0.00	0.00	0.00	0.00	0.00

8.75	0.00	0.00	0.00	0.00	0.00	0.02
9	0.00	0.00	0.00	0.00	0.00	0.04
9.25	0.00	0.00	0.00	0.00	0.01	0.08
9.5	0.00	0.00	0.00	0.00	0.04	0.11
9.75	0.00	0.00	0.00	0.00	0.07	0.14
10	0.00	0.00	0.00	0.01	0.10	0.18
10.25	0.00	0.00	0.00	0.03	0.14	0.21
10.5	0.00	0.00	0.00	0.06	0.17	0.25
10.75	0.00	0.00	0.01	0.09	0.20	0.29
11	0.00	0.00	0.03	0.12	0.24	0.32
11.25	0.00	0.00	0.06	0.15	0.27	0.36
11.5	0.00	0.00	0.08	0.18	0.31	0.40
11.75	0.00	0.01	0.11	0.22	0.34	0.43
12	0.00	0.02	0.14	0.25	0.38	0.47
12.25	0.00	0.04	0.17	0.28	0.41	0.51
12.5	0.00	0.06	0.20	0.31	0.45	0.54
12.75	0.01	0.08	0.23	0.35	0.48	0.58
13	0.02	0.10	0.26	0.38	0.52	0.62
13.25	0.04	0.13	0.29	0.41	0.56	0.65
13.5	0.05	0.16	0.32	0.45	0.59	0.69
13.75	0.07	0.18	0.35	0.48	0.63	0.73
14	0.09	0.21	0.38	0.52	0.66	0.77
14.25	0.11	0.24	0.41	0.55	0.70	0.80
14.5	0.13	0.26	0.45	0.58	0.73	0.84
14.75	0.16	0.29	0.48	0.62	0.77	0.88
15	0.18	0.32	0.51	0.65	0.80	0.91
15.25	0.20	0.35	0.54	0.68	0.84	0.95
15.5	0.23	0.38	0.57	0.72	0.88	0.99
15.75	0.25	0.41	0.60	0.75	0.91	1.02
16	0.27	0.44	0.63	0.79	0.95	1.06
16.25	0.30	0.46	0.67	0.82	0.98	1.10
16.5	0.32	0.49	0.70	0.85	1.02	1.14
16.75	0.35	0.52	0.73	0.89	1.05	1.17
17	0.38	0.55	0.76	0.92	1.09	1.21
17.25	0.40	0.58	0.79	0.96	1.13	1.25
17.5	0.43	0.61	0.82	0.99	1.16	1.28
17.75	0.45	0.64	0.86	1.02	1.20	1.32
18	0.48	0.67	0.89	1.06	1.23	1.36
18.25	0.50	0.70	0.92	1.09	1.27	1.40
18.5	0.53	0.73	0.95	1.13	1.30	1.43
18.75	0.55	0.75	0.98	1.16	1.34	1.47
19	0.58	0.78	1.02	1.19	1.38	1.51
19.25	0.61	0.81	1.05	1.23	1.41	1.55
19.5	0.63	0.84	1.08	1.26	1.45	1.58
19.75	0.66	0.87	1.11	1.30	1.48	1.62
20	0.68	0.90	1.14	1.33	1.52	1.66

20.25	0.71	0.93	1.17	1.36	1.55	1.69
20.5	0.74	0.96	1.21	1.40	1.59	1.73
20.75	0.76	0.99	1.24	1.43	1.63	1.77
21	0.79	1.02	1.27	1.47	1.66	1.81
21.25	0.81	1.05	1.30	1.50	1.70	1.84
21.5	0.84	1.08	1.33	1.53	1.73	1.88
21.75	0.86	1.10	1.37	1.57	1.77	1.92
22	0.89	1.13	1.40	1.60	1.81	1.96
22.25	0.92	1.16	1.43	1.64	1.84	1.99
22.5	0.94	1.19	1.46	1.67	1.88	2.03
22.75	0.97	1.22	1.49	1.70	1.91	2.07
23	0.99	1.25	1.53	1.74	1.95	2.10
23.25	1.02	1.28	1.56	1.77	1.98	2.14
23.5	1.05	1.31	1.59	1.81	2.02	2.18
23.75	1.07	1.34	1.62	1.84	2.06	2.22
24	1.10	1.37	1.65	1.88	2.09	2.25
24.25	1.13	1.40	1.69	1.91	2.13	2.29
24.5	1.15	1.43	1.72	1.94	2.16	2.33
24.75	1.18	1.46	1.75	1.98	2.20	2.37
25	1.20	1.49	1.78	2.01	2.24	2.40
25.25	1.23	1.52	1.82	2.05	2.27	2.44
25.5	1.26	1.55	1.85	2.08	2.31	2.48
25.75	1.28	1.58	1.88	2.12	2.34	2.52
26	1.31	1.60	1.91	2.15	2.38	2.55
26.25	1.33	1.63	1.94	2.18	2.42	2.59
26.5	1.36	1.66	1.98	2.22	2.45	2.63
26.75	1.39	1.69	2.01	2.25	2.49	2.66
27	1.41	1.72	2.04	2.29	2.52	2.70
27.25	1.44	1.75	2.07	2.32	2.56	2.74
27.5	1.47	1.78	2.11	2.36	2.60	2.78
27.75	1.49	1.81	2.14	2.39	2.63	2.81
28	1.52	1.84	2.17	2.42	2.67	2.85
28.25	1.55	1.87	2.20	2.46	2.70	2.89
28.5	1.57	1.90	2.23	2.49	2.74	2.93
28.75	1.60	1.93	2.27	2.53	2.78	2.96
29	1.62	1.96	2.30	2.56	2.81	3.00
29.25	1.65	1.99	2.33	2.60	2.85	3.04
29.5	1.68	2.02	2.36	2.63	2.89	3.08
29.75	1.70	2.05	2.40	2.67	2.92	3.11
30	1.73	2.08	2.43	2.70	2.96	3.15
30.25	1.76	2.11	2.46	2.73	2.99	3.19
30.5	1.78	2.14	2.49	2.77	3.03	3.23
30.75	1.81	2.17	2.52	2.80	3.07	3.26
31	1.84	2.20	2.56	2.84	3.10	3.30
31.25	1.86	2.23	2.59	2.87	3.14	3.34
31.5	1.89	2.26	2.62	2.91	3.17	3.38

31.75	1.92	2.29	2.65	2.94	3.21	3.41
32	1.94	2.32	2.69	2.98	3.25	3.45
32.25	1.97	2.35	2.72	3.01	3.28	3.49
32.5	2.00	2.38	2.75	3.04	3.32	3.53
32.75	2.02	2.41	2.78	3.08	3.35	3.56
33	2.05	2.44	2.82	3.11	3.39	3.60
33.25	2.08	2.47	2.85	3.15	3.43	3.64
33.5	2.10	2.50	2.88	3.18	3.46	3.68
33.75	2.13	2.53	2.91	3.22	3.50	3.71
34	2.15	2.56	2.95	3.25	3.54	3.75
34.25	2.18	2.59	2.98	3.29	3.57	3.79
34.5	2.21	2.62	3.01	3.32	3.61	3.83
34.75	2.23	2.65	3.04	3.35	3.64	3.86
35	2.26	2.68	3.08	3.39	3.68	3.90
35.25	2.29	2.71	3.11	3.42	3.72	3.94
35.5	2.31	2.73	3.14	3.46	3.75	3.98
35.75	2.34	2.76	3.17	3.49	3.79	4.01
36	2.37	2.79	3.21	3.53	3.82	4.05
36.25	2.40	2.82	3.24	3.56	3.86	4.09
36.5	2.42	2.85	3.27	3.60	3.90	4.13
36.75	2.45	2.88	3.30	3.63	3.93	4.16
37	2.48	2.91	3.34	3.67	3.97	4.20
37.25	2.50	2.94	3.37	3.70	4.01	4.24
37.5	2.53	2.97	3.40	3.73	4.04	4.28
37.75	2.56	3.00	3.43	3.77	4.08	4.31
38	2.58	3.03	3.47	3.80	4.11	4.35
38.25	2.61	3.06	3.50	3.84	4.15	4.39
38.5	2.64	3.09	3.53	3.87	4.19	4.43
38.75	2.66	3.12	3.56	3.91	4.22	4.46
39	2.69	3.15	3.60	3.94	4.26	4.50
39.25	2.72	3.18	3.63	3.98	4.30	4.54
39.5	2.74	3.21	3.66	4.01	4.33	4.58
39.75	2.77	3.24	3.69	4.05	4.37	4.62
40	2.80	3.27	3.73	4.08	4.40	4.65
40.25	2.82	3.30	3.76	4.12	4.44	4.69
40.5	2.85	3.33	3.79	4.15	4.48	4.73
40.75	2.88	3.36	3.82	4.18	4.51	4.77
41	2.90	3.40	3.86	4.22	4.55	4.80
41.25	2.93	3.43	3.89	4.25	4.59	4.84
41.5	2.96	3.46	3.92	4.29	4.62	4.88
41.75	2.99	3.49	3.96	4.32	4.66	4.92
42	3.01	3.52	3.99	4.36	4.69	4.95
42.25	3.04	3.55	4.02	4.39	4.73	4.99
42.5	3.07	3.58	4.05	4.43	4.77	5.03
42.75	3.09	3.61	4.09	4.46	4.80	5.07
43	3.12	3.64	4.12	4.50	4.84	5.10

43.25	3.15	3.67	4.15	4.53	4.88	5.14
43.5	3.17	3.70	4.18	4.57	4.91	5.18
43.75	3.20	3.73	4.22	4.60	4.95	5.22
44	3.23	3.76	4.25	4.64	4.99	5.25
44.25	3.25	3.79	4.28	4.67	5.02	5.29
44.5	3.28	3.82	4.31	4.70	5.06	5.33
44.75	3.31	3.85	4.35	4.74	5.09	5.37
45	3.34	3.88	4.38	4.77	5.13	5.40
45.25	3.36	3.91	4.41	4.81	5.17	5.44
45.5	3.39	3.94	4.45	4.84	5.20	5.48
45.75	3.42	3.97	4.48	4.88	5.24	5.52
46	3.44	4.00	4.51	4.91	5.28	5.56
46.25	3.47	4.03	4.54	4.95	5.31	5.59
46.5	3.50	4.06	4.58	4.98	5.35	5.63
46.75	3.53	4.09	4.61	5.02	5.38	5.67
47	3.55	4.12	4.64	5.05	5.42	5.71
47.25	3.58	4.15	4.67	5.09	5.46	5.74
47.5	3.61	4.18	4.71	5.12	5.49	5.78
47.75	3.63	4.21	4.74	5.16	5.53	5.82
48	3.66	4.24	4.77	5.19	5.57	5.86
48.25	3.69	4.27	4.81	5.23	5.60	5.89
48.5	3.71	4.30	4.84	5.26	5.64	5.93
48.75	3.74	4.33	4.87	5.30	5.68	5.97
49	3.77	4.36	4.90	5.33	5.71	6.01
49.25	3.80	4.39	4.94	5.36	5.75	6.05
49.5	3.82	4.42	4.97	5.40	5.78	6.08
49.75	3.85	4.45	5.00	5.43	5.82	6.12
50	3.88	4.48	5.03	5.47	5.86	6.16

Appendix A.2

Vensim model outputs in tabular format for the influence of fly ash replacement of cement on carbonation depth due to carbonation of concrete when water / binder ratio is 0.5. (Table 5.7)

Time (Year)	Fly Ash Replacement					
	0.5	0.4	0.3	0.2	0.1	0
0	0	0	0	0	0	0
0.5	5.56	4.31	3.95	4.22	5.08	5.85
1	6.95	5.36	4.86	5.08	5.95	6.70
1.5	7.93	6.11	5.49	5.68	6.56	7.28
2	8.72	6.71	6.01	6.17	7.04	7.74
2.5	9.41	7.22	6.45	6.58	7.45	8.13
3	10.01	7.68	6.84	6.95	7.82	8.47
3.5	10.55	8.10	7.19	7.27	8.14	8.77
4	11.05	8.48	7.51	7.58	8.44	9.05
4.5	11.52	8.83	7.81	7.85	8.71	9.31
5	11.95	9.16	8.09	8.12	8.96	9.54
5.5	12.36	9.47	8.36	8.36	9.20	9.77
6	12.75	9.76	8.61	8.59	9.43	9.98
6.5	13.12	10.04	8.84	8.81	9.64	10.18
7	13.47	10.31	9.07	9.02	9.85	10.37
7.5	13.81	10.57	9.29	9.22	10.04	10.55
8	14.13	10.82	9.50	9.42	10.23	10.72
8.5	14.45	11.05	9.70	9.60	10.41	10.89
9	14.75	11.28	9.89	9.78	10.59	11.05
9.5	15.04	11.51	10.08	9.96	10.75	11.20
10	15.32	11.72	10.27	10.13	10.92	11.35
10.5	15.60	11.93	10.44	10.29	11.07	11.50
11	15.87	12.14	10.62	10.45	11.23	11.64
11.5	16.13	12.33	10.78	10.60	11.38	11.77
12	16.38	12.53	10.95	10.75	11.52	11.90
12.5	16.63	12.72	11.11	10.90	11.66	12.03
13	16.87	12.90	11.26	11.04	11.80	12.16
13.5	17.10	13.08	11.41	11.18	11.93	12.28
14	17.33	13.25	11.56	11.32	12.06	12.40
14.5	17.56	13.43	11.71	11.45	12.19	12.52
15	17.78	13.60	11.85	11.58	12.32	12.63
15.5	17.99	13.76	11.99	11.71	12.44	12.74
16	18.21	13.92	12.13	11.84	12.56	12.85
16.5	18.41	14.08	12.26	11.96	12.68	12.96
17	18.62	14.24	12.39	12.08	12.79	13.07
17.5	18.82	14.39	12.52	12.20	12.91	13.17

18	19.02	14.54	12.65	12.32	13.02	13.27
18.5	19.21	14.69	12.78	12.43	13.13	13.37
19	19.40	14.84	12.90	12.54	13.24	13.47
19.5	19.59	14.98	13.02	12.65	13.34	13.56
20	19.77	15.12	13.14	12.76	13.45	13.66
20.5	19.95	15.26	13.26	12.87	13.55	13.75
21	20.13	15.40	13.37	12.98	13.65	13.84
21.5	20.31	15.54	13.49	13.08	13.75	13.93
22	20.48	15.67	13.60	13.19	13.85	14.02
22.5	20.66	15.80	13.71	13.29	13.94	14.11
23	20.83	15.93	13.82	13.39	14.04	14.19
23.5	20.99	16.06	13.93	13.49	14.13	14.28
24	21.16	16.19	14.04	13.58	14.23	14.36
24.5	21.32	16.31	14.14	13.68	14.32	14.45
25	21.48	16.43	14.25	13.78	14.41	14.53
25.5	21.64	16.56	14.35	13.87	14.50	14.61
26	21.80	16.68	14.45	13.96	14.58	14.69
26.5	21.95	16.80	14.55	14.05	14.67	14.77
27	22.11	16.91	14.65	14.15	14.76	14.84
27.5	22.26	17.03	14.75	14.23	14.84	14.92
28	22.41	17.15	14.85	14.32	14.93	14.99
28.5	22.56	17.26	14.94	14.41	15.01	15.07
29	22.70	17.37	15.04	14.50	15.09	15.14
29.5	22.85	17.49	15.13	14.58	15.17	15.22
30	22.99	17.60	15.23	14.67	15.25	15.29
30.5	23.13	17.70	15.32	14.75	15.33	15.36
31	23.27	17.81	15.41	14.84	15.41	15.43
31.5	23.41	17.92	15.50	14.92	15.49	15.50
32	23.55	18.03	15.59	15.00	15.57	15.57
32.5	23.69	18.13	15.68	15.08	15.64	15.64
33	23.82	18.24	15.77	15.16	15.72	15.71
33.5	23.95	18.34	15.85	15.24	15.79	15.77
34	24.09	18.44	15.94	15.32	15.87	15.84
34.5	24.22	18.54	16.03	15.40	15.94	15.90
35	24.35	18.64	16.11	15.47	16.01	15.97
35.5	24.48	18.74	16.20	15.55	16.08	16.03
36	24.61	18.84	16.28	15.63	16.16	16.10
36.5	24.73	18.94	16.36	15.70	16.23	16.16
37	24.86	19.04	16.44	15.78	16.30	16.22
37.5	24.98	19.13	16.53	15.85	16.37	16.29
38	25.11	19.23	16.61	15.92	16.44	16.35
38.5	25.23	19.32	16.69	16.00	16.50	16.41
39	25.35	19.42	16.77	16.07	16.57	16.47
39.5	25.47	19.51	16.84	16.14	16.64	16.53

40	25.59	19.60	16.92	16.21	16.71	16.59
40.5	25.71	19.70	17.00	16.28	16.77	16.65
41	25.83	19.79	17.08	16.35	16.84	16.71
41.5	25.94	19.88	17.15	16.42	16.90	16.77
42	26.06	19.97	17.23	16.49	16.97	16.82
42.5	26.17	20.06	17.30	16.56	17.03	16.88
43	26.29	20.14	17.38	16.62	17.09	16.94
43.5	26.40	20.23	17.45	16.69	17.16	16.99
44	26.51	20.32	17.53	16.76	17.22	17.05
44.5	26.63	20.41	17.60	16.82	17.28	17.11
45	26.74	20.49	17.67	16.89	17.34	17.16
45.5	26.85	20.58	17.74	16.96	17.41	17.21
46	26.96	20.66	17.82	17.02	17.47	17.27
46.5	27.06	20.75	17.89	17.08	17.53	17.32
47	27.17	20.83	17.96	17.15	17.59	17.38
47.5	27.28	20.91	18.03	17.21	17.65	17.43
48	27.39	21.00	18.10	17.28	17.71	17.48
48.5	27.49	21.08	18.17	17.34	17.76	17.53
49	27.60	21.16	18.24	17.40	17.82	17.59
49.5	27.70	21.24	18.30	17.46	17.88	17.64
50	27.80	21.32	18.37	17.52	17.94	17.69

Appendix B.1

Crack width predictions by Vensim software due to chloride ingress into concrete when saturation ratio is 65%

		Water / Binder Ratio						Influence	Average Influence
		0.3	0.4	0.5	0.6	0.7	0.8		
Fly Ash Ratio	0	1.33	1.61	1.88	2.10	2.29	2.44	1.11	1.41
	0.1	1.13	1.40	1.71	1.96	2.20	2.38	1.25	
	0.2	1.04	1.16	1.49	1.80	2.04	2.27	1.23	
	0.3	0.90	0.89	1.23	1.60	1.92	2.16	1.27	
	0.4	0.45	0.49	0.88	1.36	1.76	2.08	1.63	
	0.5	0.05	0.04	0.41	1.02	1.57	1.99	1.95	
Influence		1.29	1.57	1.46	1.08	0.73	0.45		
Average Influence		1.10							

Crack width predictions by Vensim software due to chloride ingress into concrete when saturation ratio is 100%

		Water / Binder Ratio						Influence	Average Influence
		0.3	0.4	0.5	0.6	0.7	0.8		
Fly Ash Ratio	0	1.33	1.61	1.88	2.10	2.29	2.44	1.11	1.41
	0.1	1.13	1.40	1.71	1.96	2.20	2.38	1.25	
	0.2	1.04	1.16	1.49	1.80	2.04	2.27	1.23	
	0.3	0.90	0.89	1.23	1.60	1.92	2.16	1.27	
	0.4	0.45	0.49	0.88	1.36	1.76	2.08	1.63	
	0.5	0.05	0.04	0.41	1.02	1.57	1.99	1.95	
Influence		1.29	1.57	1.46	1.08	0.73	0.45		
Average Influence		1.10							

Appendix B.2

		Water / Binder Ratio						Influence	Average Influence
		0.3	0.4	0.5	0.6	0.7	0.8		
Fly Ash	0	9.55	13.89	17.69	20.31	23.67	26.12	16.57	19.83
	0.1	8.71	13.69	17.94	20.87	24.46	27.08	18.36	
	0.2	7.10	12.76	17.52	20.83	24.71	27.53	20.43	
	0.3	7.21	13.30	18.37	21.86	25.91	28.83	21.63	
	0.4	9.89	16.19	21.32	24.72	28.80	31.68	21.78	
	0.5	16.92	23.03	27.80	30.67	34.54	37.11	20.19	
Influence		9.81	10.27	10.28	10.36	10.87	10.99		
Average Influence		10.43							

Carbonation depth predictions by Vensim software when relative humidity is 80%

		Water / Binder Ratio						Influence	Average Influence
		0.3	0.4	0.5	0.6	0.7	0.8		
Fly Ash	0	6.09	8.57	11.43	13.18	14.84	16.44	10.35	12.52
	0.1	5.56	8.45	11.61	13.56	15.36	17.08	11.52	
	0.2	4.53	7.87	11.34	13.54	15.53	17.39	12.86	
	0.3	4.59	8.21	11.90	14.24	16.32	18.26	13.66	
	0.4	6.33	10.04	13.87	16.17	18.23	20.16	13.82	
	0.5	10.93	14.43	18.27	20.26	22.09	23.84	12.91	
Influence		6.41	6.57	6.94	7.07	7.25	7.40		
Average Influence		6.94							

Carbonation depth predictions by Vensim software when relative humidity is 100%